AD-A070 995   TORONTO UNIV DOWNSVIEW (ONTARIO) INST FOR AEROSPACE --ETC F/G 14/2
                A NEW TYPE FLAP VALVE FOR GENERATING SONIC BOOMS IN A PYRAMIDAL--ETC(U)
                OCT 78   J J GOTTLIEB, W CZERWINSKI, N N WAHBA   AFOSR-77-3303

UNCLASSIFIED   UTIAS-208   AFOSR-TR-79-0768   NL
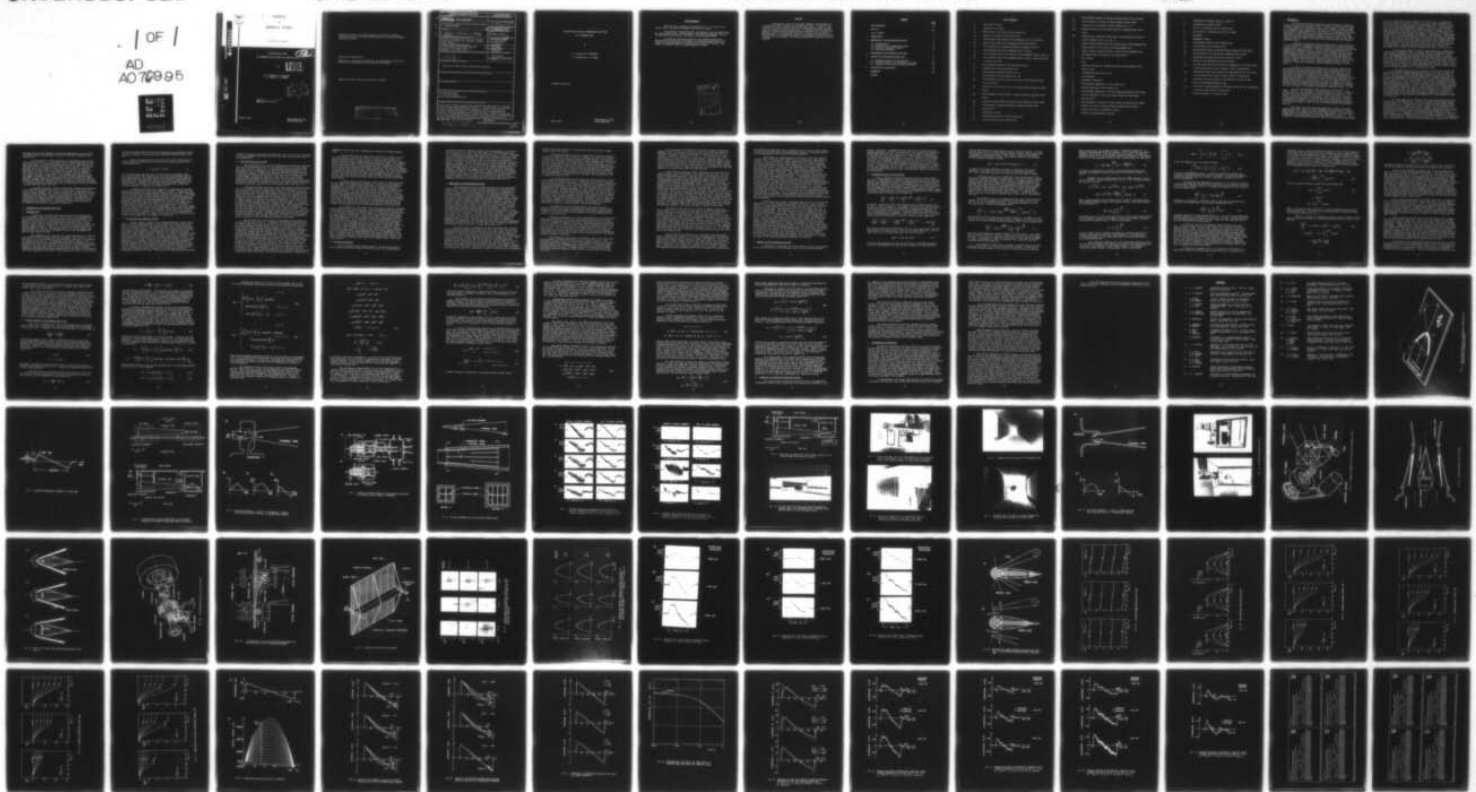
| OF |
AD
A070995

END
DATE
FILMED
8--79
DDC
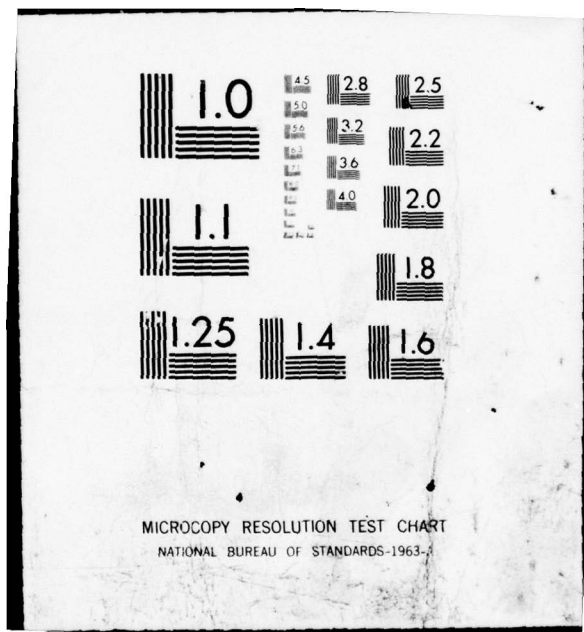
1.0

1.1

1.25   1.4   1.6

2.8   2.5

3.2   2.2

3.6

4.0   2.0

1.8

4.5
5.0
5.6
6.3

MICROCOPY RESOLUTION TEST CHART
NATIONAL BUREAU OF STANDARDS-1963-A

INSTITUTE

FOR

AEROSPACE STUDIES

UNIVERSITY OF TORONTO

A NEW TYPE FLAP VALVE

FOR GENERATING SONIC BOOMS IN A PYRAMIDAL HORN

by

J. J. Gottlieb, W. Czerwinski
N. N. Wahba, R. E. Gnoyke

D D C
RECEIVED
JUL 10 1979
C

October, 1978

79 07 09 011
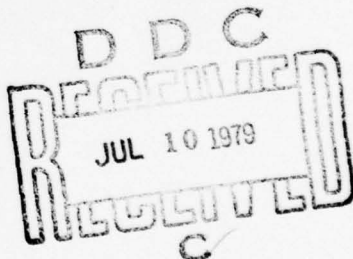
Qualified requestors may obtain additional copies from the Defense
Documentation Center, all others should apply to the National Technical
Information Service.

Conditions of Reproduction:

Reproduction, translation, publication, use and disposal in whole or in
part by or for the United States Government is permitted.

Approved for public release; distribution unlimited.

REPORT DOCUMENTATION PAGE

READ INSTRUCTIONS
BEFORE COMPLETING FORM

1. REPORT NUMBER	2. GOVT ACCESSION NO.	3. RECIPIENT'S CATALOG NUMBER
AFOSR-TR- 79-0768		

4. TITLE (and Subtitle)

A NEW TYPE FLAP VALVE FOR GENERATING SONIC BOOMS
IN A PYRAMIDAL HORN.

5. TYPE OF REPORT & PERIOD COVERED

Interim rept.,

6. PERFORMING ORG. REPORT NUMBER

UTIAS Report No. 208

7. AUTHOR(s)

J. J. Gottlieb, W. Czerwinski, N. N. Wahba,
R. E. Gnoyke

8. CONTRACT OR GRANT NUMBER(s)

AF-AFOSR-77-3303

9. PERFORMING ORGANIZATION NAME AND ADDRESS

University of Toronto, Institute for Aerospace
Studies, 4925 Dufferin St., Downsview, Ontario,
Canada, M3H 5T6

10. PROGRAM ELEMENT, PROJECT, TASK
AREA & WORK UNIT NUMBERS

2307 A3

61102F

11. CONTROLLING OFFICE NAME AND ADDRESS
Air Force Office of Scientific Research,
Bolling Air Force Base, Bldg. 410,
Washington, D.C. 20332, U.S.A.

12. REPORT DATE

Oct. 1978

13. NUMBER OF PAGES

76 pages

14. MONITORING AGENCY NAME & ADDRESS(if different from Controlling Office)

82p.

15. SECURITY CLASS. (of this report)

Unclassified

15a. DECLASSIFICATION/DOWNGRADING
SCHEDULE

16. DISTRIBUTION STATEMENT (of this Report)

Approved for public release; distribution unlimited.

17. DISTRIBUTION STATEMENT (of the abstract entered in Block 20, if different from Report)

18. SUPPLEMENTARY NOTES

19. KEY WORDS (Continue on reverse side if necessary and identify by block number)

NEW TYPE FLAP VALVE
SONIC-BOOM SIMULATORS
LOW-JET-NOISE SONIC-BOOM VALVE

20. ABSTRACT (Continue on reverse side if necessary and identify by block number)

A description is given of the design, operation and performance of a radically
new type of sonic-boom generating flap-valve. Included are the ancillary cam,
clutch, flywheel and electric motor system, as well as a much larger air
reservoir than used previously. An updated and greatly extended analysis
describes the time varying reservoir conditions (e.g., pressure) and mass-flow
rate of air through the flap valve, as well as the wave motion or characteristics
of the travelling N-wave in the pyramidal concrete horn (25 m long with a
3 m × 3 m base) of the UTIAS
travelling-wave sonic-boom
simulation facility.

DD FORM 1473 EDITION OF 1 NOV 65 IS OBSOLETE
1 JAN 73

UNCLASSIFIED

A NEW TYPE FLAP VALVE FOR GENERATING SONIC BOOMS

IN A PYRAMIDAL HORN

by

J. J. Gottlieb, W. Czerwinski,

N. N. Wahba and R. E. Gnoyke

Submitted July, 1978

Acknowledgements

ii

Abstract

A description is given of the design, operation and performance of a radically new type of sonic-boom generating flap-valve. Included are the ancillary cam, clutch, flywheel and electric motor system, as well as a much larger air reservoir than used previously. An updated and greatly extended analysis describes the time varying reservoir conditions (e.g., pressure) and mass-flow rate of air through the flap valve, as well as the wave motion or characteristics of the travelling N-wave in the pyramidal concrete horn (25 m long with a 3 m x 3 m base) of the UTIAS travelling-wave sonic-boom simulation facility.

CONTENTS

List of Symbols

a	sound speed of a gas
$\bar{a}$	atmospheric sound speed
a_o	time-dependent sound speed of the reservoir gas
$\bar{a}_o$	initial sound speed of the reservoir gas
a_*	time-dependent sound speed of the flowing gas at the valve throat
$\bar{a}_*$	initial sound speed of the flowing gas at the valve throat
a_i	i^{th} coefficient of a polynomial equation as defined in Eq. 18
A	cross-sectional area of the pyramidal horn at radius r
A_e	cross-sectional area of the large end of the pyramidal horn at radius r_e
$\bar{A}_o$	cross-sectional area of the pyramidal horn at radius r_o where the valve is joined to the horn
A_*	time-dependent variation of the valve-throat area
$\bar{A}_*$	maximum value of the valve-throat area
f	time-dependent function defined in Eq. 20
I	time-dependent function defined in Eq. 18
m_*	time-dependent mass flow rate per unit area of gas flowing through the valve throat
$\bar{m}_*$	initial mass flow rate per unit area of gas flowing through the valve throat
M_*	time-dependent flow Mach number of the gas flowing through the valve throat
$\bar{M}_*$	initial flow Mach number of the gas flowing through the valve throat
N_*	time-dependent, normalized variation of the valve-throat area
p	gas pressure
$\bar{p}$	atmospheric pressure
p_o	time-dependent pressure of the reservoir gas
$\bar{p}_o$	initial pressure of the reservoir gas

p_* time-dependent pressure of the gas flowing through the valve throat

$\bar{p}_*$ initial pressure of the gas flowing through the valve throat

Δp overpressure or perturbation pressure defined as $p - \bar{p}$

Δp_m maximum overpressure of the front shock of a simulated sonic boom or N-wave

$\overline{\Delta p}$ characteristic overpressure amplitude of the simulated sonic boom or N-wave as defined in Eq. 30 or Eq. 31

r radial distance measured from the projected apex of the pyramidal horn

r_e radial location of the large end of the pyramidal horn

r_o radial location at which the valve is joined to the pyramidal horn

r_* equivalent radius for area $\bar{A}_*$ of the valve throat

R gas constant

t time

t_o duration of the gas flow through the valve and the simulated sonic boom or N-wave

T nondimensional time t/t_o and τ/τ_o

T gas temperature

$\bar{T}$ atmospheric temperature

T_o time-dependent temperature of the reservoir gas

$\bar{T}_o$ initial temperature of the reservoir gas

T_* time-dependent temperature of the gas flowing through the valve throat

$\bar{T}_*$ initial temperature of the gas flowing through the valve throat

u gas flow speed

u_* time-dependent flow speed of the gas flowing through the valve throat

$\bar{u}_*$ initial flow speed of the gas flowing through the valve throat

Δu particle velocity or perturbation velocity

V volume of the high-pressure reservoir

α	nondimensional parameter $\bar{a}_* \bar{A}_* t_o / V$ or $\bar{a}_* \bar{A}_* \tau_o / V$
β	nondimensional parameter $r_o / \bar{a} \tau_o$
γ	ratio of the specific heats of a perfect gas
λ_o	wave length of a simulated sonic boom or N-wave
ρ	gas density
$\bar{\rho}$	atmospheric density
ρ_o	time-dependent density of the reservoir gas
$\bar{\rho}_o$	initial density of the reservoir gas
ρ_*	time-dependent density of the gas flowing through the valve throat
$\bar{\rho}_*$	initial density of the gas flowing through the valve throat
τ	time measured from the wave front as defined in Eq. 20
τ_o	duration of the simulated sonic boom or N-wave
τ_{10}	time after the wave front at which the overpressure of the front shock of the simulated sonic boom or N-wave is 10% of its peak value
τ_{90}	time after the wave front at which the overpressure of the front shock of the simulated sonic boom or N-wave is 90% of its peak value
$\Delta\tau_m$	rise time of the front shock of a simulated sonic boom or N-wave based on the maximum overpressure Δp_m
$\Delta\tau_p$	rise time of a shock defined as 1.25 times the time for the overpressure to rise from 10% to 90% of its peak value
ϕ	velocity potential of an acoustic wave

1. INTRODUCTION

With each new year more of mankind is being subjected to additional noise and its consequent increased stress. Research into the effects of noise on humans, animals and structures, as well as its abatement, is also expanding at an accelerated pace, fortunately. Results of such work can provide a base for establishing safe guidelines of noise exposure. One important and currently active area of noise research is the study of the effects of impulse sound. Furthermore, a particularly important impulse sound is the sonic boom, whose impact is now being assessed before supersonic transport (SST) aircraft such as the Anglo-French Concorde and the Soviet TU-144 are introduced into extensive commercial service.

A sketch of the shock-wave pattern emanating from a SST aircraft and the trailing N-shaped overpressure signature at the Earth's surface are shown in Fig. 1 (Ref. 1). Furthermore, a better illustration of the ground-intercepted sonic-boom path appears in Fig. 2. The most important parameters which are commonly used to describe the various parts of the signature include the peak overpressure, rise-time, duration (or wave length), and wave form which may deviate somewhat from the ideal N-shape. It is worth noting that respective values of peak overpressure, duration and rise-time are 100 N/m^2, 300 ms and 1 ms for a typical sonic boom from a current SST and also from a large military supersonic bomber. In the case of a shorter supersonic fighter, only the duration is significantly different, being correspondingly shorter at about 100 ms.

In order to successfully simulate a sonic boom from a SST aircraft, any simulation facility must have the capability of repeatedly producing an N-wave having the correct peak overpressure, rise-time and duration. In the late 1960's and early 1970's, many different types of sonic-boom simulation devices and techniques were proposed and most simulators or prototypes were constructed and tested. A description of such simulators and their test results cannot be given here, but the interested reader can find much information in various review articles or reports (Refs. 2, 3 and 4). However, it is worth mentioning that most simulators were only partially successful (e.g., produced an N-wave having the correct peak overpressure and rise time but not duration), and only a few met all of the desired requirements adequately (Refs. 5 to 10).

The sonic-boom program at UTIAS started in the late 1960's. For example, see Ref. 1 for a review of the work completed up to 1974. A good part of this program was the development of suitable sonic-boom simulators. One portable sonic-boom simulator in the form of a shock tube (11 kg, 1 m long), having a constant-area driver and exponential horn, can easily be transported and operated by one person to conduct wildlife field tests (Refs. 1 and 11). A simulated short-duration sonic boom can be produced and directed at wildlife in its natural habitat, in order to study its startle response and subsequent behaviour.

The first of two major laboratory facilities at UTIAS is the Loud-speaker-Driven Booth, which can easily accommodate one human subject or small caged animals in its solidly built and sealed chamber (about 2 m^3) to facilitate response tests to a simulated full-scale sonic boom (Refs. 1, 9 and 12). The second major laboratory facility is the Travelling-Wave Horn (Refs. 1, 4, 10, 12, 13 and 14), and its essential features are shown in the elevation and plan views

1

of Fig. 3. The large horizontal pyramid is 25 m long, has a 3 m square base, and is made mainly of concrete. Near the horn apex a sonic-boom generator in the form of either a mass-flow valve or a shock-tube driver is used to control the air flow from the high-pressure reservoir into the horn. The expanding air flow near the horn apex simulates the expansion process occurring in a weak spherical explosion and produces the travelling N-wave or simulated sonic boom which propagates from the small to the large end of the horn. For studies of the effects of sonic boom on humans and animals, a human subject or small caged animals can be put in the interior test section or alternatively in the psycho-acoustic test room which is joined to the horn interior by a suitably sized open window. For structural tests, one large or many small panels representative of a house interior wall can be installed in the cutout, or one or more walls of the psychoacoustic test room can be used directly for full-scale wall response and fatigue tests. Many such studies and also others which utilized the Travelling-Wave Horn have already been completed (see Refs. 13 and 15 to 22).

In the shock-tube mode of operation, high-pressure air contained in a constant-area or pyramidal driver is suddenly released by breaking a diaphragm which initially separates the driver gas from the lower pressure air in the horn. The expanding driver gas generates the travelling N-wave or simulated sonic boom. Although the peak overpressure of the N-wave can be easily controlled to be less than, equivalent to or greater than that of an actual sonic boom, the duration is short (up to 20 ms) and the rise time is rapid (about 20 μs). Such a short N-wave can be useful for certain human and animal response studies, but it is more suitable for studies of N-wave diffraction over and into a model building, and also N-wave propagation over a reduced-scale topology.

For the mass-flow-valve mode of operation of the Travelling-Wave Horn a specially designed, pneumatically-operated plug valve is used to control the mass-flow rate of air from the high-pressure reservoir into the horn (Figs. 4 and 5). The peak overpressure and wave length of the simulated sonic boom can be controlled independently such that either one is less than, equivalent to or greater than that of an actual sonic boom. The rise time of the simulated sonic boom is typically 3 to 6 ms. The interior of the horn is equipped with a special high-frequency sound absorber or low-pass acoustic filter for removing jet noise from the passing N-wave (Figs. 3 and 6). This undesirable jet noise is generated by the high-speed turbulent air flow at the plug valve, and it is superposed on the simulated sonic boom. The open base of the pyramidal horn is covered by a specially-designed reflection-eliminator (Fig. 3), which is in the form of a recoiling porous piston. This device adequately minimizes the undesirable re-flected wave which is generated when the simulated sonic boom reaches the large end of the horn.

Jet noise superposed on simulated sonic booms generated with the plug valve is well illustrated in Figs. 7 and 8 for different N-wave amplitudes and durations (Ref. 10) Without the use of the jet-noise absorber (first column) the superposed noise is normally very severe, whereas with the absorber (second column) the noise is markedly less intense. However, even in the latter case, the subjective loudness of the boom can be increased substantially by the presence of the jet noise, and thus results of human and animal-response tests can be affected (Ref. 13). Furthermore, since structural panels respond not only to the basic N-shaped pressure signature but also to the lower frequencies of the jet noise, panel response is affected by the jet noise (Refs. 18 and 19). Consequently, it was concluded in Ref. 10 that the Travelling-Wave Horn, when operated with the

plug valve and jet-noise absorber, is limited in performance by the jet noise to N-waves having a peak amplitude less than 200 N/m^2 and a duration shorter than 150 ms.

The possibility of greatly improving the performance of the facility was pointed out in Ref. 10. An analysis of the jet noise showed that the noise could be reduced to inconsequential significance by using a valve which has a much larger throat area (e.g., tenfold larger at about 350 cm^2). For the same mass-flow rate of air through the valve, which would produce an equivalent amplitude and duration N-wave, the larger valve would result in a much lower flow speed at the valve throat (well below sonic speed) and thus markedly-less intense jet noise. It was realized that scaling up the plug valve to a much larger size might be impractical. The resulting larger and more massive plug might be very difficult to accelerate quickly to high speed when needed, maintain a constant high speed and decelerate in order to control with precision the mass-flow rate of air through the valve. Consequently, a radically new mass-flow valve was designed and constructed, and the Travelling-Wave Horn was modified to operate with this large flap valve.

A detailed description is given of the design, operation and performance of the UTIAS Travelling-Wave Horn with the new flap valve. This description covers the basic elements of the facility including the air-compressor and large-reservoir system, pyramidal horn, reflection eliminator, and flap valve with its unique electric-motor drive, flywheel, fast-acting clutch and cam system. This is followed by an updated and greatly extended analysis to describe the time-varying reservoir conditions (e.g., reservoir pressure), valve operation and wave motion in the pyramidal horn. The amplitude, duration and wave form of the simulated sonic boom can be predicted successfully.

2. DESCRIPTION OF THE TRAVELLING-WAVE HORN

2.1 Pyramidal Horn

A plan view of the UTIAS sonic-boom laboratory and Travelling-Wave Horn when operated with the flap valve is shown in Fig. 9. The pyramidal horn is enclosed at the small end by a building called the control room and at the large end by the test room, as depicted in Fig. 9 and also shown in Fig. 10. Pictures of those parts of the horn contained in the control and test rooms appear in Figs. 11 and 12, respectively. The interior of the horn, looking from the base towards the apex, is shown in Fig. 13, and the opposite view of the interior appears in Fig. 14. The illusory effects that the horn appears infinitely long in Fig. 13 and has no divergence in Fig. 14 are also experienced when one stands inside the horn.

The pyramidal horn is 25 m long, has a square base which is 3 m on each side, and has a total divergence angle of 7.2 degrees. The first part of the horn which is 2.4 m long is made of 2.5-cm-thick steel plate, and it is supported by a special stand (Fig. 11). The remainder of the horn is made of steel-reinforced concrete, and this monolithic structure also has extremely rigid walls which are 20 cm thick. The steel and concrete portions of the horn were purposely designed to have very rigid, nonporous and flat walls, in order to minimize undesirable wave-energy losses and resulting wave-form distortion as the simulated sonic boom propagates from the small to the large end of the horn. The horn walls

3

are plane to within 0.2% of the duct width where the wall perturbation occurs, and such protuberances should not produce significant transverse waves in the horn.

The cross-sectional area of the horn (A) increases continuously with radial distance (r) measured from the projected horn apex, as given by the following expression:

$$A = A_e(r/r_e)^2 = (r/8)^2 \qquad (1)$$

The area at the large end (A_e) equals 9.30 m^2 and the corresponding radius (r_e) equals 24.38 m. This expression for the plane cross-sectional area is a good approximation for the curved surface area associated with the spherical wave front of the simulated sonic boom, and it is used for simplicity in the analytical work. Note that the percentage difference between the plane and curved surface areas amounts to only 0.3% for the UTIAS horn, because the divergence angle of 7.2 degrees is relatively small.

A pyramidal horn instead of a hyperbolic or wedgy duct was selected because this type of horn forms a solid angle of a sphere. Consequently, the expansion flow process of a weak spherical explosion (Ref. 14) can be simulated and a travelling N-wave produced from the onset near the horn apex. Only a small portion of a full sphere is incorporated in the horn in order to minimize the source energy required to produce the simulated sonic boom. The source energy required for the operation of the UTIAS facility is about three orders of magnitude ($1/256\pi$) less than that needed for the case of a full sphere, which is calculated by taking the ratio of the cross-sectional area of the horn ($r^2/64$) to the full area of the corresponding sphere ($4\pi r^2$). The source energy cannot be reduced much further because a sufficiently large interior test section is required (about 2.5 m square) to accommodate a human subject or a structure and the horn length is limited (about 25 m) by cost and space considerations. Note also that a pyramidal horn having a plane floor, walls and ceiling provides a better working space than, for example, a conical horn.

2.2 Air Reservoir and Compressor System

The air reservoir system for the Travelling-Wave Horn consists essentially of a large cylindrical tank (3.4 m^3) located inside the control room (Fig. 11) and two additional long cylindrical tanks (3.4 m^3 each) outside the control room (Figs. 9 and 10). The three tanks are interconnected by suitable short pipes of large diameter to minimize unnecessary pressure differences and wave motion between tanks during the generation of a simulated sonic boom. Furthermore, their combined volume is sufficient to provide a reasonably constant reservoir pressure during operation. The large indoor tank is connected via a short transition duct directly to the flap-valve housing (Figs. 9 and 11). Low-pressure air (1 to 2 atm) is supplied to the reservoir by means of a two-stage, high-pressure (1 to 18 atm), reciprocating compressor (16 brake horsepower, 0.025 m^3 capacity at 850 rpm) and its small self-contained reservoir (0.5 m^3). The high-pressure air in the compressor reservoir maintains the facility reservoir at a desired, preselected lower pressure by means of a suitable pressure sensor and electronics, pressure throttle, and electrically controlled, pneumatically actuated ball valve. Note that the air compressor has been housed

4

outdoors in a special acoustically insulated shed (Fig. 10) to provide a virtually noise-free atmosphere inside the control and test rooms as well as the inside of the pyramidal horn.

2.3 Flap Valve and Control System

The flap valve and its essential requirements for producing a simulated sonic boom are illustrated in Fig. 15. The primary function of the mass-flow valve (Fig. 15a) is to release in a controlled manner higher pressure air from the reservoir into the pyramidal horn, where the expanding flow generates the simulated sonic boom. To achieve this simulation each valve flap must execute a one-cycle, oscillatory rotational motion such that the valve-throat area (A) is approximately a "parabolic" function of time (Fig. 15b). For constant reservoir-state conditions the mass-flow rate (m) of air through the valve throat has the same parabolic profile (Fig. 15b). This particular mass-flow-rate distribution, from zero to a maximum and back to zero again, produces the desired N-shaped overpressure signature (Δp) of the simulated sonic boom (Fig. 15c).

The mass-flow valve, dual flaps in the valve housing, three-bar linkage, cam, clutch, flywheel, electric motor and control system are shown in the two pictures of Fig. 16 and also illustratively in Fig. 17. When the flaps are in their normally closed state the higher pressure reservoir air is prevented from flowing into the horn. Although the electric motor turns the flywheel and the nearest part of the disengaged clutch at constant speed, the other part of the disengaged clutch, the cam and valve flaps are motionless. To actuate the valve in order to generate a simulated sonic boom the stationary half of the clutch is allowed to move axially towards the rotating half and engage it, causing the cam shaft and cam to suddenly rotate at constant speed. The rotating cam forces the three-bar linkage to synchronously rotate the flaps, first outwards to increase the throat area and mass flow rate of air from the reservoir into the horn and then inwards to decrease the throat area and mass flow rate. After one cam-shaft revolution the clutch disengages automatically and also suddenly stops the cam and cam-shaft rotation. The flaps have now returned to their original locations and the one-cycle operation has ended. The cycle can be repeated, of course, to produce a second and subsequent simulated sonic booms.

The flap valve has a centre section or aerodynamic fairing which has not been shown in Figs. 15 and 17. A drawing of the fairing in the flap valve is, however, shown in Fig. 18, and the motion of the flaps and various parts of the fairing during the opening stage of the valve are illustrated in Fig. 19. In Fig. 19a the flaps are shown in their normally closed state. The spring-loaded plates of the fairing are pressed together and a good seal is maintained to prevent air leakage from the reservoir into the horn. During the initial outward motion of the flaps, the fairing plates are forced outwards to follow the flaps and maintain the air seal (Fig. 19b). Eventually the plates are stopped suddenly by the fairing front stops, as the flaps go beyond the fairing edge (Fig. 19c). At this time the transition from no flow to flow through the valve is rapid, and it helps to produce a rapid rise time on the front shock of the simulated sonic boom. As the flaps continue to move outwards, the first half of the boom is generated by the increasing flow of air into the horn. The second half of the boom is generated as the flaps move inwards and decrease the flow back to zero. A rapid transition from flow to no flow, when the flaps re-establish contact with the central fairing, helps to produce a rapid rise time on the second shock of the boom. Note that the central fairing is shaped like a

symmetrical airfoil (Fig. 18) to minimize flow turbulence and high-frequency noise.

The two valve flaps are each 28.0 cm long and 19.7 cm wide, and they are firmly screwed to their pivot shafts which are 21.6 cm apart (Fig. 18). Nearly synchronous motion of the two flaps is achieved with a simple but completely adequate three-bar linkage between the flap pivot shafts. The rotational motion of the flaps, which produces the desired parabolic throat-area variation and mass-flow-rate profile, is controlled by the cam. Although the cam shape must be quite precise to produce the desired flap motion, the cam can be designed on the basis of the predicted shape. When the flaps are in the fully open position the valve-throat area can be as large as 250 cm^2. However, the cam of the present system does not utilize this whole area, as the maximum throat area is only 156 cm^2. Note that the flaps are quite light for rapid acceleration response, and they have O-ring seals along their sides which slide over the valve-housing inner surfaces.

A variable-speed, direct-current, electric motor (5 brake horsepower) has the capability of handling the average but not peak torque requirement of the flap valve. The reservoir pressure acting on the flaps during the valve opening period can produce a large counter torque. However, the flywheel (diameter of 31 cm, width of 10 cm) adds the extra capability to meet the peak torque requirements. Its large rotational inertia is sufficient to give an essentially constant-speed cam rotation during the valve operation. The motor speed or the flywheel and cam speed control the open-to-close time of the valve and hence the duration of both the air flow through the valve and the simulated sonic boom. The flywheel and cam speed can be conveniently varied from as high as 600 rpm to 100 rpm and even lower to give corresponding boom durations as short as 100 ms to 500 ms and even longer. Note that the reservoir pressure dictates the boom amplitude, and the cam shape determines the boom wave form.

An illustration of the details of the fast-acting, one-cycle, mechanical clutch appears in Fig. 20a and Fig. 20b. When the trigger mechanism (Fig. 20a) is actuated electrically, the stationary part of the clutch on the cam shaft next to the coupling is released and forced by means of a compression spring along the shaft into the rotating part of the clutch linked to the spinning flywheel. The quick engaging of the clutch suddenly rotates the coupling and cam shaft at the flywheel speed. As the cam shaft is rotated by the flywheel, the clutch pin follows the outward spiral contour of the clutch housing and subsequently causes the clutch to disengage just prior to the end of one revolution (Figs. 20a and 20b). The continuing cam-shaft rotation, owing to rotational inertia, is then stopped suddenly by means of the clutch pin when it strikes the rubber-cushioned pin stop. Recoiling rotation of the cam shaft and cam is restrained by a special spring-loaded catch mechanism (Fig. 20b), and re-engaging of the clutch is prevented by the trigger mechanism which resets automatically (Fig. 20a). To minimize both the acceleration and deceleration forces imposed on the clutch components during the sudden starting and stopping phases, the cam, cam shaft and associated rotating clutch parts were designed to have a small rotational inertia.

2.4 Reflection Eliminator

When the simulated sonic boom propagates to the base of the horn it would normally be partially reflected from the open end. This reflected wave

would then disrupt the simulated pressure and flow conditions in the interior test section (Fig. 9), because the wave length of the simulated sonic boom can be as many as four times longer than the entire horn. In order to eliminate or at least adequately minimize this undesirable reflection and its subsequent echoes, a reflection eliminator was built to cover the base of the horn. The reflection eliminator is basically a huge porous piston, as illustrated in Fig. 21. The porous part of this piston is a 2.5-cm-thick blanket of microlite material (12 kg/m^3). Because the porous piston is free to move on a special roller-and-track support, it can respond to the incident simulated sonic boom, being accelerated by the drag forces of the air flowing through the porous microlite. Significant air leakage around the porous piston is prevented by enclosing the piston at its periphery with a special skirt which is attached to the base of the horn. The correct flow resistance of the porous microlite and correct piston weight, as well as the ability of the piston to move, provides a matching of the impedance of the duct exit to that of the incident simulated sonic boom, thereby eliminating the reflected wave (Ref. 10).

3. PERFORMANCE OF THE TRAVELLING-WAVE HORN

The Travelling-Wave Horn utilizing the flap valve has proven experimentally to be a practical facility for the simulation of a sonic boom from either a SST or supersonic military aircraft, because the air compressor and reservoir system, flap valve, pyramidal horn and reflection eliminator all essentially function correctly as designed. The simulated sonic boom in the horn has an N-shaped overpressure signature for the following reasons. Firstly, the electric motor, flywheel, clutch, cam and three-bar linkage move the flaps correctly to give the desired parabolic throat-area variation. Secondly, the reservoir volume is sufficiently large to maintain a nearly constant driving pressure during the valve operation such that the flow through the valve has the desired corresponding parabolic mass-flow-rate variation, which generates a boom having the required N-shaped overpressure signature. Thirdly, the reflection eliminator adequately minimizes the wave reflection from the large end of the horn such that the N-wave flow and pressure conditions in the interior test section are not disrupted. Fourthly, jet noise superposed on a simulated sonic boom is not a problem, because the large throat area of the flap valve can easily pass the required flow rate at a low flow speed and consequently generates little jet noise. Note that more jet noise than is desirable is superposed on high-amplitude and long-duration booms, which are only infrequently needed for sonic-boom tests, but even this noise could be adequately diminished by utilizing a large cam and thus a larger valve throat area.

The N-wave duration requirements are more than sufficiently satisfied because the easily adjusted motor speed can be set to give valve open-to-close times and thus boom durations from 100 to 300 ms and even longer. Owing to the flexibility of setting the reservoir pressure from as low as 1 atm (absolute) to as high as 2 atm, the facility has the capability of producing an N-wave having a lower, equivalent or higher amplitude than that of an actual sonic boom. Peak overpressures as high as 1200, 600 and 400 N/m^2 can be achieved easily for respective N-wave durations of 100, 200 and 300 ms. The rise times of the front and rear shocks of the simulated sonic boom are not constant but depend very weakly on N-wave amplitude and more strongly on duration. For example, a typical rise time of the front shock, defined as 1.25 times the time for the overpressure to rise from 10 to 90% of its peak value, is about 6, 8 and 10 ms for corresponding

7

ruations of 100, 200 and 300 ms. The rise time of the rear shock is always somewhat longer (10 to 25%).

The Travelling-Wave Horn has been designed for continuous operation such that a sufficiently rapid sequence of simulated sonic booms can be produced to facilitate structural response, fatigue and damage studies. The number of booms per unit time depends on both the mass of air discharged from the reservoir per boom and the capacity of the compressor to refill the reservoir. For the case of a long-duration N-wave of 300 ms having a modest peak overpressure of 100 N/m^2, the generation rate has been found to be about three booms per minute. For a shorter duration boom of 200 ms having the same amplitude, the facility can easily produce six booms per minute. If the duration is still shorter at 100 ms the generation rate increases to about fifteen booms per minute. When the N-wave amplitude is doubled from 100 to 200 N/m^2, then the generation rate is reduced by a factor of two.

As already mentioned, the valve flaps move correctly and give a parabolic throat-area variation with time. Although the area variation cannot be measured directly during the generation of a simulated sonic boom to substantiate the preceding statement, it can be inferred directly from a measurement of the angular-displacement history of a flap. Note that the throat area is directly proportional to the angular displacement of f flap, provided that the rotation is sufficiently small. Measured angular-displacement histories of the top flap, which are virtually the same as those for the bottom flap, are shown in Fig. 22. Results are given not only for three different N-wave durations of 100, 200 and 300 ms, but also for three different reservoir overpressures of 6.9, 13.8 and 20.7 kN/m^2. These measured profiles have been reproduced in Fig. 23 where they can be better compared to a parabolic profile. From these and other angular-displacement histories it can be concluded that the cam shape and associated flap rotation produce the desired parabolic throat-area variation.

The capability of the Travelling-Wave Horn for generating both different amplitude and duration simulated sonic booms having a good N-shaped signature is aptly demonstrated by the measured overpressure signatures shown in Figs. 24, 25 and 26. These N-shaped signatures are quite representative of those of actual sonic booms.

The measured signatures also show that low-amplitude and short-duration booms are virtually free of jet noise, and significant jet noise only occurs superposed on infrequently used booms having a high amplitude and long duration. It is now worthwhile to compare the virtually noise-free signatures of Figs. 24, 25 and 26 for the case of the flap valve to the noisy signatures of Figs. 7 and 8 for the other case of a plug valve and pyramidal horn with and without a jet-noise absorber. From this comparison it is quite obvious that the facility modification from a plug valve to a much larger flap valve was more effective in reducing the jet noise than the addition of a jet-noise absorber to the original facility utilizing a plug valve.

Some additional high-frequency noise appears ahead of the front shock of short-duration simulated sonic booms, as can be seen in Fig. 24. Such undesirable precursor noise is due to mechanical banging of mainly clutch parts during the fast clutch engaging process. This noise is of course more severe for higher flywheel and cam-shaft speeds required for short-duration N-waves. Precursor noise is not much of a problem because it is virtually absent from overpressure signatures having a duration greater than about 100 ms (see Figs. 25 and 26).

8

The low-frequency perturbations in the basic N-shaped overpressure signatures shown in Figs. 24, 25 and 26 are not due to a defective reflection eliminator, but result instead from enclosing the large end of the horn and reflection eliminator in the test room (Fig. 9). The simulated sonic boom, on passing out of the horn through the porous piston into the test room, cause low-frequency wave motion in the test room (Helmholtz resonator effect). Such waves subsequently enter the horn through the porous piston and slightly disrupt the flow and pressure conditions in the interior test section, thereby causing undesirable perturbations in the N-shaped signature. To minimize the enclosing effect of the test room, two large test-room doors directly behind the reflection eliminator are opened during normal facility operation.

Before discussing the rise times of the front and rear shocks of the simulated sonic boom it is important to first define the rist time. The rise time is defined herein to be 1.25 times the time for the overpressure to rise from 10 to 90% of its peak value. The peak value should be that of the basic N-shaped signature and thus exclude any spurious peak caused by the jet noise or perturbation caused by the test-room enclosing effect. This rise-time definition gave consistent and meaningful results. The measured rise times for repeated trials were very similar because the 10 and 90% points of the shock profile were well defined in each case and also consistent, as was the rapid overpressure rise between these two points. Note that the 0 and 100% points of the shock profile were not well defined and varied substantially from one test to the next. The rise-time definition gave meaningful results not only because the measured rise times were consistent, but also because the subjective loudness of a shock is mainly a function of the rapid rate of change of overpressure and only weakly dependent on the total overpressure change. Furthermore, in the case of a shock profile which rises asymptotically to its peak value (rear shock of an N-wave), a rise-time definition based on the overpressure change from a minimum (0% point) to a maximum (100% point) would yield an infinite rise time, whereas the definition adopted in this work would give a realistic finite value.

Rise times of the front and rear shocks of simulated sonic booms shown in Figs. 24, 25 and 26 are not all equal or constant, but depend mainly on the valve open-to-close time or N-wave duration and to some extent on reservoir pressure or N-wave amplitude. Neglecting the small effect of reservoir pressure, the rise time of the front shock averages about 6, 8 and 10 ms for a duration of 100, 200 and 300 ms respectively. The average rise time of the rear shock is generally 10 to 25% longer. These rise times of simulated sonic booms are certainly longer than most of those taken from measurements of actual sonic booms. For example, the rise time of the front shock of a sonic boom from the Anglo-French Concorde SST ranges from as low as 0.1 ms to 5 ms and sometimes even longer (Ref. 23), and probably has an average of about 1 ms. On the other hand, the average rise time of 638 sonic booms from military aircraft was found to be 4 to 5 ms (Ref. 24).

The rise time of the simulated sonic boom from the Travelling-Wave Horn is certainly short enough at 6 to 10 ms to facilitate most room-resonance studies and structural-panel response and damage investigations. However, most human-response studies (startle, hearing, heart rate, sleep) and also animal-response tests (cochlea damage) require a sonic boom having a much shorter rise time. Additionally, it is important to control the rise time and be able to vary it from 1 ms or even shorter if possible to 10 ms and longer. Although the complementary UTIAS Loudspeaker-Driven Booth can generate a simulated sonic

boom having a rise time which can be controlled from 1 to 10 ms and even longer, in order to facilitate human and animal-response studies, it was hoped that the UTIAS Travelling-Wave Horn would have a similar capability.

Much thought was originally given to the design of the flap valve to achieve a short rise time on both shocks of the simulated sonic boom, hopefully as short as 1 ms. Furthermore, a simple scheme was contrived to control the rise time, such that it could be varied from 1 to 10 ms or longer as desired. The first central-fairing design, shown schematically in Fig. 27, featured two very thin steel plates. As the valve flaps initially move outwards (Fig. 27a) and break free of the central fairing, the steel plates are simultaneously translated and rotated outwards from their normally retracted position into their outermost location (Fig. 27b). Later, when each flap returns, each associated steel plate is quickly retracted to clear the space for the flap and thus avoid severe flap impact with the plate. In experiments with this first central fairing, short rise times of about 1 ms on the front shock and 2 to 3 ms on the rear shock were achieved, provided that the steel plates moved very quickly into their outermost location and later back into their retracted position. On the other hand, when the plates were not allowed to move and fixed in their retracted state, both rise times were very long at about 15 ms. By simply controlling how quickly the steel plates could be extended or retracted, it was found that the rise time of the front shock could be correspondingly controlled and varied from 1 to 15 ms. Also, the rise time was not strongly affected by the N-wave duration or amplitude. These experiments were very important in that they confirmed the two-fold concept of generating a simulated sonic boom having a short rise time of about 1 ms and controlling the rise time with a special control-fairing mechanism.

Difficulties were, however, encountered with the first control-fairing design (Fig. 27), which unfortunately prohibited its use for normal facility operation. On the return motion of the flaps to the central fairing, the flaps would occasionally strike the steel plates with sufficient impact to cause permanent plate bending. This bending would often cause other valve parts to bind and sometimes fail. Such valve failure occurred as frequently as once for every 20 to 50 simulated sonic booms, and valve repair generally required a few man days of effort. To overcome this problem a second central fairing (Figs. 18 and 19), which was used for all work given in this report, was designed and tested. This second central fairing has never failed because each of the two plates is firstly hinged at the centre to reduce impact forces and secondly thicker to avoid bending failure. However, the penalty of using this second central fairing has been that the rise time of the front and rear shocks of the simulated sonic boom are undesirably long at 6 to 10 ms and longer. The thick, hinged plates of the central fairing unfortunately do not move sufficiently fast or in just the correct manner to produce the rapid starting and stopping flow processes needed to produce short rise times on the front and rear shocks respectively. If simulated sonic booms having a short rise time of less than 6 ms are required for normal facility operation, then modification or possibly new design of the central fairing and valve flaps is necessary.

4. ANALYSIS FOR THE TRAVELLING-WAVE HORN

A combination of gasdynamic and acoustic theory is used to successfully predict the main features of the simulated sonic boom (wave form, amplitude,

duration, rise time). Gasdynamic theory is used first to describe the time-varying conditions of the air in the reservoir (e.g., pressure and temperature) and the mass flow rate of air out of the reservoir through the opening and closing flap valve into the pyramidal horn. Acoustic theory is then employed to describe the resulting wave motion in the horn. Because of certain assumptions made in the gasdynamic analysis, the mass-flow rate of air out of the reservoir can be determined without solving for the wave motion in the horn, and it thus serves as a convenient boundary condition for the separate acoustic analysis. Although this type of analysis for a travelling-wave horn is based on work given originally in Refs. 6 and 7 and much more completely in Ref. 10, the present analysis features not only a new interesting method of solution but also new results.

4.1 Gasdynamic Analysis of the Reservoir

The air reservoir of the Travelling-Wave Horn has a finite volume (10.2 m^3). Consequently the properties of the reservoir air are not fixed with time but vary continuously as the air discharges out through the flap valve and generates the simulated sonic boom in the pyramidal horn. In order to predict the reservoir conditions, assume that the state properties are spatially uniform and all changes with time are adiabatic and reversible. Then the following isentropic expressions can be used to relate the time-dependent reservoir temperature $T_o(t)$, sound speed $a_o(t)$, pressure $p_o(t)$ and density $\rho_o(t)$ to their initial fixed values which are denoted by an overhead bar.

$$\frac{T_o(t)}{\bar{T}_o} = \left[\frac{a_o(t)}{\bar{a}_o} \right]^2 = \left[\frac{p_o(t)}{\bar{p}_o} \right]^{\frac{\gamma-1}{\gamma}} = \left[\frac{\rho_o(t)}{\bar{\rho}_o} \right]^{\gamma-1} \tag{2}$$

The symbol γ denotes the ratio of the specific heat at constant pressure (C_p) to that at constant volume (C_v). Now assume that the air flow from the reservoir through the flap valve, which is essentially a convergent-divergent duct flow with a slowly varying throat area, is not only adiabatic and reversible but also one-dimensional and quasisteady. Isentropic expressions given below then relate the time-dependent properties of the reservoir air to those at the valve throat (denoted by the subsciprt *) and also to the flow Mach number $M_*(t)$.

$$\frac{T_o(t)}{T_*(t)} = \left[\frac{a_o(t)}{a_*(t)} \right]^2 = \left[\frac{P_o(t)}{P_*(t)} \right]^{\frac{\gamma-1}{\gamma}} = \left[\frac{\rho_o(t)}{\rho_*(t)} \right]^{\gamma-1} = 1 + \frac{\gamma-1}{2} M_*^2(t) \tag{3}$$

The following equation for the mass-flow rate of air per unit area at the valve throat $m_*(t)$ can be expressed as a function of the Mach number $M_*(t)$, which is simply the ratio of the flow speed $u_*(t)$ and sound speed $a_*(t)$.

$$m_*(t) - \rho_*(t) \, a_*(t) \, M_*(t) \tag{4}$$

If the flow-area variation $A_*(t)$ at the valve throat is expressed as $\bar{A}_* N_*(t)$, where $\bar{A}_*$ is the maximum throat area and $N_*(t)$ describes the area variation,

11

then the mass flow rate is $m_*(t)\,\bar{A}_*N_*(t)$ or $\rho_*(t)\,a_*(t)\,M_*(t)\,\bar{A}_*N_*(t)$. For this mass flow rate of air out of the reservoir having a volume V, the resulting rate of decrease of reservoir-air mass is simply $V\rho_o'(t)$, where the prime denotes differentiation with respect to time. The reservoir density is thus governed by the following differential equation.

$$\rho_o'(t) + \rho_*(t)\,a_*(t)\,M_*(t)\,\bar{A}_*N_*(t)/V = 0 \tag{5}$$

In order to solve this differential equation in conjunction with previous expressions, the equation of state ($p = \rho RT$) and sound-speed expression ($a^2 = \gamma RT$), a boundary condition for the flow at the valve throat is needed.

Consider first the case of choked flow at the valve throat for which $M_*(t)$ does not change with time but equals unity. This is the required boundary condition if the flow is choked. Choked flow can be assumed to persist with time as long as the throat pressure $p_*(t)$ exceeds the ambient pressure in the pyramidal horn, which can be taken to be atmospheric pressure ($\bar{p}$). Or, choked flow occurs when the reservoir to atmospheric pressure ratio $p_o(t)/\bar{p}$ exceeds the reservoir to throat pressure ratio $p_o(t)/p_*(t)$. From Eq. 3 with $M_*(t)$ equal to unity, this critical pressure ratio $p_o(t)/p_*(t)$ is constant and simply equal to $(\gamma+1)/2$ raised to the power of $\gamma/(\gamma-1)$. For the case of air with γ equal to 1.4 the critical pressure ratio is thus 1.892 or the reciprocal of 0.528.

By using Eqs. 2 and 3 and letting $M_*(t)$ equal unity, the differential equation (Eq. 5) can be expressed in terms of only one unknown $T_o(t)$, $a_o(t)$, $p_o(t)$ or $\rho_o(t)$ and integrated explicitly. The simplest procedure is to use the unknown $a_o(t)$ to obtain the following result.

$$\frac{a_o(t)}{\bar{a}_o} = \left[1 + \frac{\gamma-1}{2}\left(\frac{2}{\gamma+1}\right)^{\frac{\gamma+1}{2(\gamma-1)}} \frac{\bar{a}_o\bar{A}_* t_o}{V} \int_0^{t/t_o} N_*(y)\,dy \right]^{-1} \tag{6}$$

Other results for $T_o(t)$, $p_o(t)$ and $\rho_o(t)$ follow from Eq. 2. The mass flow rate per unit area $m_*(t)$, normalized by the product of atmospheric density $\bar{\rho}$ and sound speed $\bar{a}$, can be derived easily from the preceding results, and it is given below.

$$\frac{m_*(t)}{\bar{\rho}\,\bar{a}} = \left(\frac{2}{\gamma+1}\right)^{\frac{\gamma+1}{2(\gamma-1)}} \frac{\bar{P}_o}{\bar{P}} \frac{\bar{a}}{\bar{a}_o}\left(\frac{a_o(t)}{\bar{a}_o}\right)^{\frac{\gamma+1}{\gamma-1}} \tag{7}$$

Note that the nondimensional parameter $\bar{a}_o\bar{A}_* t_o/V$ and the integral of $N_*(t)$ determine how fast the reservoir conditions and mass flow rate per unit area change with time. The changes are rapid and large if $N_*(t)$ is unity and the parameter is large, corresponding to a small air reservoir (V), large valve ($\bar{A}_*$) and a long valve open-to-close time (t_o).

Now consider the other case of unchoked or subsonic flow at the valve throat for which $M_*(t)$ is less than unity and not constant. For this case a reasonable boundary condition for the flow at the valve throat is to take the

static pressure $p_*(t)$ as constant and equal to atmospheric pressure $\bar{p}$. An immediate consequence which follows from Eqs. 2 and 3 is that all other throat conditions such as $T_*(t)$, $a_*(t)$ and $\rho_*(t)$ are also constant. By using this assumption and Eqs. 2 and 3, the previous differential equation for the density (Eq. 5) can now be expressed in terms of only one unknown $M_*(t)$ as shown below.

$$\left[1 + \frac{\gamma - 1}{2} M_*^2(t) \right]^{\frac{2-\gamma}{\gamma-1}} M_*'(t) + \frac{\bar{a}_* \bar{A}_* N_*(t)}{V} = 0 \qquad (8)$$

Once $M_*(t)$ is obtained from a solution to this differential equation the reservoir time-dependent conditions and mass flow rate follow from Eqs. 2, 3 and 4.

Equation 8 can be solved exactly for only certain values of γ (e.g., 5/3, 3/2 and 7/5). For the relevant case of air ($\gamma = 7/5$), the exact solution can be given as follows,

$$x\sqrt{1+x^2}(5+2x) - \bar{x}\sqrt{1+\bar{x}^2}(5+2\bar{x}) + 3\ln(x+\sqrt{1+x^2})$$

$$- 3\ln(\bar{x}+\sqrt{1+\bar{x}^2}) + \frac{8\bar{a}_*\bar{A}_* t_0}{V} \int_0^{t/t_0} N_*(y)\,dy = 0, \qquad (9)$$

where x equals $M_*(t)/\sqrt{5}$ and the initial value $\bar{x}$ is $\bar{M}_*/\sqrt{5}$. The initial flow Mach number $\bar{M}_*$ at time t equal to zero follows from Eq. 3 with $p_*(t)$ replaced by $\bar{p}$ as shown below.

$$\bar{M}_*^2 = \frac{2}{\gamma - 1}\left[\left(\frac{\bar{p}_0}{\bar{p}}\right)^{\frac{\gamma-1}{\gamma}} - 1 \right] \qquad (10)$$

Note that $\bar{a}_*$ in Eq. 9 is the sound speed of the air at the valve throat and not in the reservoir. However, it is related to the initial values of reservoir sound speed and pressure by Eqs. 2 and 3, as shown below.

$$\bar{a}_* = \bar{a}_0 \left(\frac{\bar{p}}{\bar{p}_0}\right)^{\frac{\gamma-1}{2\gamma}} \qquad (11)$$

Now, for a given initial reservoir sound speed $\bar{a}_0$, pressure ratio $\bar{p}_0/\bar{p}$ and volume V, valve open-to-close time or flow duration t_0, and throat-area distribution $\bar{A}_* N_*(t)$, the flow Mach number $M_*(t)$ can be obtained from Eq. 9 by an iterative procedure.

The normalized function $N_*(t)$ for the throat-area variation has thus far been left in a general form such that any actual or idealized form of $N_*(t)$ can be used in the analysis. At this stage, however, it is worthwhile to introduce an ideal "parabolic" form for $N_*(t)$, which is given below.

13

$$N_*(t) = \begin{cases} 0 & t < 0 \\ 4\left(1 - \dfrac{t}{t_o}\right)\dfrac{t}{t_o} & 0 < t < t_o \\ 0 & t_o < t \end{cases} \qquad (12)$$

Hence, the integral in Eq. 9 is given as follows,

$$\int_0^{t/t_o} N_*(y)\,dy = \frac{2}{3}\left[3\left(\frac{t}{t_o}\right)^2 - 2\left(\frac{t}{t_o}\right)^3 \right], \qquad (13)$$

and it has a maximum value of 2/3. It should be noted that in practice the cam shape and resulting valve-flap motion are designed to produce this parabolic throat-area variation (Eq. 12), in order to generate a simulated sonic boom having a duration t_o.

Once $M_*(t)$ has been determined by using Eqs. 9, 10, 11 and 12 or 13 for a fixed initial reservoir pressure $\bar{p}_o$ and sound speed $\bar{a}_o$, the reservoir conditions with time follow from Eqs. 2 and 3. For example, the expression for the reservoir pressure is given below.

$$\frac{p_o(t)}{\bar{p}_o} = \frac{\bar{p}}{\bar{p}_o}\left[1 + \frac{\gamma - 1}{2}M_*^2(t) \right]^{\frac{\gamma}{\gamma-1}} \qquad (14)$$

Furthermore, by using Eq. 3 and previous results, the mass flow rate per unit area $m_*(t)$ can be expressed in the following nondimensional form.

$$\frac{m_*(t)}{\bar{\rho}\,\bar{a}} = \frac{\bar{a}}{a_o}\left[\frac{\bar{p}_o}{\bar{p}} \right]^{\frac{\gamma-1}{2\gamma}} M_*(t) \qquad (15)$$

Although it may not be readily apparent from Eqs. 9, 14 and 15, the nondimensional parameter $a_*\bar{A}_*t_o/V$ in the solution for $M_*(t)$, $p_o(t)$ and $m_*(t)$ determines how fast the reservoir conditions and mass flow rate change with time, like the previous case for choked flow at the valve throat.

In past work with the Travelling-Wave Horn utilizing a plug valve (Ref. 10) the reservoir pressure was most often sufficiently high to produce choked flow ($\bar{p}_o > 1.89\bar{p}$). In some cases, however, the reservoir pressure would decrease sufficiently such that the flow would become unchoked at later times. When the reservoir pressure falls to $1.89\bar{p}$, the new reservoir conditions ($\bar{T}_o$, a_o, $\bar{p}_o$ and $\bar{\rho}_o$) at this time can be determined from the choked-flow solution and then used as input for the unchoked-flow solution. This procedure may be tedious but it is not unduly difficult. In the present work for a large flap valve, however, the reservoir pressure is always sufficiently low ($\bar{p}_o < 1.89\bar{p}$) such that the two cases of choked flow and a combination of choked and unchoked flow are of no concern to this work. Henceforth the work will pertain solely to the case of unchoked flow at the valve throat.

For the case of unchoked flow it is inconvenient in the analysis to obtain $M_*(t)$ iteratively from the exact solution (Eq. 9) for γ equal to 1.4, or

14

numerically from the original differential equation (Eq. 8) for other values of γ. Fortunately, this inconvenience can be circumvented by using an approximate but very accurate explicit expression for $M_*(t)$. This approximate expression imposes no restriction on the value of γ for normal values between 1 and 5/3. To obtain this expression the variable coefficient in Eq. 8, namely $1 + (\gamma-1)M_*^2(t)/2$ raised to the power of $(2-\gamma)/(\gamma-1)$, is first expanded in a binomial series. Such an expansion is valid because $(\gamma-1)M_*^2(t)/2$ is a small parameter less than unity which never exceeds $(\gamma-1)/2$ (e.g., 0.2 for air). Then the differential equation can be integrated easily to give the following result.

$$M_*(t) - \bar{M}_* + \frac{2-\gamma}{6}\left[M_*^3(t) - \bar{M}_*^3\right] + \frac{(2-\gamma)(3-2\gamma)}{40}\left[M_*^5(t) - \bar{M}_*^5\right]$$
$$+ \ldots + \frac{\bar{a}_*\bar{A}_*t_o}{V}\int_0^{t/t_o} N_*(y)dy = 0 \tag{16}$$

Now let an explicit solution for $M_*(t)$ take the following form,

$$M_*(t) = \bar{M}_* \sum_{i=0}^{\infty} a_i \alpha^i I^i(t), \tag{17}$$

$$\alpha = \bar{a}_*\bar{A}_*t_o/V,$$

$$I(t) = \frac{3}{2}\int_0^{t/t_o} N_*(y)dy,$$

which is reasonable provided that $\alpha I(t)$ is a small parameter having an absolute value less than unity. Note that in the present work $I(t)$ never exceeds unity and α typically varies from 0 to 0.2.

When Eq. 17 for $M_*(t)$ is substituted into Eq. 16 and all terms of third order and lower are retained, the following approximate results for $M_*(t)$ can be obtained.

$$\frac{M_*(t)}{\bar{M}_*} = 1 + a_1 \alpha I(t) + a_2 \alpha^2 I^2(t) + a_3 \alpha^3 I^3(t) \tag{18}$$

$$\alpha = \bar{a}_*\bar{A}_*t_o/V, \qquad I(t) = \frac{3}{2}\int_0^{t/t_o} N_*(y)dy$$

$$a_1 = \frac{-4}{3\bar{M}_*[2 + (2-\gamma)\bar{M}_*^2]}$$

$$a_2 = \frac{-16(2 - \gamma)}{9\bar{M}_*[2 + (2 - \gamma)\bar{M}_*^2]^3}$$

$$a_3 = \frac{64(2 - \gamma)[2 - 5(2 - \gamma)\bar{M}_*^2]}{81\bar{M}_*[2 + (2 - \gamma)\bar{M}_*^2]5}$$

This explicit expression for $M_*(t)$ can, of course, be used in Eqs. 14 and 15 to evaluate the reservoir pressure $p_o(t)$ and mass flow rate per unit area $m_*(t)$.

Results of the unchoked-flow analysis are illustrated graphically in Figs. 28 to 33. In each case the throat-area variation with time, $N_*(t)$, was taken to be parabolic (Eqs. 12 and 13). Consider first the results for the flow Mach number $M_*(t)$ given by Eq. 18 and shown in Fig. 28. Three plots for three different but typical values of the nondimensional grouping $\bar{a}_*\bar{A}_*t_o/V$ are shown in this figure. In each plot four different variations of $M_*(t)$ appear, corresponding to four different initial values of the reservoir to atmospheric pressure ratio $\bar{p}_o/\bar{p}$ (or equivalently the Mach number $\bar{M}_*$). From these results it can be seen that $M_*(t)$ changes from its initial value $\bar{M}_*$ more markedly when $\bar{p}_o/\bar{p}$ (or $\bar{M}_*$) is lower and also when the value of $\bar{a}_*\bar{A}_*t_o/V$ is larger (large throat area, long valve open-to-close time, small reservoir volume). It should be noted here that, for normal operation of the Travelling-Wave Horn to generate a simulated sonic boom having an amplitude from 20 to 200 N/m^2 and a duration from 100 to 300 ms, the change in $M_*(t)$ is small (less than 20%) because the reservoir was intentionally designed to have a large volume.

It is worth mentioning that the flow Mach number $M_*(t)$ can diminish to zero if the valve open-to-close time is sufficiently long. One such result is shown for interest in Fig. 28c ($\bar{p}_o/\bar{p} = 1.007$). Once the Mach number diminishes to zero the flow from the reservoir ceases, even though the valve may still be partly open and Eq. 18 predicts a negative Mach number or reverse flow. It should be noted that there is no mechanism in the present quasisteady gasdynamic analysis to predict a reverse flow or flow oscillations like that of a second-order differential equation describing a Helmholtz resonator (spring, mass and damper system).

The mass flow rate per unit area at the valve throat, $m_*(t)$, changes with time like the Mach number $M_*(t)$ shown in Fig. 28, because it is directly proportional to $M_*(t)$ (see Eq. 15). Consequently, these results are not shown graphically. Of more interest, however, is the variation of the mass flow rate $m_*(t)\bar{A}_*N_*(t)$. Although $N_*(t)$ is a parabolic function of time (Eq. 12), the mass flow rate will deviate from this ideal profile because $m_*(t)$ is not constant but varies like $M_*(t)$. The degree of deviation for different values of $\bar{p}_o/\bar{p}$ and $\bar{a}_*\bar{A}_*t_o/V$ can readily be seen in Fig. 29, where the nondimensional mass flow rate $m_*(t)/\bar{\rho}\bar{a}$ is plotted versus time t/t_o and compared directly to the corresponding parabolic profile given by $\bar{m}_*N_*(t)/\bar{\rho}\bar{a}$ [$\bar{m}_*$ is the initial value of $m_*(t)$]. For a small value of $\bar{p}_o/\bar{p}$ and a large value of $\bar{a}_*\bar{A}_*t_o/V$, it can be seen that the mass flow rate deviates more markedly from the ideal parbolic profile.

The variation of the nondimensional pressure $p_o(t)/\bar{p}$, density $\rho_o(t)/\bar{\rho}$ and temperature $T_o(t)/\bar{T}$ with nondimensional time t/t_o, which are each given by a combination of Eqs. 2, 14 and 18, are shown in Figs. 30, 31 and 32 respectively. The marked effects of large values of both $\bar{p}_o/\bar{p}$ and $\bar{a}_*\bar{A}_*t_o/V$ on making the variation large can readily be seen. However, by noting that the ordinate scale

16

has been greatly expanded, it can also be seen that the total relative change in each $p_o(t)/\bar{p}$, $\rho_o(t)/\bar{\rho}$ and $T(t)/\bar{T}$ profile is normally small, even for the largest values of $\bar{p}_o/p$ and $\bar{a}_*\bar{A}_*t_o/V$.

The results for the reservoir pressure, density and temperature shown in Figs. 30, 31 and 32 do not bring out certain information pertinent to the selection of the reservoir volume for a sonic-boom simulator. Since the driving force for the air flow from the reservoir into the horn is not directly due to the absolute reservoir pressure $p_o(t)$ or pressure ratio $p_o(t)/\bar{p}$ but rather to the pressure difference $p_o(t) - \bar{p}$, it is important that this pressure difference remains essentially constant during the generation of a simulated sonic boom. Results for the nondimensional pressure difference $(p_o(t) - \bar{p})/(\bar{p}_o - \bar{p})$ versus time t/t_o are shown in Fig. 33. They exhibit the same temporal variation and dependence on $\bar{a}_*\bar{A}_*t_o/V$ as the previous results for $p_o(t)/\bar{p}$ (Fig. 30) but an opposite dependence on $\bar{p}_o/\bar{p}$. The change in $(p_o(t) - \bar{p})/(\bar{p}_o - \bar{p})$ with time is larger for smaller values of $\bar{p}_o/\bar{p}$. Consequently, the reservoir volume for a facility must be sufficiently large or $\bar{a}_*\bar{A}_*t_o/V$ sufficiently small such that $(p_o(t) - \bar{p})/(\bar{p}_o - \bar{p})$ varies insignificantly for the lowest value of the reservoir pressure $\bar{p}_o$ which one expects to use.

4.2 Acoustic Analysis of the Simulated Sonic Boom

The sound or simulated sonic boom in the pyramidal horn is generated by the influx of air at the horn apex. The well-known spherical wave equation which is given below is employed to describe the wave motion in the horn (Ref. 25).

$$\frac{\partial^2(r\phi)}{\partial t^2} = \bar{a}^2 \frac{\partial^2(r\phi)}{\partial r^2} \tag{19}$$

The respective symbols ϕ and r denote the velocity potential and the radial distance measured from the horn apex. Because only an outward moving wave is generated by the air entering the horn and the reflection of this wave at the large end is neglected or considered eliminated by the reflection eliminator, the general solution of the wave equation can be expressed in the following simple form.

$$\phi = f(\tau)/r \tag{20}$$

$$\tau = t - (r - r_o)/\bar{a}$$

The symbol r_o denotes the radial distance (1.58 m) at which the flap valve is attached to the pyramidal horn, and τ is a retarded time having an initial value of zero at the wave front.

The overpressure Δp and particle velocity Δu of the wave in the horn are related to the velocity potential ϕ, and also to the general function $f(\tau)$ which describes the wave signature, as illustrated below.

$$\Delta p = -\bar{\rho}\frac{\partial\phi}{\partial t} = -\frac{\bar{\rho}}{r}f'(\tau) \tag{21}$$

17

$$\Delta u = \frac{\partial \phi}{\partial r} = -\frac{1}{\bar{a}\,r}\,f'(\tau) - \frac{1}{r^2}\,f(\tau) \tag{22}$$

The prime denotes differentiation of the variable with respect to the argument given in the following brackets. It is worth noting that the overpressure is directly proportional to the derivative of $f(\tau)$ and decays with distance like $1/r$. The particle velocity, however, is essentially directly proportional to $f(\tau)$ at small radii or in the so-called near-field and diminishes like $1/r^2$, whereas at large radii or in the far-field it is directly proportional to $f'(\tau)$ and decays like $1/r$. Hence, the overpressure and particle-velocity signatures have the same shape only in the far-field.

In order to determine the function $f(\tau)$ and thus the overpressure and particle velocity of the wave in the horn, the mass flow rate at the valve throat from the gasdynamic analysis, $m_*(t)\bar{A}_* N_*(t)$, is used as the boundary condition for the acoustic analysis. Firstly, it is assumed that the flow is quasisteady from the valve throat to the downstream location where the flap valve is joined to the horn. This location is at a radial distance r_o, and the corresponding area is denoted by $\bar{A}_o$. The mass flow rate at this location is $m_o(t)\bar{A}_o$ or $\bar{\rho}A_o\Delta u$ to first order. Then, this mass flow rate can be equated to $m_*(t)\bar{A}_* N_*(\tau)$ from the gasdynamic analysis, and Δu can be eliminated from the resulting expression by using Eq. 22, to give the following first-order, linear differential equation for $f(\tau)$.

$$f'(\tau) + \frac{\bar{a}}{r_o}\,f(\tau) = -\frac{\bar{a}r_o}{\bar{\rho}}\,\frac{\bar{A}_*}{\bar{A}_o}\,m_*(\tau)N_*(\tau) \tag{23}$$

When the mass flow rate $m_*(\tau)\bar{A}_* N_*(\tau)$ is zero before time τ equal to zero, the function $f(\tau)$ and its derivatives are all equal to zero. For a mass flow rate starting at τ equal to zero and ending at τ equal to τ_o, the solutions for $f(\tau)$ and $f'(\tau)$ during this time interval can be obtained easily from Eq. 23, and they are given below.

$$f(\tau) = -\frac{\bar{a}r_o}{\bar{\rho}}\,\frac{\bar{A}_*}{\bar{A}_o}\,\exp\left(-\frac{\bar{a}\tau}{r_o}\right)\int_0^\tau m_*(y)N_*(y)\exp\left(\frac{\bar{a}y}{r_o}\right) dy \tag{24}$$

$$f'(\tau) = -\frac{\bar{a}r_o}{\bar{\rho}}\,\frac{\bar{A}_*}{\bar{A}_o}\,\exp\left(-\frac{\bar{a}\tau}{r_o}\right)\int_0^\tau [m_*(y)N_*'(y) + m_*'(y)N_*(y)]\exp\left(\frac{\bar{a}y}{r_o}\right) dy \tag{25}$$

When the mass flow rate is zero at times greater than τ_o, the following solutions for $f(\tau)$ and $f'(\tau)$ can be obtained.

$$f(\tau) = f(\tau_o)\exp\left[-\frac{\bar{a}}{r_o}(\tau - \tau_o)\right] \tag{26}$$

$$f'(\tau) = f'(\tau_o)\exp\left[-\frac{\bar{a}}{r_o}(\tau - \tau_o)\right] \tag{27}$$

18

Now that the results for $f(\tau)$ and $f'(\tau)$ are available, Eqs. 21 and 22 for the overpressure and particle velocity can be expressed as shown below.

$$
\Delta p(\tau) = \begin{cases} 0 & \text{if } \tau < 0 \\[2mm] \dfrac{\bar{a}r_o}{r}\dfrac{\bar{A}_*}{\bar{A}_o}\exp\left(-\dfrac{\bar{a}\tau}{r_o}\right)\displaystyle\int_0^\tau [m_*(y)N_*'(y) \\[2mm] \qquad + m_*'(y)N_*(y)]\exp\left(\dfrac{\bar{a}y}{r_o}\right)dy & \text{if } 0 < \tau < \tau_o \\[4mm] \Delta p(\tau_o)\exp\left[-\dfrac{\bar{a}}{r_o}(\tau - \tau_o)\right] & \text{if } \tau > \tau_o \end{cases}
$$

(28)

$$
\Delta u(\tau) = \begin{cases} 0 & \text{if } \tau < 0 \\[2mm] \dfrac{r_o}{\bar{\rho}r}\dfrac{\bar{A}_*}{\bar{A}_o}\exp\left(-\dfrac{\bar{a}\tau}{r_o}\right)\displaystyle\int_0^\tau [m_*(y)N_*'(y) + m_*'(y)N_*(y) \\[2mm] \qquad + \dfrac{\bar{a}}{r}m_*(y)N_*(y)]\exp\left(\dfrac{\bar{a}y}{r_o}\right)dy & \text{if } 0 < \tau < \tau_o \\[4mm] \Delta u(\tau_o)\exp\left[-\dfrac{\bar{a}}{r_o}(\tau - \tau_o)\right] & \text{if } \tau > \tau_o \end{cases}
$$

(29)

These results complete the general solution for the wave motion in the pyramidal horn, for any specified time distributions of the mass flow rate per unit area $m_*(\tau)$ and throat area $N_*(\tau)$. In most cases the integrations would have to be done numerically to obtain final results for the overpressure and particle-velocity signatures.

Let the mass flow rate per unit area be given by the gasdynamic analysis (Eqs. 15 and 18), and also let the throat-area variation be parabolic (Eq. 12). After these expressions are substituted into Eqs. 28 and 29, the integrals can be evaluated analytically. The integration procedure is not unduly difficult, but it is a rather long and tedious process. The final results for the overpressure signature are summarized below, in a simple and convenient form.

19

$$\Delta p(T) = 0 \qquad \text{if } T < 0$$

$$\Delta p(T) = \overline{\Delta p}[\{1 - 2T + 2\beta - (1 + 2\beta)\exp(-T/\beta)\}$$

$$+ a_1\epsilon\{10T^4 - 20T^3 + 9T^2\}$$

$$+ a_1\epsilon\beta\{-40T^3 + 60T^2 - 18T\}$$

$$+ a_2\epsilon^2\{-32T^7 + 112T^6 - 126T^5 + 45T^4\}$$

$$+ a_1\epsilon\beta^2\{120T^2 - 120T + 18(1 - \exp(-T/\beta))\}$$

$$+ a_2\epsilon^2\beta\{224T^6 - 672T^5 + 630T^4 - 180T^3\}$$

$$+ a_3\epsilon^3\{88T^{10} - 440T^9 + 810T^8 - 648T^7$$

$$+ 189T^6\}] \qquad \text{if } 0 < T < 1 \qquad (30)$$

$$\Delta p(T) = \Delta p(1)\exp[-(T - 1)/\beta] \qquad \text{if } T > 1$$

$$\overline{\Delta p} = \frac{4r_o^2 \bar{m}_*}{r\tau_o}\frac{\bar{A}_*}{\bar{A}_o}, \qquad T = \frac{\tau}{\tau_o}$$

$$\beta = \frac{r_o}{\bar{a}\tau_o}, \qquad \epsilon = \frac{\bar{a}_*\bar{A}_*\tau_o}{V}$$

In the above results the coefficients a_1, a_2 and a_3 are not new but have been given previously in Eq. 18, and $\overline{\Delta p}$ is a characteristic amplitude of the overpressure signature. Note that both parameters β and ϵ are typically small compared to unity, and that the expression for the overpressure signature is thus accurate to third order.

The characteristic amplitude $\overline{\Delta p}$ in Eq. 30 can be expressed in an alternate and more convenient form. Firstly, $\bar{A}_*/\bar{A}_o$ can be replaced by r_*^2/r_o^2, where r_* is an equivalent radius corresponding to the maximum throat area $\bar{A}_*$. For example, if $\bar{A}_*$ is 156 cm^2 for the Travelling-Wave Horn, then r_* equals 1.0 m by using Eq. 1. Secondly, the initial mass flow rate per unit area $\bar{m}_*$ or $m_*(\tau = 0)$ can be eliminated by using Eq. 15, and the initial Mach number $\bar{M}_*$ in the resulting expression can be removed by using Eq. 10. Finally, after some rearrangement, the desired expression for $\overline{\Delta p}$ is given below.

20

$$\overline{\Delta p} = 4\gamma\bar{p}\,\frac{r_*}{r}\,\frac{r_*}{\bar{a}_o\tau_o}\left[\frac{2}{\gamma-1}\left(\frac{\bar{p}_o}{\bar{p}}\right)^{\frac{\gamma-1}{\gamma}}\left\{\left(\frac{\bar{p}_o}{\bar{p}}\right)^{\frac{\gamma-1}{\gamma}}-1\right\}\right]^{1/2} \tag{31}$$

Hence, this result is expressed in terms of the initial reservoir pressure $\bar{p}_o$ and sound speed $\bar{a}_o$, atmospheric pressure $\bar{p}$, flow or N-wave duration τ_o and equivalent radius r_*.

The expression for the particle-velocity signature can be derived in a manner similar to that used to obtain the expression for the overpressure signature. However, now that the results for the overpressure are known, it is much simpler to use these known results in the following equation to obtain the expression for the particle-velocity signature.

$$\Delta u(T) = \frac{\Delta p(T)}{\bar{\rho}\,\bar{a}} + \frac{\tau_o}{\bar{\rho}\,r}\int_0^T \Delta p(y)\,dy \tag{32}$$

Because the integration in this equation can be done rather easily to obtain the final results for the particle velocity, these quite lengthy results are not presented. Note that Eq. 32, which conveniently expresses the particle velocity in terms of the overpressure, can be obtained directly from Eqs. 21 and 22.

In order to illustrate some interesting and important features of the overpressure and particle-velocity signatures, consider the following simplified case. Let ϵ or $\bar{a}_*\bar{A}_*\tau_o/V$ be zero, which corresponds to the case of a reservoir having an infinite volume. Hence, the reservoir conditions such as the pressure and temperature are constant during the generation of a simulated sonic boom. Also, let β or $r_o/\bar{a}\tau_o$ be zero. This corresponds to the case of a point source (Ref. 10) or the reservoir air entering the horn at its apex ($r_o = 0$). Then, the resulting simple expressions from Eqs. 30, 31 and 32 for the overpressure and particle-velocity signatures are given below.

$$\Delta p = \begin{cases} \overline{\Delta p}(1 - 2T) & \text{if } 0 < T < 1 \\ 0 & \text{if } T < 0 \text{ or } T > 1 \end{cases} \tag{33}$$

$$\Delta u = \begin{cases} \dfrac{\overline{\Delta p}}{\bar{\rho}\,\bar{a}}\left[1 - 2T + \dfrac{\bar{a}\tau_o}{r}(T - T^2)\right] & \text{if } 0 < T < 1 \\ 0 & \text{if } T < 0 \text{ or } T > 1 \end{cases} \tag{34}$$

A number of important observations can be made from these simple results.

21

The wave or simulated sonic boom that propagates from the small to the large end of the pyramidal horn has a predicted N-shaped signature (Eq. (33)), which is illustrated graphically in Fig. 34a. Remember that the throat-area variation was taken to be parabolic for this prediction. The two shocks in the signature have an instantaneous or zero rise time and an identical amplitude $\overline{\Delta p}$ (Eq. 31). This amplitude increases with increasing reservoir-pressure ratio $\overline{p}_0/\overline{p}$, and it is inversely proportional to both the flow or N-wave duration τ_0 and radius r_0. Hence, the overpressure profile is invariant with distance but the overpressure diminishes like $1/r$.

Although the particle-velocity signature also exhibits two shocks of equal amplitude $(\overline{\Delta p}/\rho \ \overline{a})$ and instantaneous rise time, it is not necessarily N shaped or invariant with distance (see Eq. 34). Velocity signatures for different fixed radii are shown in Fig. 34b. All of these signatures, characterized by different values of the parameter $\overline{a}\tau_0/r$, have been normalized and given on the same diagram to illustrate the change in wave form from an almost parabolic shape in the near-field to an N-shaped profile in the far-field. Often it is convenient to use the inverse parameter $r/\overline{a}\tau_0$ to identify a velocity profile at a relatively large radius. Because $\overline{a}\tau_0$ equals the wave length λ_0, the inverse parameter $r/\overline{a}\tau_0$ or r/λ_0 is a direct measure of how many wavelengths the wave is from its source.

The interior test section of the UTIAS Travelling-Wave Horn is not located in the far-field but rather in the so-called mid-field, as the radial distance to this section (20 to 25 m) is only a fraction of a wave length. For example, the values of r/λ_0 are equal to 0.45, 0.30 and 0.15 for simulated sonic booms having different durations of 100, 200 and 300 ms respectively. Consequently the particle-velocity profile as predicted at the interior test section is not N shaped, although the signature is not too different than the N shape. Because the signature has a convex curvature between the two shocks the positive velocity portion has a greater duration than the negative velocity portion. These results can be interpreted from the velocity profiles given in Fig. 34b, by noting that $\overline{a}\tau_0/r$ equals 2, 3 and 6 for the respective durations of 100, 200 and 300 ms. These particular profiles are not shown for clarity.

More interesting and important features of the overpressure signature can be illustrated by letting β or $r_0/\overline{a}\tau_0$ be zero as for the previous case but now letting ϵ or $\overline{a}_*\overline{A}_*\tau_0/V$ be nonzero. Since the parameter $\overline{a}_*\overline{A}_*\tau_0/V$ is a function of the reservoir volume (V), N-wave duration (τ_0) and flap-valve throat area $(\overline{A}_*)$, their influence on the overpressure signature can be jointly evaluated. The required expression for the overpressure can be obtained from Eq. 30, and it is given below.

$$\Delta p = 0 \quad \text{if} \quad T < 0 \quad \text{or} \quad T > 1$$

$$\Delta p = \overline{\Delta p}[1 - 2T + a_1\epsilon\{10T^4 - 20T^3 + 9T^2\}$$

$$+ a_2\epsilon^2\{-32T^7 + 112T^6 - 126T^5 + 45T^4\} \tag{35}$$

$$+ a_3\epsilon^3\{88T^{10} - 440T^9 + 810T^8 - 648T^7$$

$$+ 189T^6\}] \quad \text{if} \quad 0 < T < 1$$

Three sets of graphical illustrations of pressure profiles for different typical values of ϵ or $\bar{a}_*\bar{A}_*\tau_0/V$ of 0.05, 0.10 and 0.15 are given in Fig. 35. In each set of results the dependence of the profile on the initial reservoir pressure ratio $\bar{p}_0/\bar{p}$ is illustrated. It can be seen that the distortion of the overpressure signature from the ideal N shape becomes worse with increasing values of $\bar{a}_*\bar{A}_*\tau_0/V$ and diminishing values of $\bar{p}_0/\bar{p}$. These results illustrate that, if a long-duration simulated sonic boom having a good N-shaped signature is to be generated with a Travelling-Wave Horn utilizing a large value, then the reservoir volume (V) must be sufficiently large to offset large values of the throat area ($\bar{A}_*$) and duration (τ_0). The parameter $\bar{a}_*\bar{A}_*\tau_0/V$ should therefore have a value which is less than about 0.1.

The results shown in Fig. 35 have been rearranged and given again in Fig. 36. The three sets of results correspond to different values of the reservoir pressure ratio $\bar{p}_0/\bar{p}$ of 1.007, 1.015 and 1.89. In each set the effects of different values of $\bar{a}_*A_*\tau_0/V$ of 0, 0.05, 0.10 and 0.15 on the signature are shown.

Further interesting and important features of the overpressure signature can be illustrated by letting β or $r_0/\bar{a}\tau_0$ be nonzero and ϵ or $\bar{a}_*\bar{A}_*\tau_0/V$ be zero (infinite reservoir volume). For this case the following expression for the overpressure can be obtained from Eq. 30.

$$\Delta p = 0 \quad \text{if} \quad T < 0$$

$$\Delta p = \overline{\Delta p}[1 - 2T + 2\beta - (1 + 2\beta)\exp(-T/\beta)] \quad \text{if} \quad 0 < T < 1 \qquad (36)$$

$$\Delta p = \overline{\Delta p}[-1 + 2\beta - (1 - 2\beta)\exp(-1/\beta)\exp -(T - 1)/\beta] \quad \text{if} \quad T > 1$$

Based on these results the effects of a nonzero value of β or $r_0/\bar{a}\tau_0$ on the N-shaped overpressure profile can be assessed, and these effects are conveniently illustrated graphically in Fig. 37. The essential result of a nonzero value of $r_0/\bar{a}\tau_0$ is that the front and rear shocks of the profile both have a finite rise time. It can be seen that the two rise times become longer relative to the N-wave duration as the value of $r_0/\bar{a}\tau_0$ increases. Actually the rise time is nearly constant, but it appears more conspicuously on shorter duration N-waves for which the value of $r_0/\bar{a}\tau_0$ is larger. Note that an instantaneous rise time would occur only when the value of $r_0/\bar{a}\tau_0$ or r_0 is zero. (The radius r_0 is the location at which the mass-flow valve is joined to the pyramidal horn.)

The peak overpressure of the front shock of an N-wave having a finite rise time is always less than that having an instantaneous rise time, and this difference becomes more marked for a shorter duration N-wave. This feature is also illustrated by the three overpressure signatures shown in Fig. 37. Quantitatively, the maximum overpressure of the front shock Δp_m and the corresponding rise time $\Delta\tau_m$ from zero to the maximum overpressure can be derived easily from Eq. 36, and these two results are given below.

$$\Delta p_m = \overline{\Delta p}\left[1 - \frac{2r_0}{\bar{a}\tau_0}\ln\left(\frac{\bar{a}\tau_0}{2r_0} + 1\right)\right]$$

$$\Delta\tau_m = \frac{r_0}{\bar{a}}\ln\left(\frac{\bar{a}\tau_0}{2r_0} + 1\right)$$

(37)

23

These results demonstrate that the rise time $\Delta\tau_m$ increases and the peak overpressure Δp_m diminishes as the N-wave duration τ_0 increases.

Previously, in Chapter 3, the rise time of a shock was defined to be equal to 1.25 times the time for the overpressure to rise from 10% to 90% of its peak value. By using Eq. 36, the respective times τ_{10} and τ_{90} for the overpressure of the front shock to rise from zero to 10% and 90% of the peak value are given by the following approximate expressions.

$$\tau_{10} \approx 0.1 \frac{r_0}{\bar{a}} \left[1 - 2\beta \ln\left(\frac{1 + 2\beta}{2\beta} \right) \right]$$

(38)

$$\tau_{90} \approx \frac{r_0}{\bar{a}} \ln\left[\frac{1 + 2\beta}{0.1 + 2\beta + 1.16\beta \ln\left(\frac{1 + 2\beta}{2\beta} \right)} \right]$$

These results are accurate for values of β or $r_0/\bar{a}\tau_0$ ranging from 0 to 0.2, which are more than sufficient for the present work. The rise time $\Delta\tau_r$ or $1.25(\tau_{90} - \tau_{10})$ is therefore given by the following approximate expression.

$$\Delta\tau_r \approx 1.25 \frac{r_0}{\bar{a}} \left[\ln\left\{ \frac{1 + 2\beta}{0.1 + 2\beta + 1.16\beta \ln\left(\frac{1 + 2\beta}{2\beta} \right)} \right\} \right.$$

$$\left. -0.1 + 0.2\beta \ln\left(\frac{1 + 2\beta}{2\beta} \right) \right]$$

(39)

Although the rise time $\Delta\tau_r$ diminishes monotonically with increasing values of β, $\Delta\tau_r$ is essentially constant at 2.75 $r_0/\bar{a}$ for small β values (< 0.005). Furthermore, for β values ranging from 0.01 to 0.05, which are typical for the UTIAS Travelling-Wave Horn, $\Delta\tau_r$ is roughly equal to $2r_0/\bar{a}$. Results such as these can be determined from Eq. 39, or from Fig. 38 where $\Delta\tau_r\bar{a}/r_0$ is plotted versus β or $r_0/\bar{a}\tau_0$. Note that for r_0 and $\bar{a}$ values of 1.58 m and 430 m/s respectively, the predicted rise time is roughly 9 ms.

As a final example of the analytical results for the overpressure signature of a simulated sonic boom, three typical signatures for the UTIAS Travelling-Wave Horn are shown in Fig. 39. It can be seen that the three N-shaped profiles (solid lines) have a nominal peak overpressure of 100 N/m^2 and different durations of 100, 200 and 300 ms. They exhibit finite rise times ($\beta \neq 0$) and distortions from the N shape due to a finite reservoir volume ($\epsilon \neq 0$). These signatures were calculated by using Eq. 30 and typical values of β or $r_0/\bar{a}\tau_0$ and ϵ or $\bar{a}_*\bar{A}_*\tau_0/V$. In each case the corresponding ideal N-wave (dotted line) featuring an instantaneous rise time ($\beta = 0$) and no distortion ($\epsilon = 0$) is shown for completeness and comparison purposes.

4.3 Comparison of Predicted and Measured Results

All of the predicted overpressure signatures which are compared to experimental results in this section have been calculated by using Eqs. 30 and

31. Implicit in the analysis and thus these equations is the assumption that the throat-area variation with time of the flap valve is parabolic, as given by Eq. 12. The maximum throat area $\bar{A}_*$ for the UTIAS Travelling-Wave Horn and the corresponding equivalent radius r_* used in the calculations were 156 cm^2 and 1.0 m respectively, and the radial location r_0 at which the valve is joined to the pyramidal horn was taken to be 1.58 m. Unless noted to the contrary the reservoir volume V was 10.2 m^3. Furthermore, the overpressure signatures were predicted for a radial location r of 21.3 m, corresponding to the interior test section of the horn where the overpressure measurements were made.

Three measured overpressure signatures having the same nominal duration of 100 ms have been traced from the oscillograms in Fig. 24 and reproduced in Fig. 40. Corresponding predicted signatures are also shown in Fig. 40, in order to facilitate their comparison to measured profiles. Two similar sets of measured signatures traced from oscillograms of Figs. 25 and 26 for nominal durations of 200 and 300 ms are reproduced in Figs. 41 and 42 respectively, where the predicted signatures are also given. It can readily be seen in all three sets of results that the predicted and measured signatures are in good agreement. In general the overpressure signatures measured in the UTIAS Travelling-Wave Horn can be predicted successfully by the analysis developed previously in this chapter.

Two additional measured overpressure signatures having a nominal duration of 200 ms are shown in Fig. 43. For this case the reservoir volume of the facility was reduced by one-third from 10.2 to 3.4 m^3. Included in the figure are the corresponding predicted profiles, which are again in good agreement with the measured signatures. Note that both the measured and predicted results differ fairly markedly from the desired N shape for good simulation of a sonic boom, owing to an inadequate reservoir volume. Such results illustrate the importance of having a reservoir with sufficient volume.

5. DISCUSSIONS AND CONCLUSIONS

The UTIAS Travelling-Wave Horn has proven to be a practical facility for the simulation of a full-scale sonic boom. The air compressor and reservoir system, flap valve and electric-drive system (including the flywheel, clutch, cam, three-bar linkage, two flaps and central fairing), pyramidal horn and porous-piston type of reflection eliminator all essentially function correctly as designed. The simulator therefore has the desired capability of producing a good N-shaped overpressure signature or simulated sonic boom in the interior test section of the pyramidal horn. The N-wave amplitude and duration can be controlled individually to be less than, equal to, or more than that of an actual sonic boom. Owing to certain design features of the compressor, reservoir, flap valve and control system, the facility has the desirable capability of producing respectable and repetitive simulated sonic booms (1 to 10 booms per minute), in order to facilitate structural response, fatigue and damage studies. Note that the primary use of the UTIAS Travelling-Wave Horn is to study the effects of simulated sonic booms on structures and their subcomponents. Hence, the generation of repeatable and repetitive N-waves at a high repetition rate is a necessary requirement of the facility.

One disadvantage of the UTIAS Travelling-Wave Horn utilizing the present flap valve is that the rise times of the front and rear shocks of the simulated

sonic boom are longer at 6 to 10 ms than those of an actual sonic boom (typically about 1 ms). Also, the rise times are not easily controlled but are essentially fixed by the valve design and N-wave duration. Since the rise times normally have very little effect on structural response, the major use of the facility for structural response, fatigue and damage studies is not impaired by the present long rise times of 6 to 10 ms, or by not being able to control the rise times. However, human and animal response tests requiring a simulated sonic boom having a short rise time which can also be varied from 0.5 to 10 ms, for example, cannot be done with the present facility. However, with additional developmental costs the rise times could be improved if the need should arise. (Note that such response tests can be done with the complementary UTIAS Loudspeaker-Driven Booth.)

It is worth mentioning that the original flap valve utilized a specially designed central fairing (Fig. 27), which resulted in a short rise time as low as 1 ms for the front shock of the simulated sonic boom. Furthermore, this central fairing had special design features which permitted the rise time to be controlled from 1 to 15 ms. However, because this central fairing suffered frequent mechanical failure, a newer present central fairing (Fig. 18) having good mechanical reliability was designed and used in the flap valve. This new central fairing resulted in the undesirably longer rise times of 6 to 10 ms. Hence, short rise-time capability was sacrificed to obtain a nonfailing mechanical operation. It is believed, however, that such a sacrifice is not necessary. A future modification to the central fairing or a whole new design should result in both good mechanical reliability and a short rise time control of the rise time from 1 to 15 ms, for example, should also be possible.

The Travelling-Wave Horn utilizing a large air reservoir and large-area flap valve produces a simulated sonic boom with very little superposed jet noise. Hence, the main problem of intense jet noise superposed on the N-wave, when the facility used the previous small-area plug valve (Ref. 10), has been virtually solved. By virtue of the large-area flap valve, the mass-flow rate of air required to produce a simulated full-scale sonic boom can be delivered at a very low flow velocity. The low flow velocity at the flap valve is the main reason that insignificant jet noise is produced. It should also be noted here that the use of a large valve results in the use of a low reservoir pressure. However, this advantage is offset because the reservoir has to have a large air-storage capacity, such that the reservoir pressure does not change significantly during the generation of a simulated full-scale sonic boom.

The combined gasdynamic and acoustic analysis successfully describes the wave motion in the pyramidal horn during the generation of a simulated sonic boom. On the one hand the gasdynamic analysis has the capability of predicting the pressure, temperature and other state properties of the expanding reservoir air and also the mass flow rate and flow Mach number of the air passing through the opening and closing flap valve. On the other hand the acoustic analysis is able to predict the overpressure and particle-velocity signatures of the simulated sonic boom in the pyramidal horn, including their main characteristics such as the peak overpressure, duration and rise time. One important result of the analysis is a suitable criterion on how large the reservoir volume must be, in order that the overpressure signature is not significantly distorted from the N shape. For normal operation of the UTIAS Travelling-Wave Horn the nondimensional parameter $\bar{a}_* \bar{A}_* \tau_0 / V$ should be less than 0.05, 0.10 and 0.15 to avoid significant distortion in an N-wave having a duration of 100, 200 and 300 ms, respectively. Note that the respective symbols $\bar{a}_*$, $\bar{A}_*$, τ_0 and V denote sound speed at the valve throat, maximum valve-throat area, N-wave duration and reservoir volume.

26

It is worth mentioning that further analysis dealing with the jet noise and reflection eliminator, and their experimental verification, can be found in Ref. 10.

REFERENCES

1. J. J. Gottlieb — Sonic-Boom Research at UTIAS. CASI Jour., 20(5), May 1974, pp. 199-222.

2. I. R. Schwartz — Sonic Boom Simulation Facilities. Aircraft Engine Noise and Sonic Boom, AGARD, No. 29, May 1969.

3. P. M. Edge
   H. H. Hubbard — Review of Simulation Devices and Techniques. J. Acoust. Soc. Amer. 51, 1972, pp. 722-728.

4. J. J. Gottlieb
   I. I. Glass — Recent Developments in Sonic-Boom Simulation Using Shock Tubes. Can. J. Phys. 52, 1974, pp. 207-218.

5. L. J. Shepherd
   W. W. Sutherland — Relative Annoyance and Loudness Judgements of Various Simulated Sonic Boom Waveforms. NASA CR-1192, 1968.

6. R. Tamboulian — Research and Development of a Sonic Boom Simulation Device. GASL TR No. 713, 1968.

7. R. Tamboulian
   W. Peschke — Description and Capabilities of a Travelling Wave Sonic Boom Simulator. NASA CR-1696, 1970.

8. C. Thery
   A. Peter
   F. Schlosser — Le Générateur de Bang de l'ISL. Institut Franco-Allemand de Recherches de St. Louis, Rapport 15/71, 1971.

9. A. Falkiewicz — Development of a Loudspeaker-Driven Simulator for Sonic Booms and Other Transient Sounds. UTIAS M.A.Sc. Thesis, 1972.

10. J. J. Gottlieb — Simulation of a Travelling Sonic Boom in a Pyramidal Horn. Prog. Aerospace Sci. 17, 1976, pp. 1-66. Also UTIAS Report No. 196, July 1974.

11. N. D. Ellis
    I. B. Rushwald
    H. S. Ribner — Development of a Portable Sonic Boom Simulator for Field Use. UTIAS Technical Note No. 190, 1974.

12. I. I. Glass
    H. S. Ribner
    J. J. Gottlieb — Canadian Sonic Boom Simulation Facilities. CASI Jour. 18(8), 1972, pp. 235-246.

13. R. Carothers — Initial Calibration and Physiological Response Data for the Travelling-Wave Sonic Boom Simulator. UTIAS Technical Note No. 180, 1972.

14. J. J. Gottlieb — Wave Motion in Low-Pressure-Ratio Rectangular and Pyramidal Shock Tubes. UTIAS Report No. 199, 1975.

15. K. W. Lips
An Unstable Steering Task With a Sonic-Boom Disturbance. UTIAS Technical Note No. 179, 1972.

16. H. S. Ribner
P. J. Morris
W. H. Chu
Laboratory Simulation of Development of Superbooms by Atmospheric Turbulence. J. Acoust. Soc. Amer. $\underline{53}$(3), 1973, pp. 926-928.

17. O. V. Nowakiwsky
Effects of Sonic Boom on Automobile-Driver Behaviour. UTIAS Technical Note No. 188, 1974.

18. B. R. Leigh
Lifetime Concept of Plaster Panels Subjected to the Sonic Boom. UTIAS Technical Note No. 191, 1974.

19. B. R. Leigh
R. C. Tennyson
I. I. Glass
Aged Plaster Panels Subjected to Sonic Booms. CASI Jour. $\underline{21}$(9), 1975, pp. 352-360.

20. I. I. Glass
K. W. Lips
O. V. Nowakiwsky
L. D. Reid
Sonic-Boom-Startle Effects during Simulated and Actual Automobile-Driving Tests. CASI Jour. $\underline{22}$(4), 1976, pp. 70-88.

21. S. Reinis
Acute Changes in Animal Inner Ears due to Simulated Sonic Booms. J. Acoust. Soc. Amer. $\underline{60}$(1), 1976, pp. 133-138.

22. N. N. Wahba
Pressure Inside a Room Subjected to Sonic Boom. UTIAS Technical Note No. 207, May 1977.

23. G. Parmentier
G. Mathieu
D. Seydel
A. Peter
Bangs Sonique de Concorde 001 en vol Rectiligne à Vitesse Constante. Institut Franco-Allemand de Recherches de St. Louis, Notice ISL SN 1/70, 1970.

24. A. D. Pierce
D. J. Maglieri
Effects of Atmospheric Irregularities on Sonic Boom Propagation. J. Acoust. Soc. Amer. $\underline{51}$, 1972, pp. 702-721.

25. L. D. Landau
E. M. Lifshitz
Mechanics of Continuous Media. Gostekhizdat, 1944. Translation: Fluid Mechanics, Second Edition, Pergamon Press, Oxford, 1959.
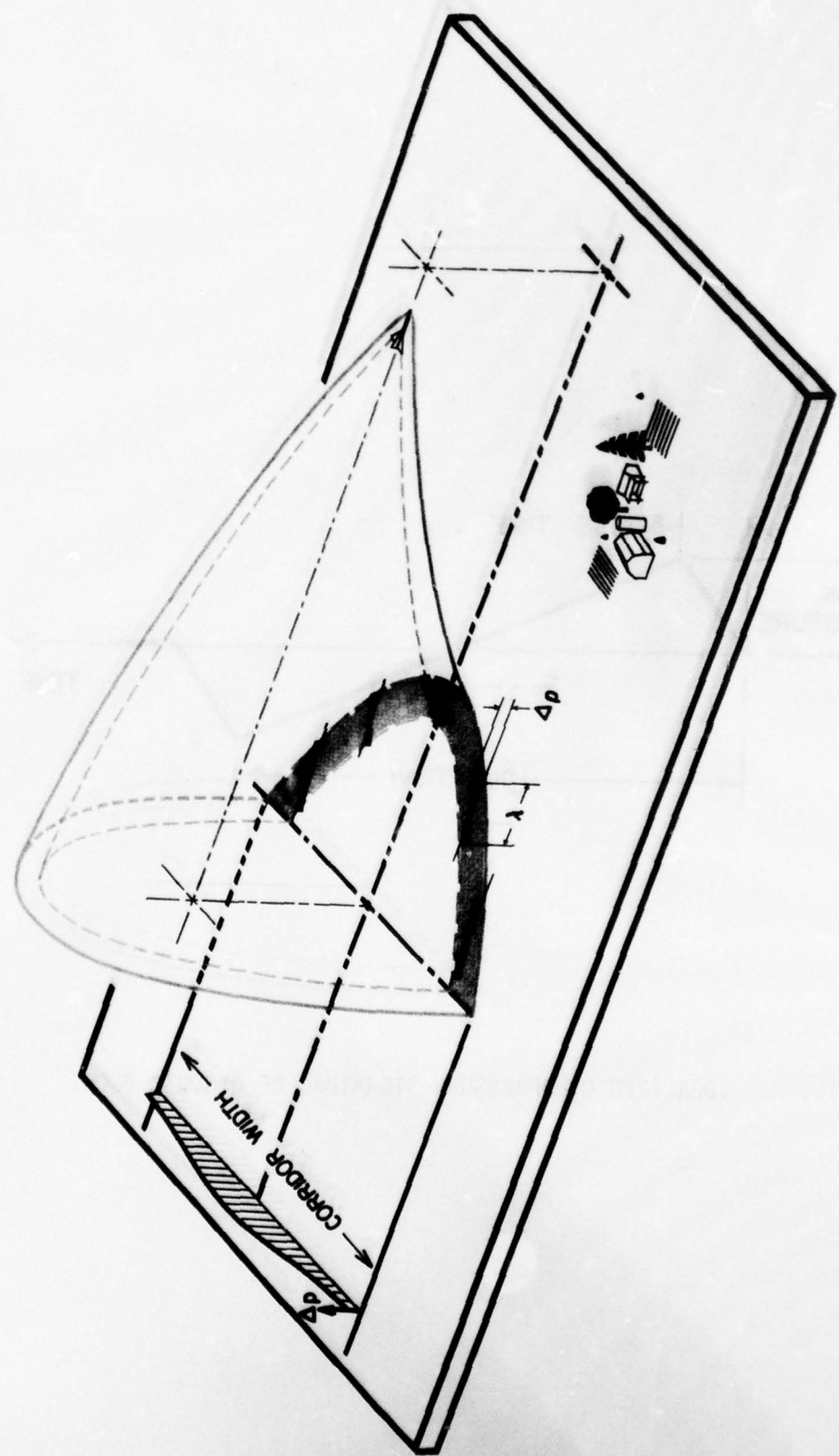
FIG. 1. WAVE PATTERN AND RESULTING OVERPRESSURE FOOTPRINT ON THE GROUND FROM A SUPERSONIC AIRCRAFT.
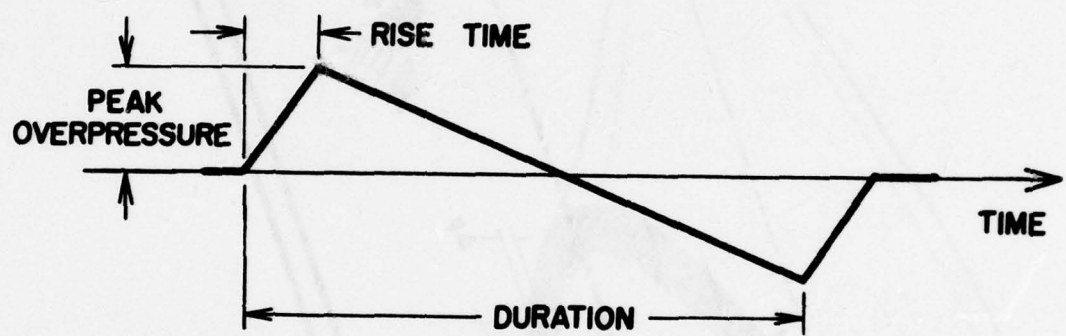
FIG. 2. IDEALIZED OVERPRESSURE SIGNATURE OF A SONIC BOOM.

1.8-m by 3.6-m
CUTOUT

TEST ROOM

PYRAMIDAL HORN

CONTROL ROOM

REFLECTION ELIMINATOR

SONIC-BOOM GENERATOR

0   5 m
SCALE

ELEVATION VIEW

PSYCHOACOUSTIC
TEST ROOM

MAIN BUILDING

PYRAMIDAL HORN

JET-NOISE
ABSORBER

CONTROL ROOM

VALVE

COMPRESSOR

REFLECTION ELIMINATOR

RESERVOIRS

INTERIOR TEST SECTION

0   5 m
SCALE
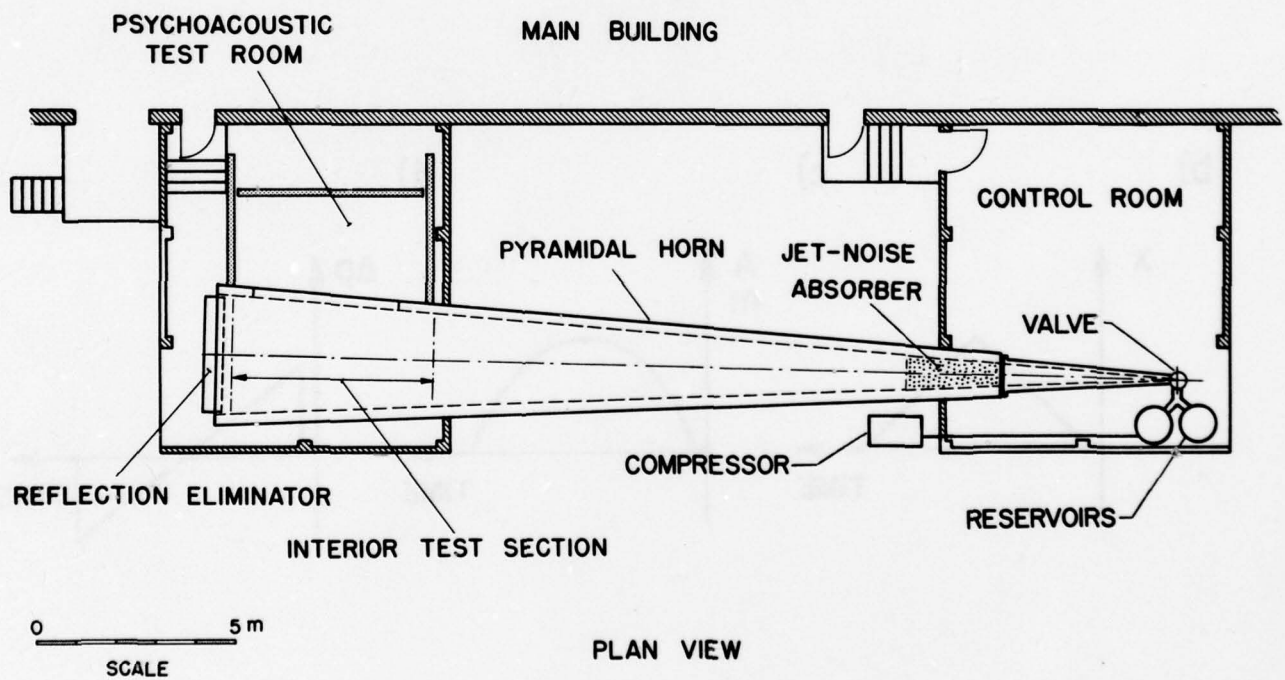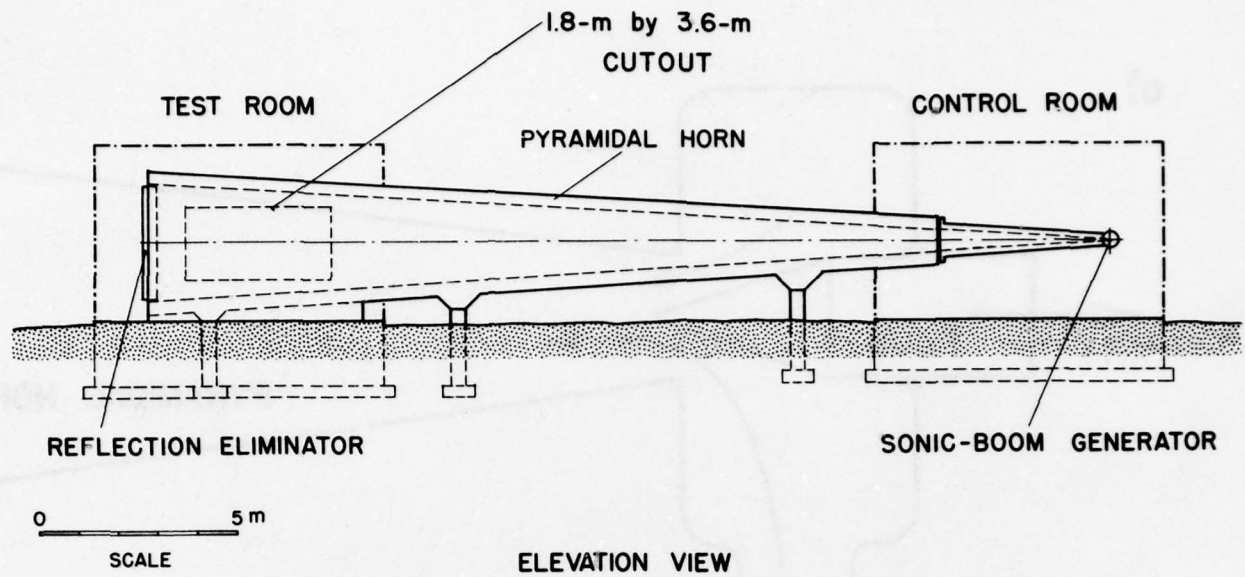
PLAN VIEW

FIG. 3. ELEVATION AND PLAN VIEWS SHOWING MOST OF THE RELEVANT
ELEMENTS OF THE TRAVELLING-WAVE HORN USING A PLUG VALVE.
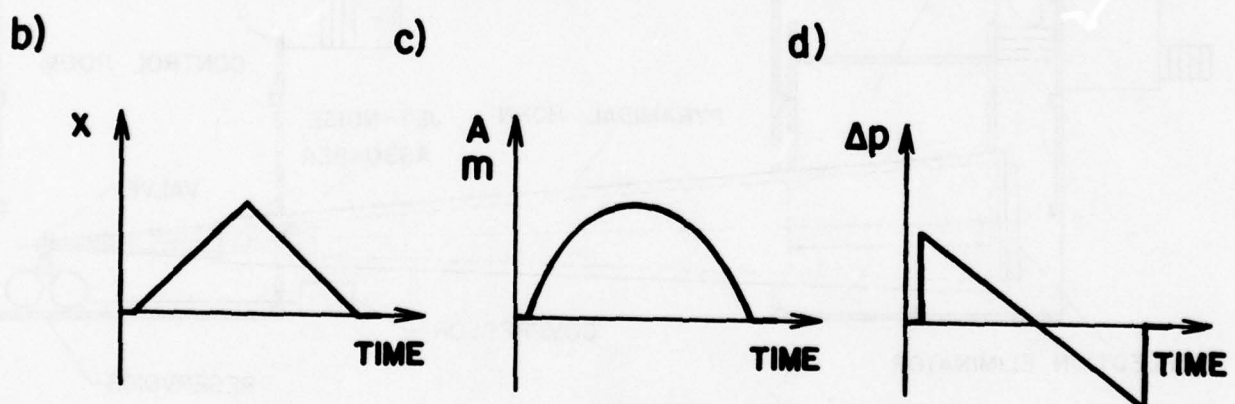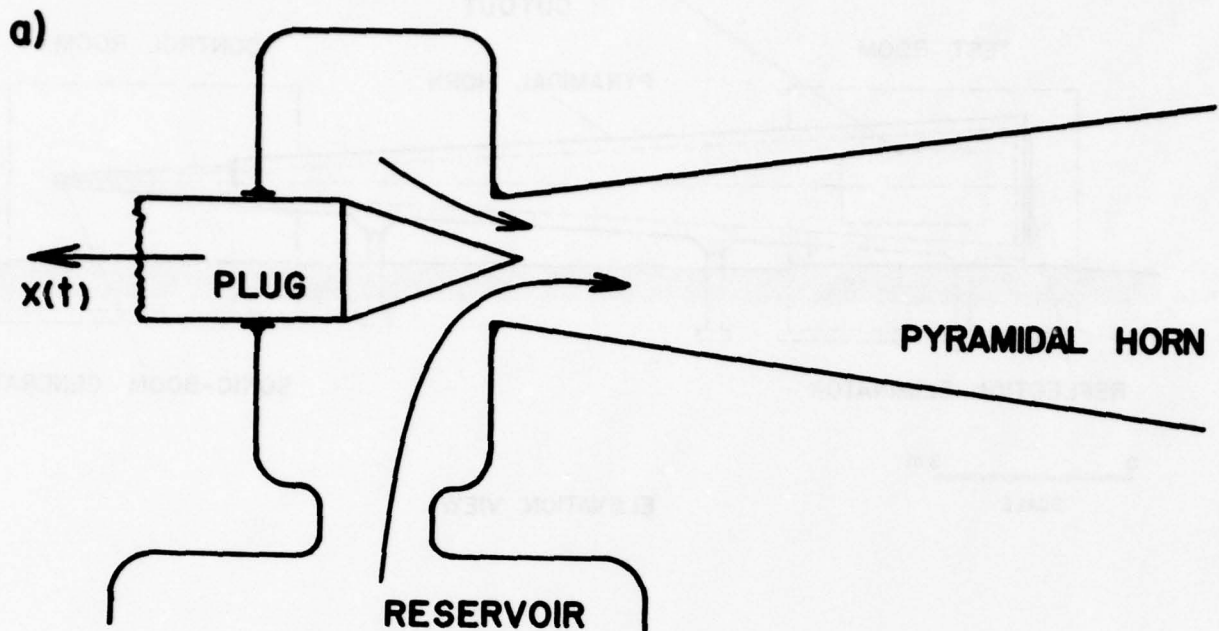
FIG. 4. PLUG VALVE OPERATION: a) VALVE, b) PLUG MOTION, c) THROAT-AREA AND MASS-FLOW-RATE PROFILES, d) OVERPRESSURE SIGNATURE.
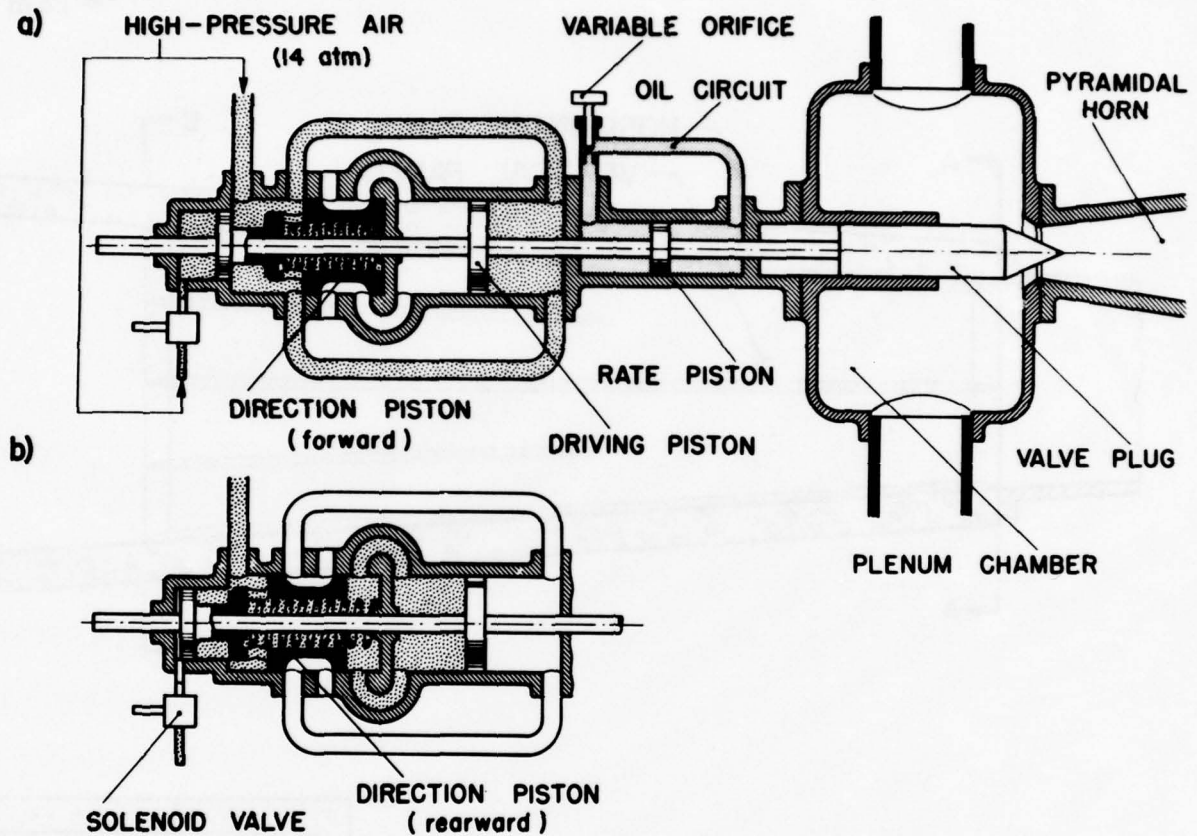
FIG. 5. SIMPLIFIED ASSEMBLY DRAWING OF THE PLUG VALVE EXHIBITING THE OPENING (a) AND CLOSING (b) MOVEMENTS.
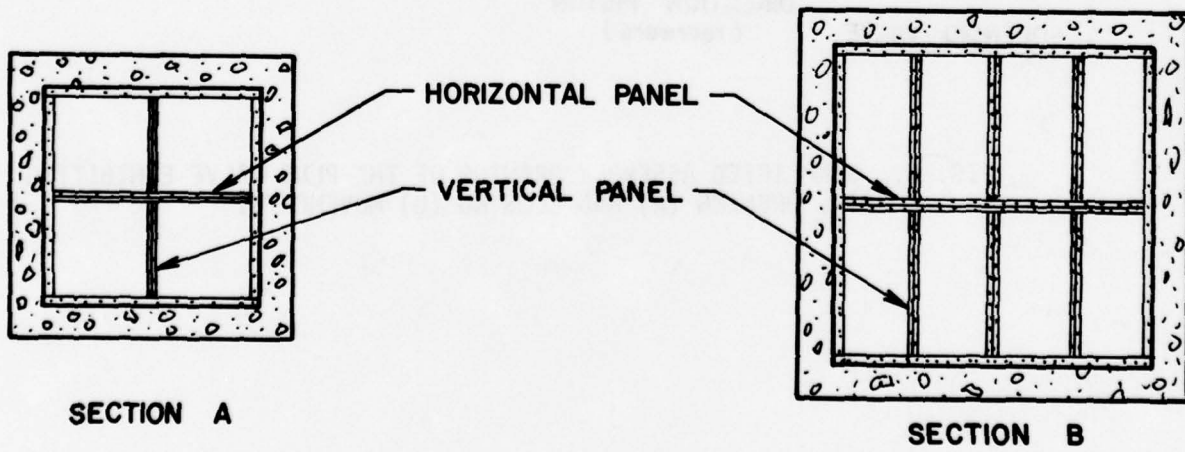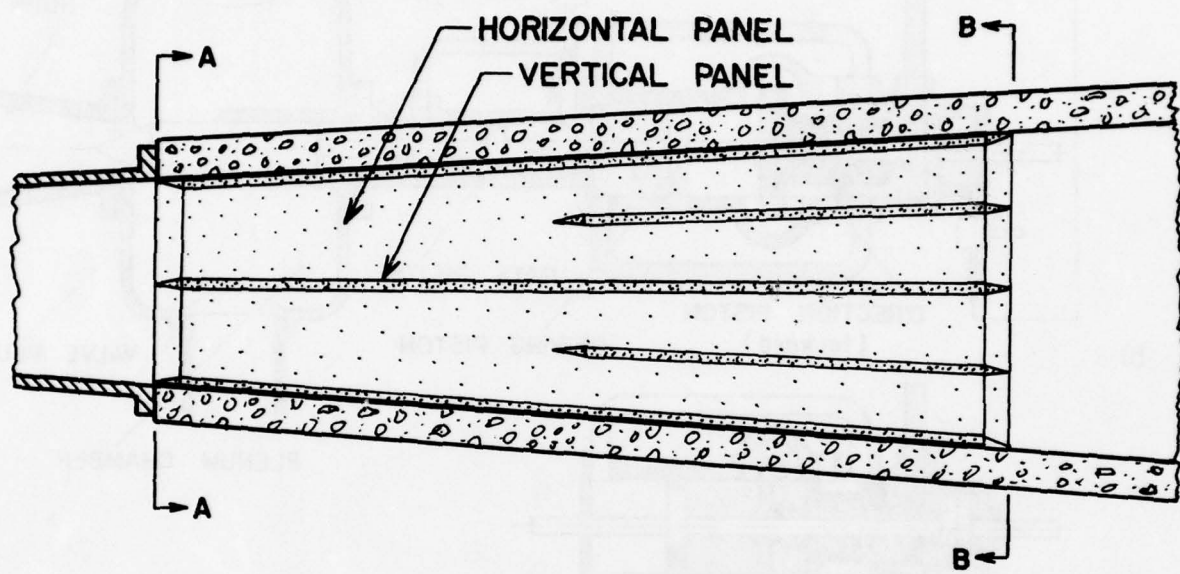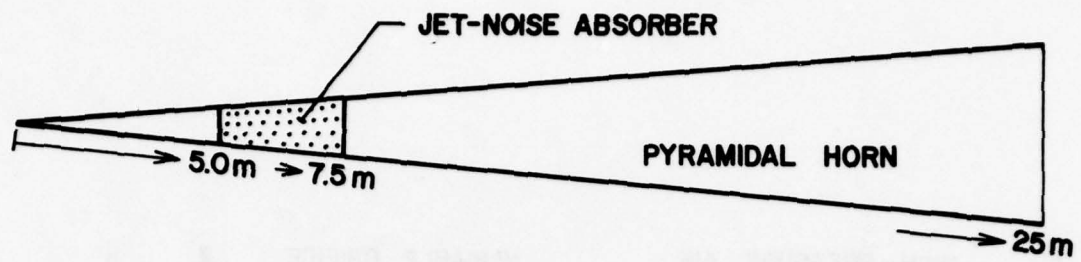
FIG. 6. JET-NOISE ABSORBER FOR THE PLUG-VALVE OPERATING MODE.
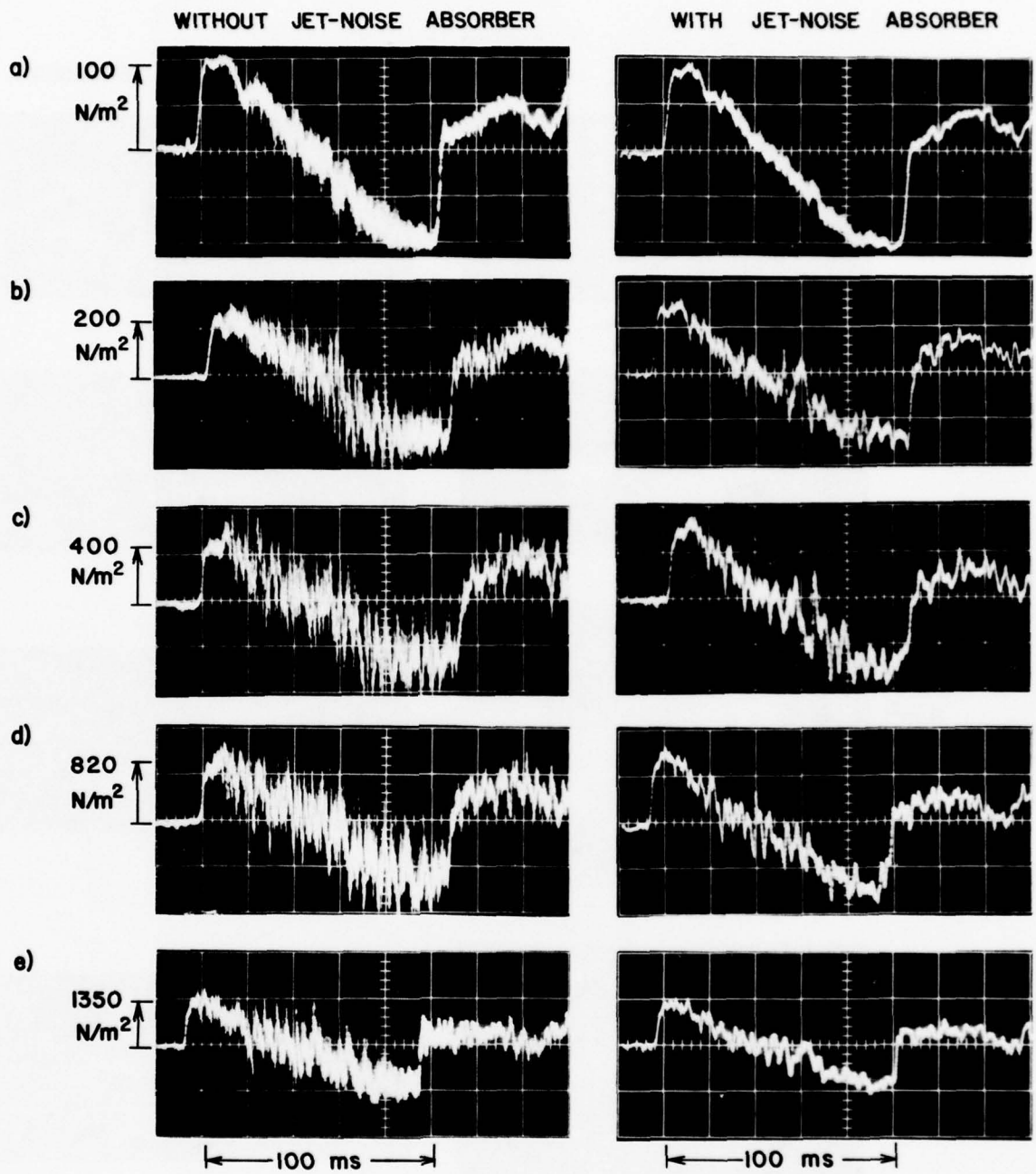
FIG. 7. SIMULATED SONIC BOOMS GENERATED WITH AND WITHOUT THE
JET-NOISE ABSORBER (plug valve, radial distance of 15.2 m,
reservoir pressures of 1.3, 2.5, 5.1, 9.2 and 13.9 atm).
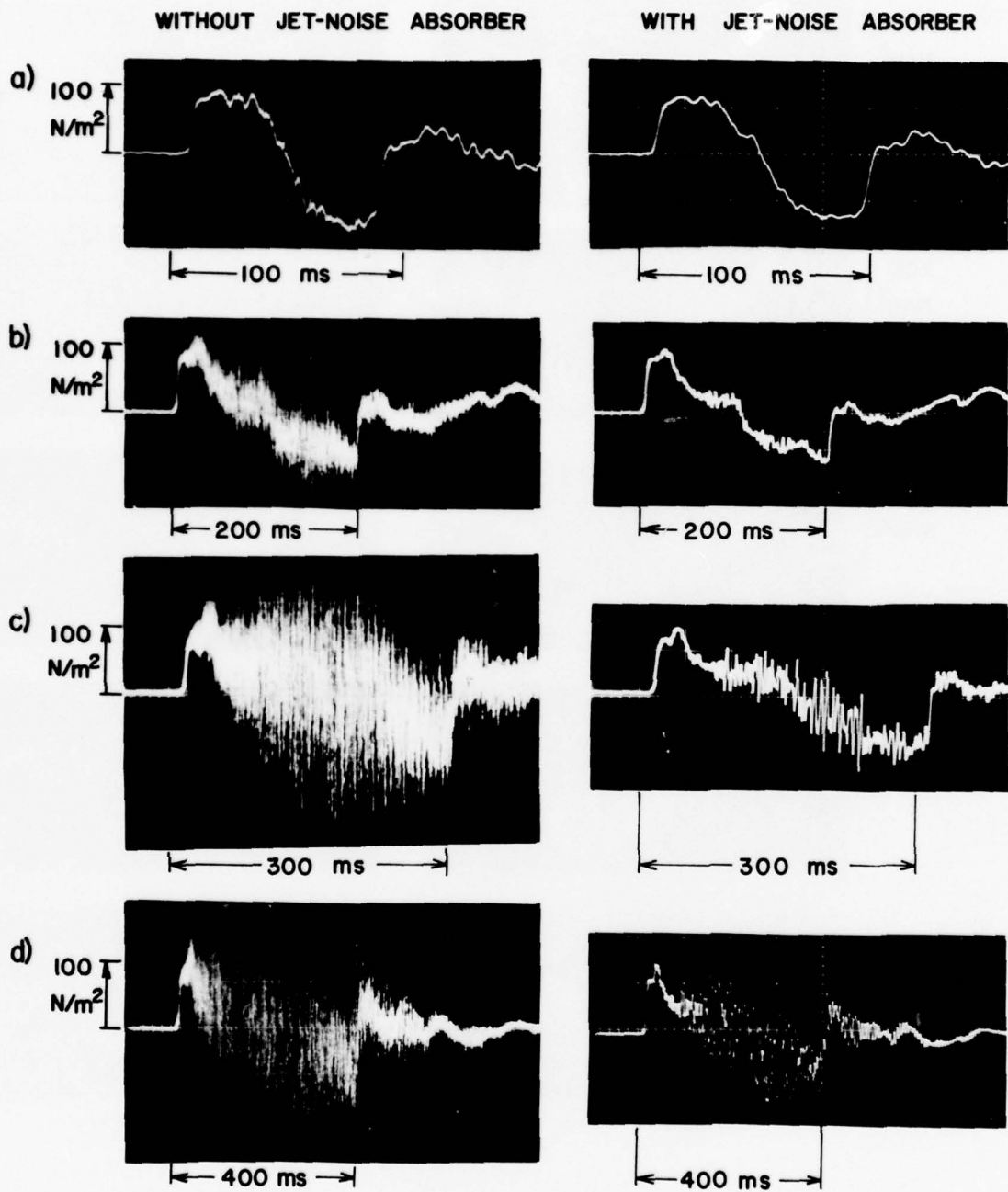
FIG. 8. SIMULATED SONIC BOOMS GENERATED WITH AND WITHOUT THE
JET-NOISE ABSORBER (plug valve, radial distance of 21.4 m,
reservoir pressures of 1.2, 1.8, 2.8 and 3.4 atm).
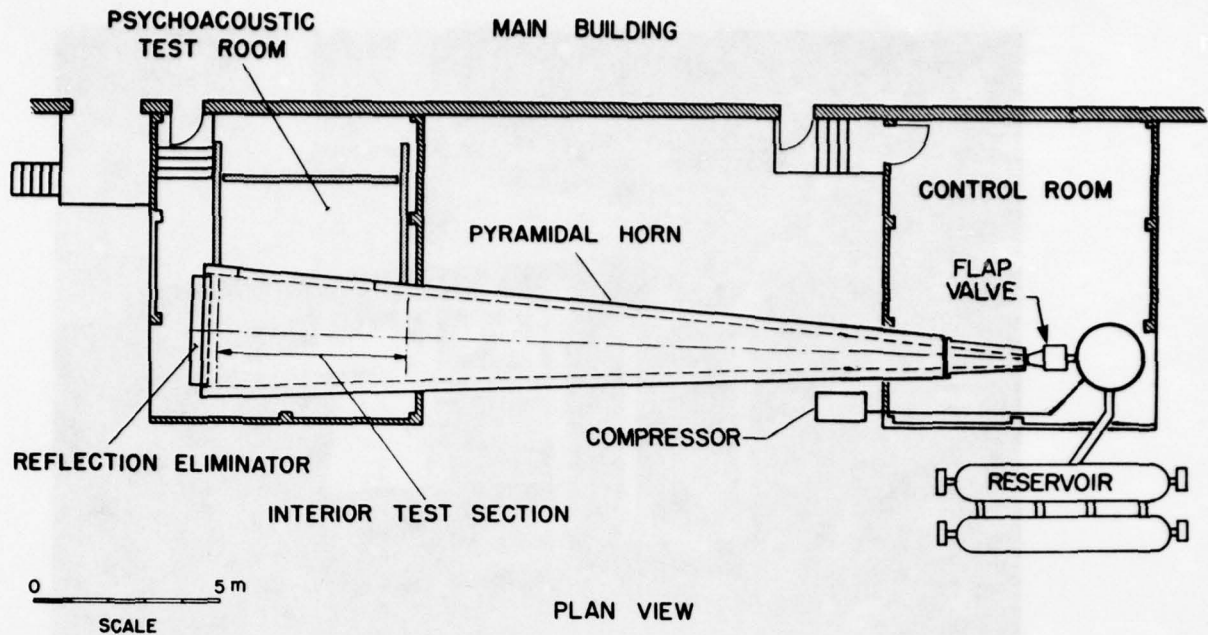
FIG. 9. PLAN VIEW ILLUSTRATING THE MOST RELEVANT ELEMENTS OF THE
TRAVELLING-WAVE HORN USING A FLAP VALVE.
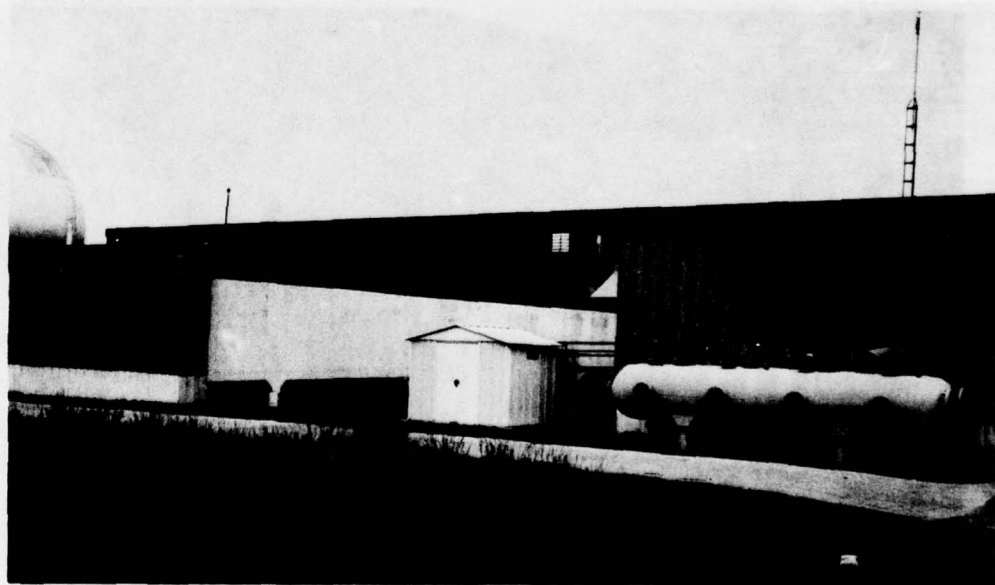
FIG. 10. OUTSIDE VIEW OF THE TRAVELLING-WAVE HORN SHOWING THE
CONCRETE HORN, TEST AND CONTROL ROOMS, COMPRESSOR SHED,
AND TWO TANKS OF THE AIR RESERVOIR SYSTEM.
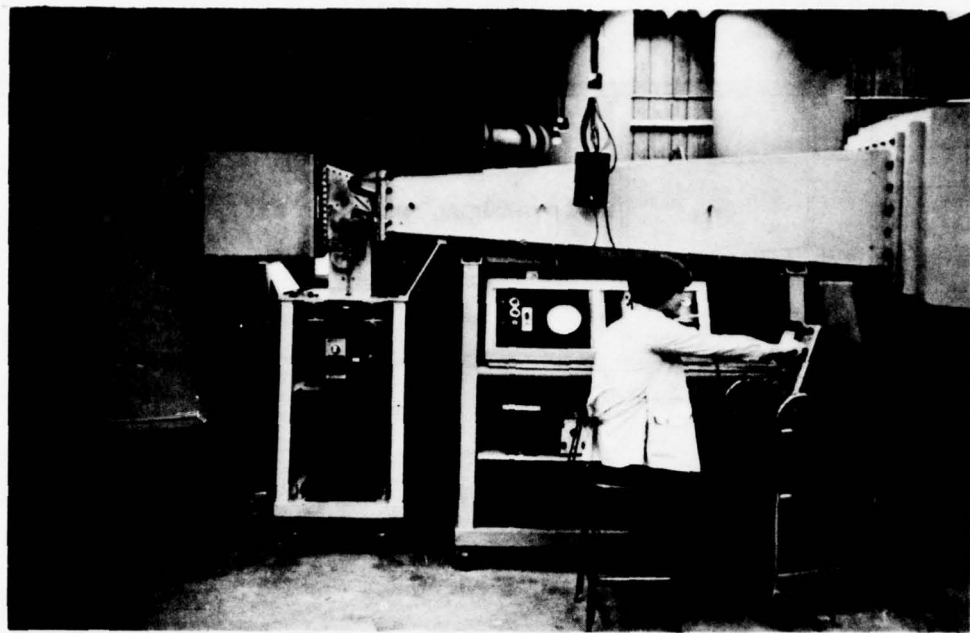
FIG. 11. VIEW OF THE SMALL END OF THE HORN SHOWING ALSO THE LARGE TANK
OF THE AIR RESERVOIR SYSTEM, FLAP VALVE AND ELECTRIC-MOTOR
DRIVE SYSTEM, CONTROL CONSOLE, AND ANCILLIARY ELECTRONICS.
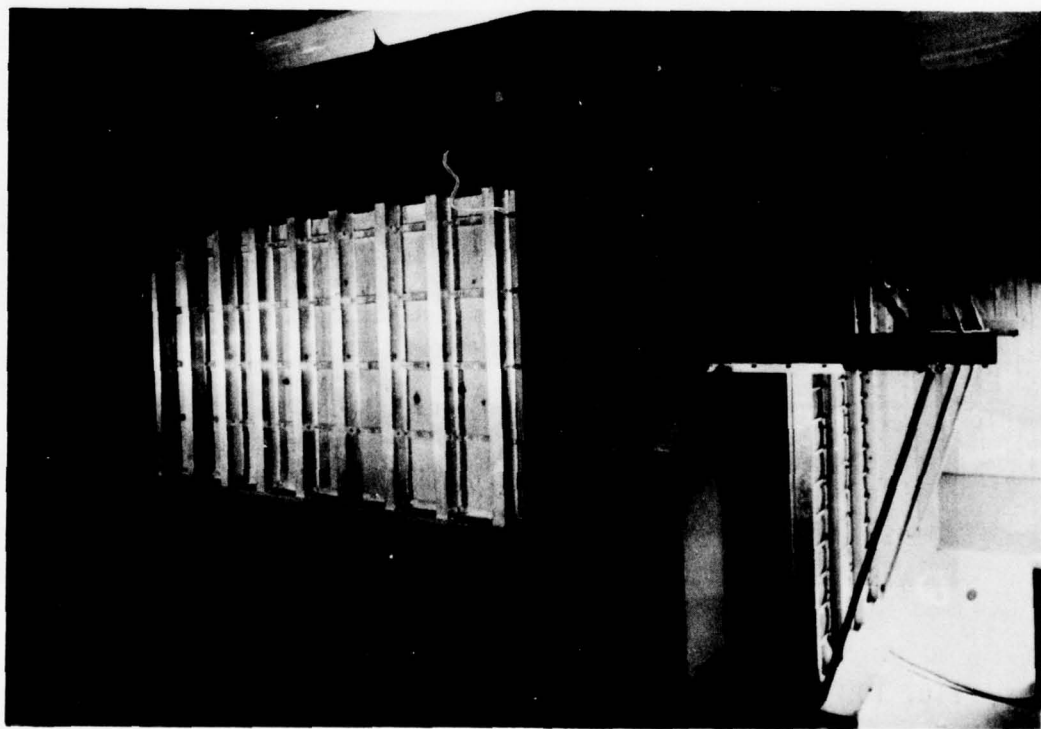
FIG. 12. VIEW OF THE LARGE END OF THE HORN SHOWING ALSO THE
REFLECTION ELIMINATOR, ACCESS DOOR TO THE HORN
INTERIOR, AND CUTOUT FOR STRUCTURAL PANEL TESTS.
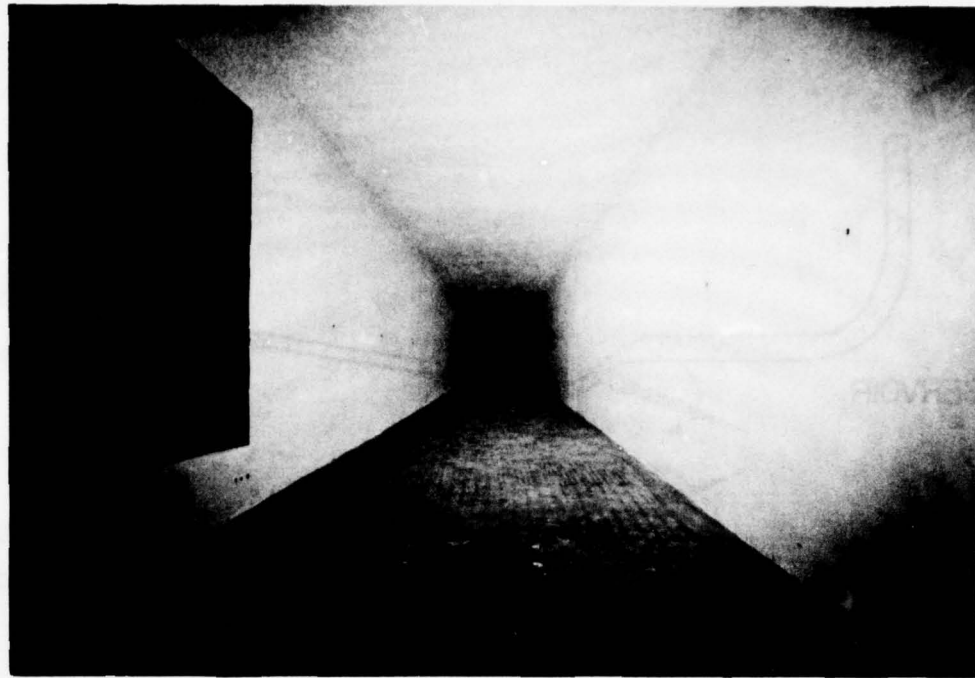
FIG. 13.   INTERIOR VIEW OF THE APEX OF THE PYRAMIDAL HORN.
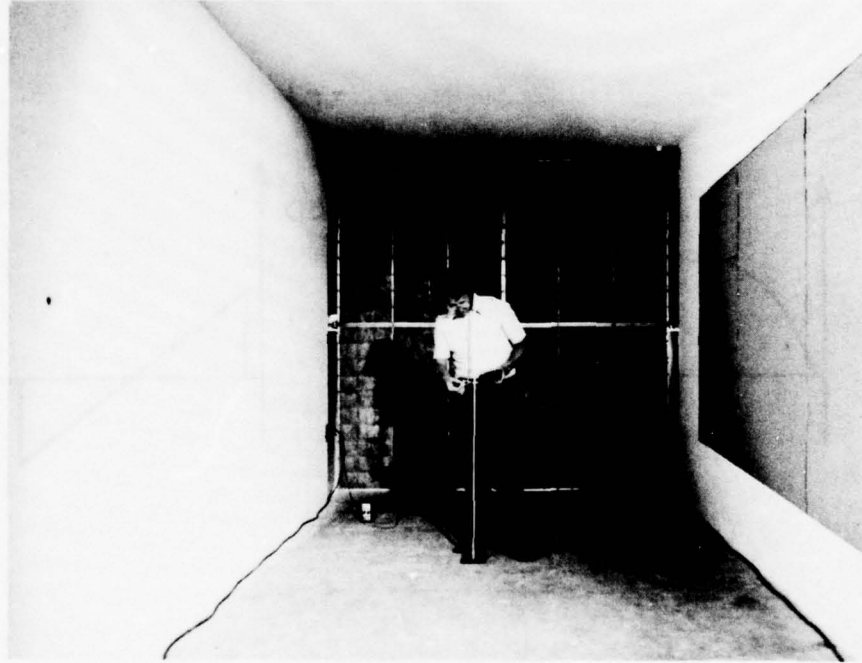
FIG. 14.   INTERIOR VIEW OF THE BASE OF THE HORN SHOWING ALSO
          THE REFLECTION ELIMINATOR AND COVERED CUTOUT.
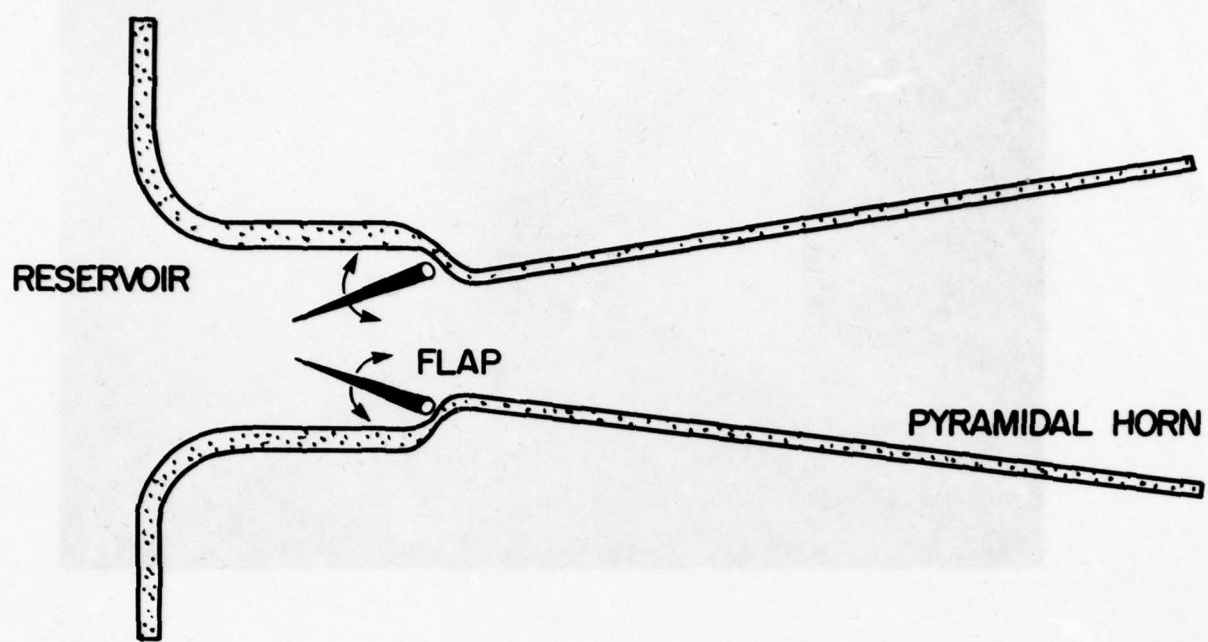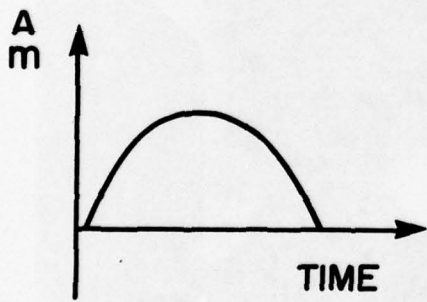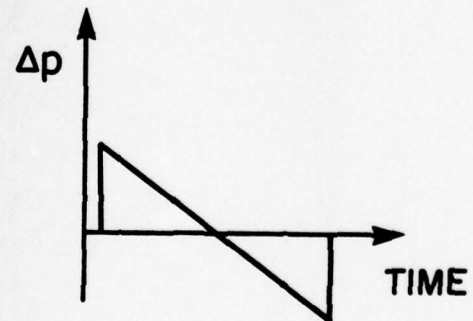
FIG. 15.   FLAP VALVE OPERATION: a) VALVE, b) THROAT-AREA AND
MASS-FLOW-RATE PROFILES, c) OVERPRESSURE SIGNATURE.
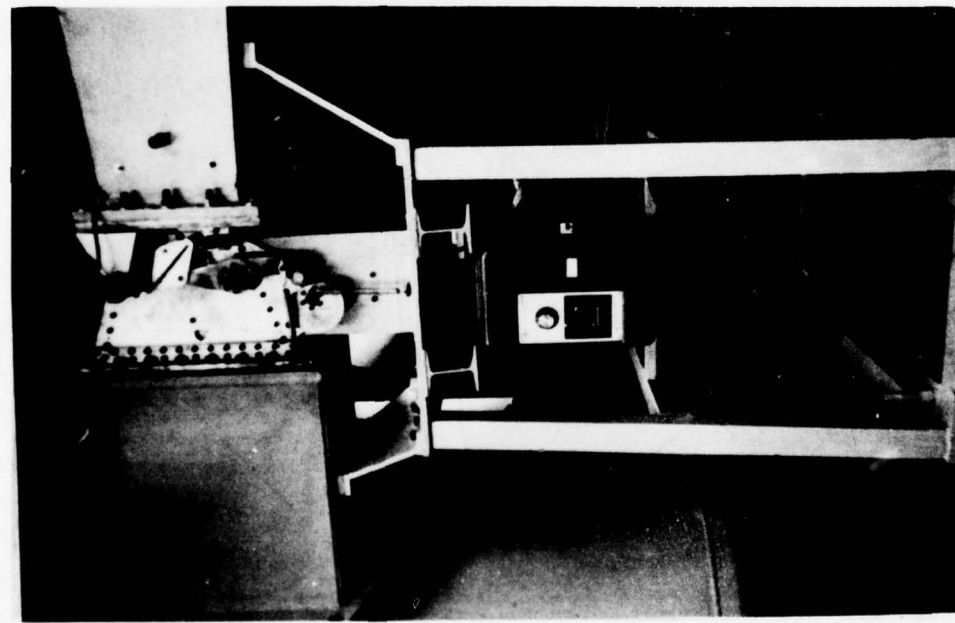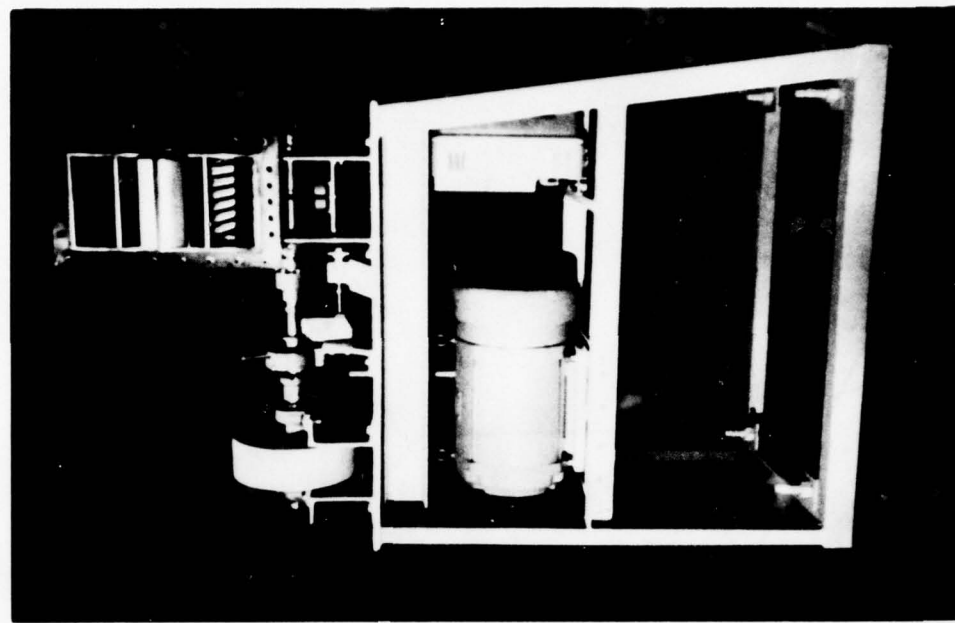
FIG. 16. FLAP VALVE AND CONTROL SYSTEM.
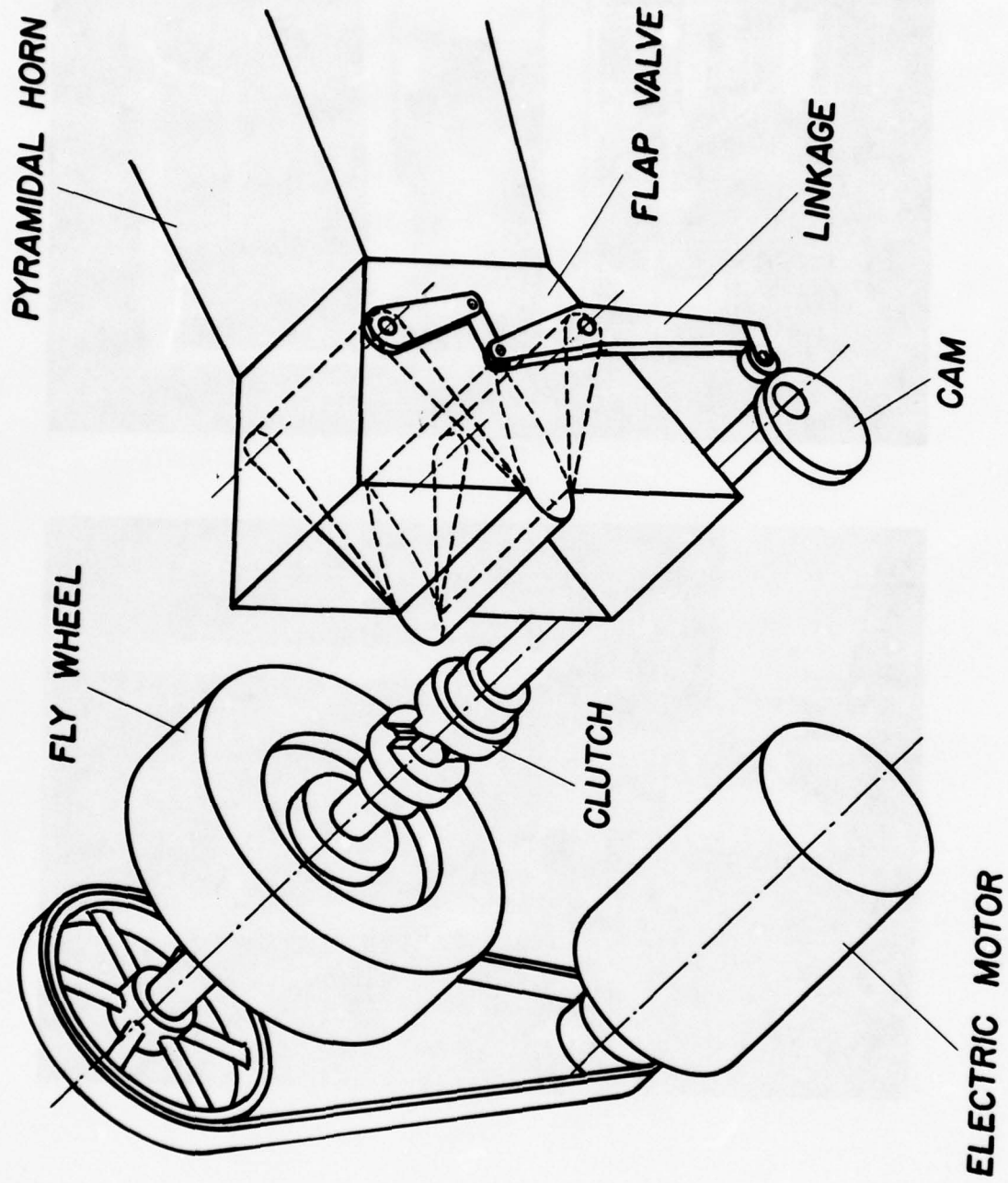
FIG. 17. SCHEMATIC DIAGRAM OF THE FLAP VALVE AND CONTROL SYSTEM.
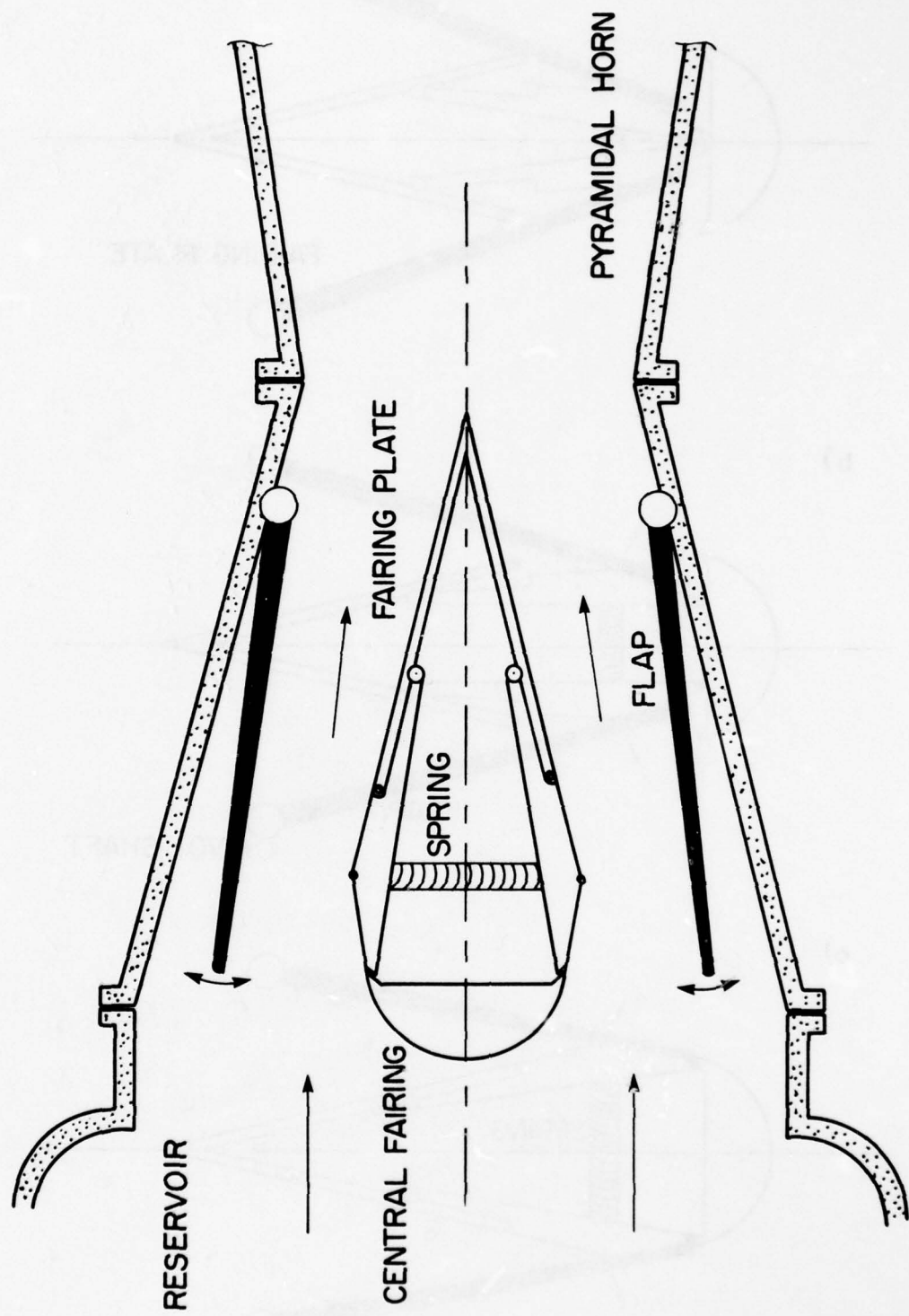
FIG. 18. CENTRAL FAIRING IN THE FLAP VALVE.
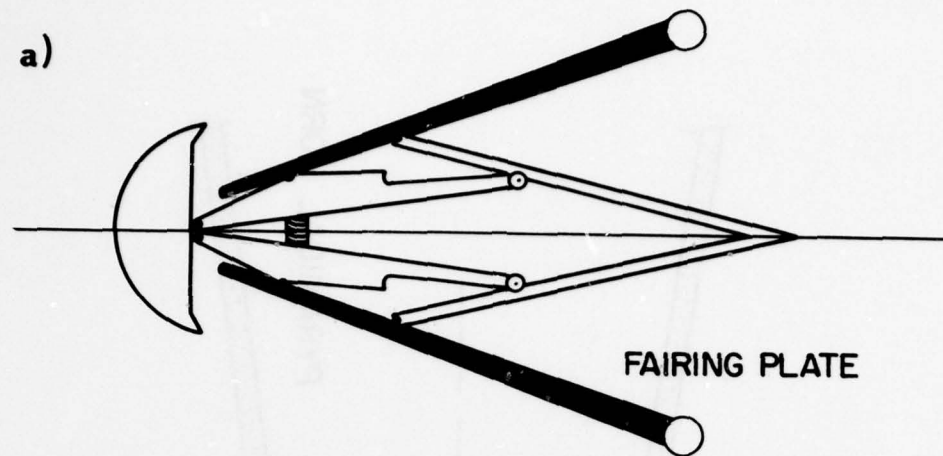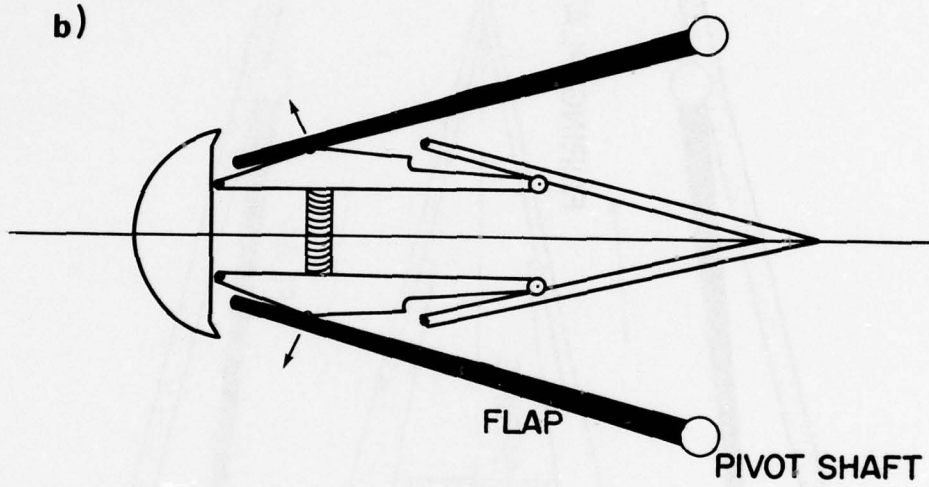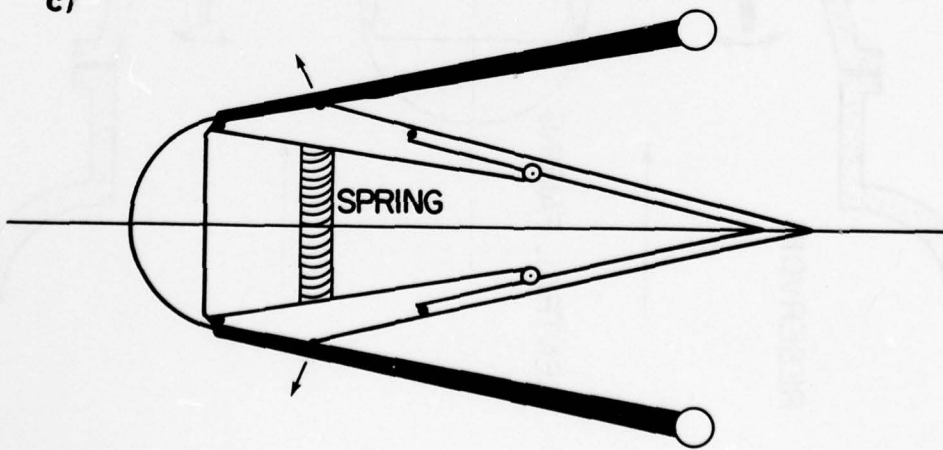
FIG. 19. MOTION OF THE FLAPS AND CENTRAL-FAIRING PLATES OF THE VALVE.

FLYWHEEL

PILLOW BLOCK

CLUTCH

CLUTCH PIN

COMPRESSION SPRING

STATIONARY CAM

PIN STOP

TRIGGER MECHANISM

COUPLING
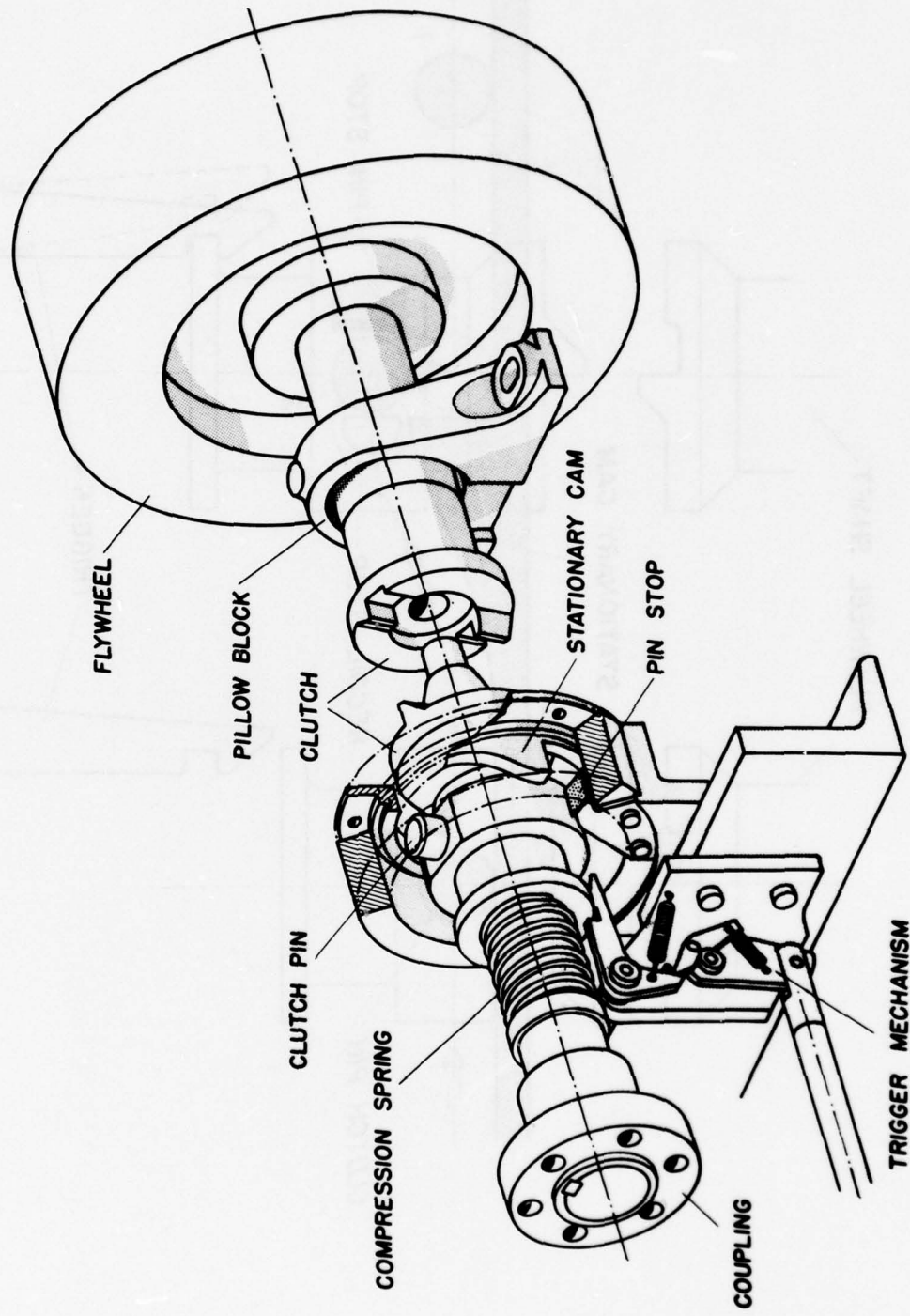
FIG. 20a.   ONE-REVOLUTION CLUTCH FOR THE FLAP VALVE.
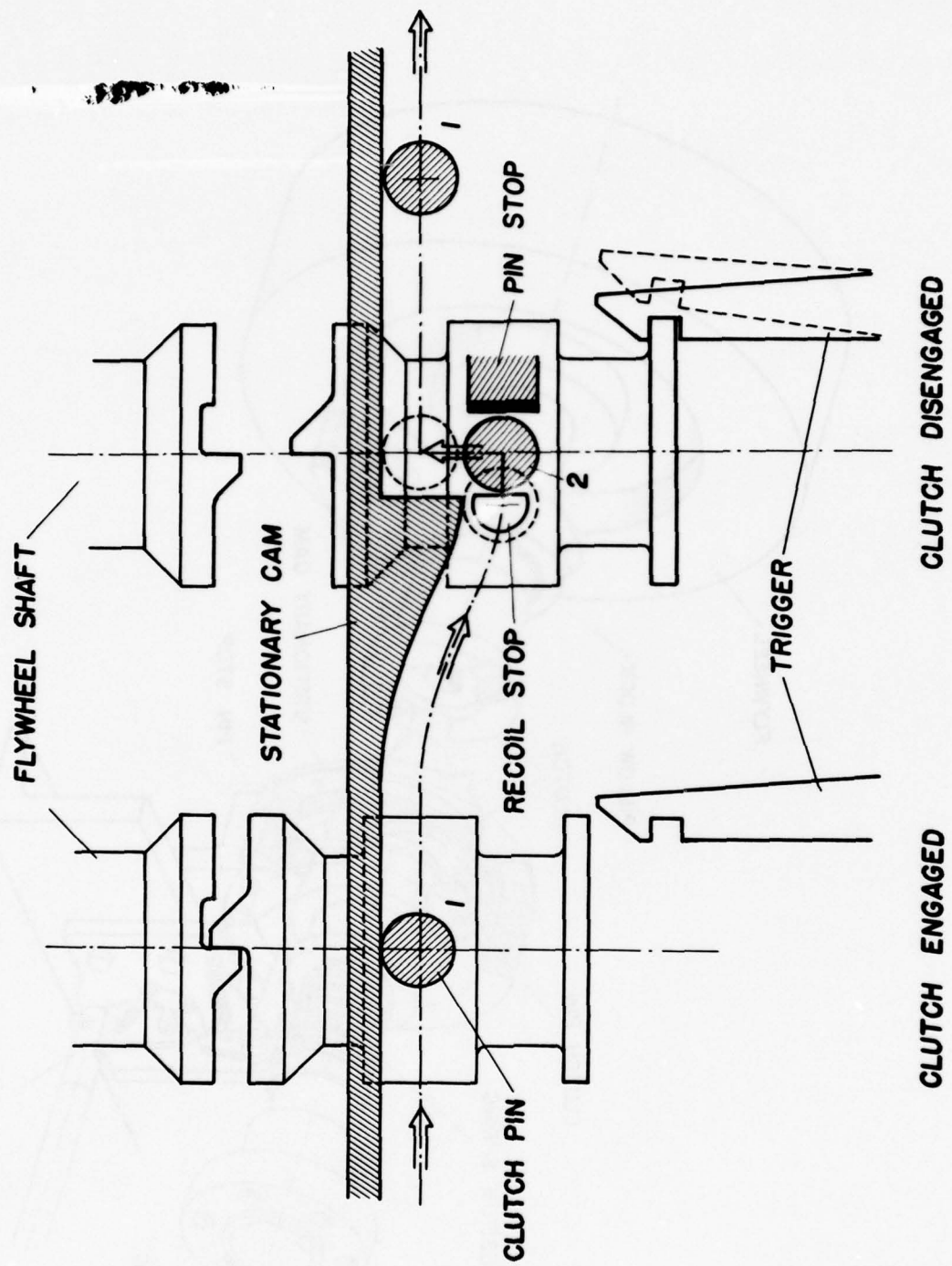
FIG. 20b. ILLUSTRATION OF THE CLUTCH PIN MOTION WHICH CAUSES THE
ONE-REVOLUTION CLUTCH TO ENGAGE AND DISENGAGE.
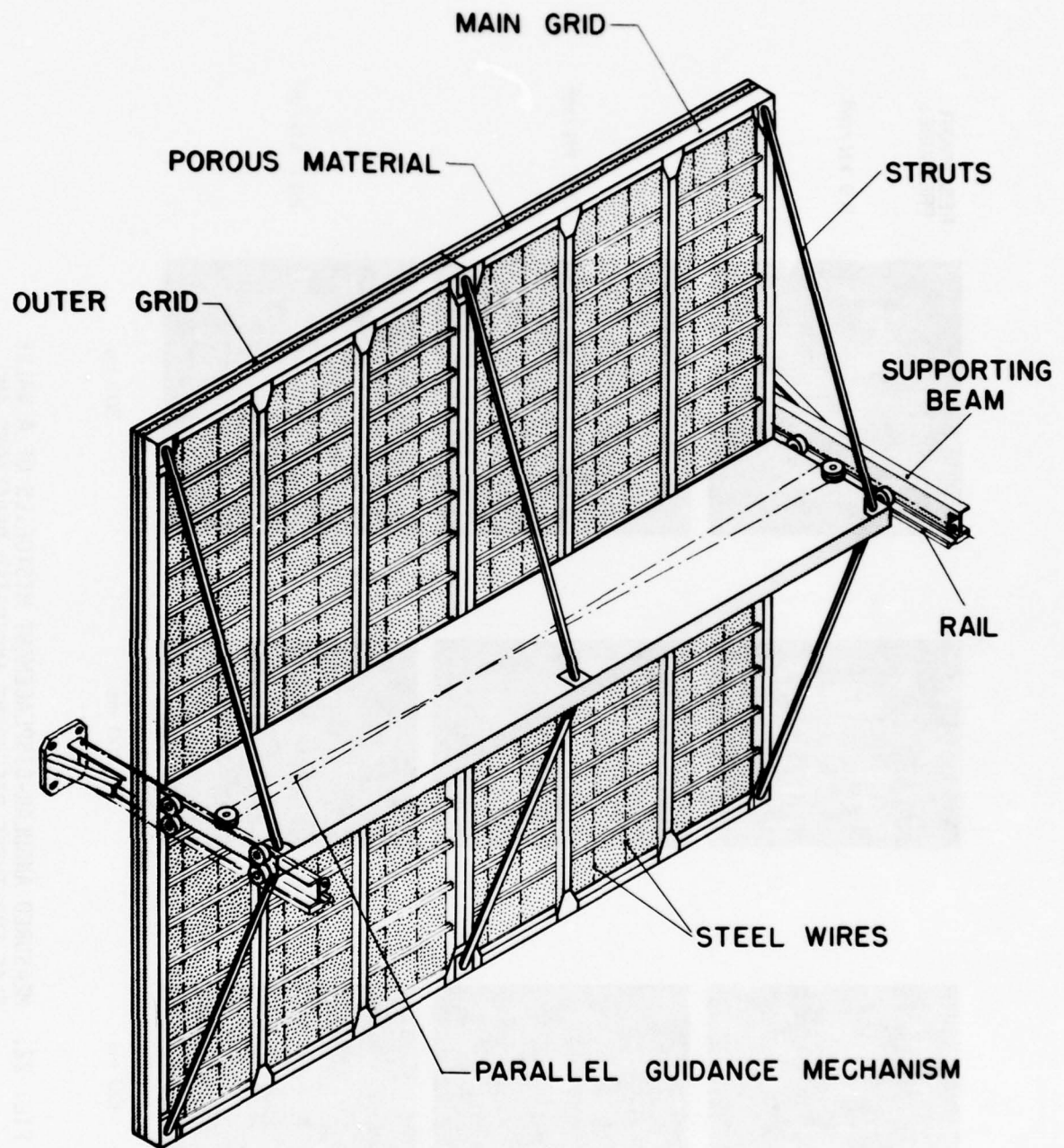
FIG. 21. POROUS-PISTON REFLECTION ELIMINATOR.

RESERVOIR PRESSURE:

6.9 kN/m²

13.8 kN/m²

20.7 kN/m²

DURATION: 100 ms   200 ms   300 ms

16.2 Degrees
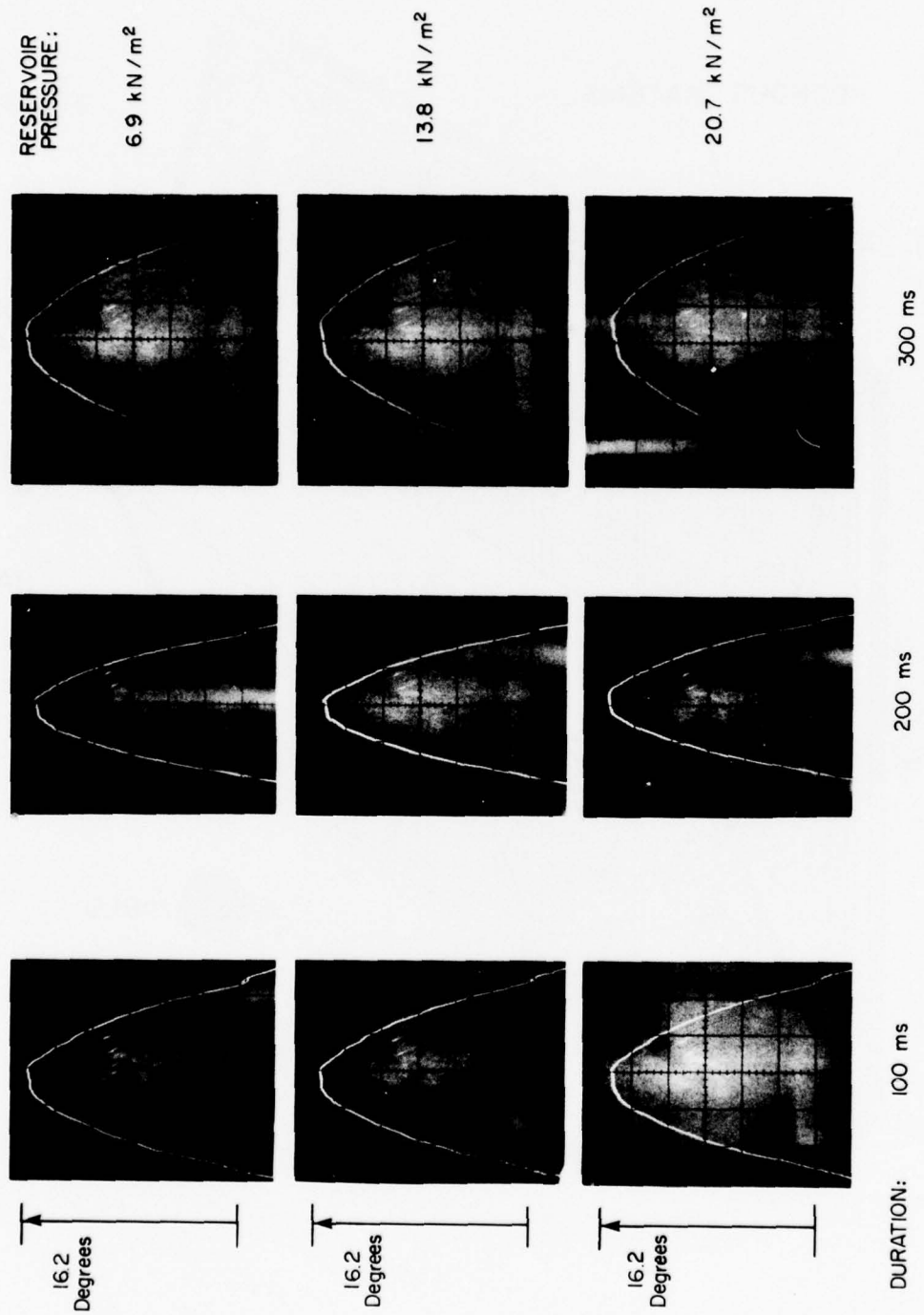
FIG. 22.   MEASURED ANGULAR-DISPLACEMENT HISTORIES OF A VALVE FLAP FOR THREE DIFFERENT INDICATED DURATIONS AND RESERVOIR PRESSURES.
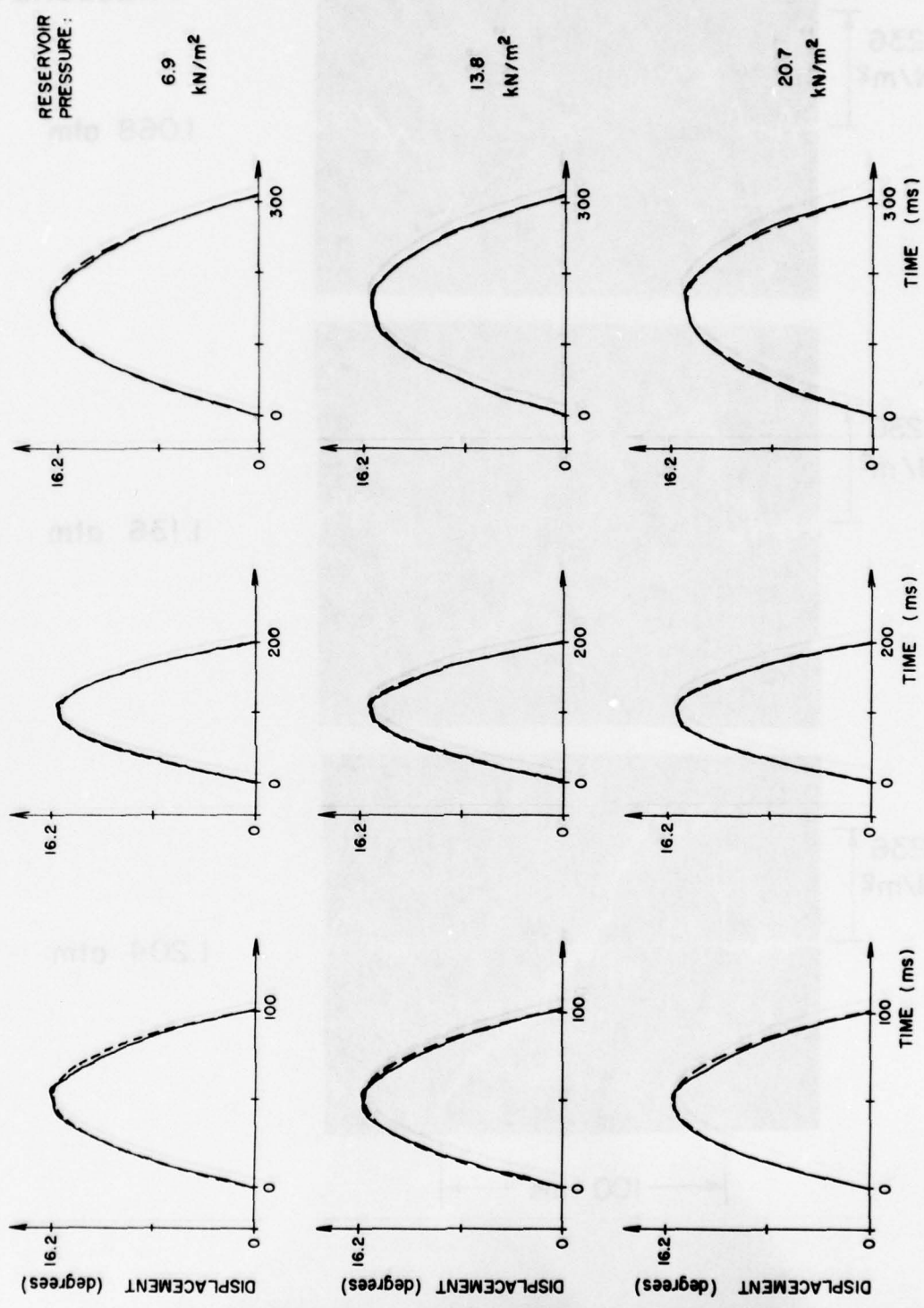
FIG. 23. MEASURED AND PARABOLIC ANGULAR-DISPLACEMENT HISTORIES OF A VALVE FLAP FOR THREE DIFFERENT INDICATED DURATIONS AND RESERVOIR PRESSURES (—— measured, --- parabolic).
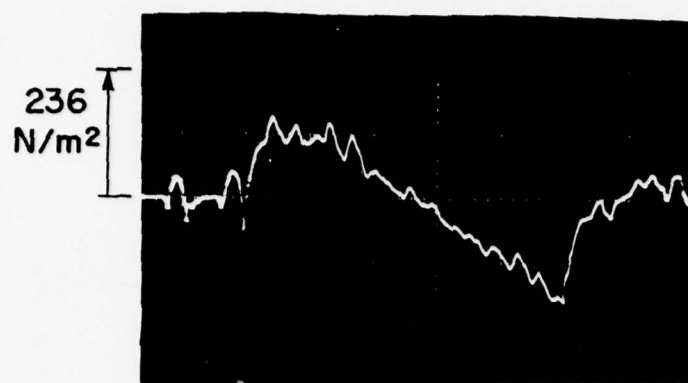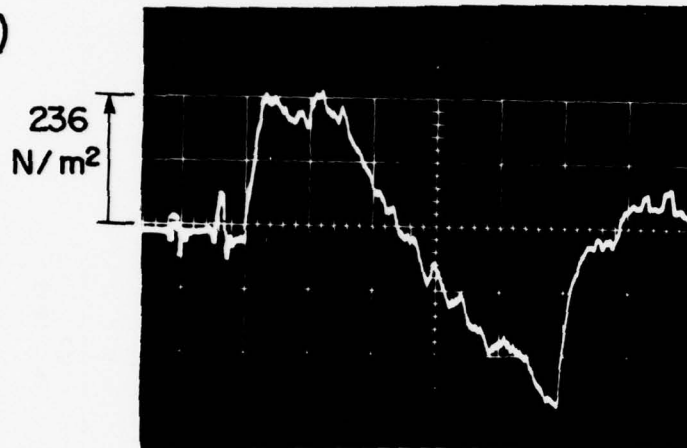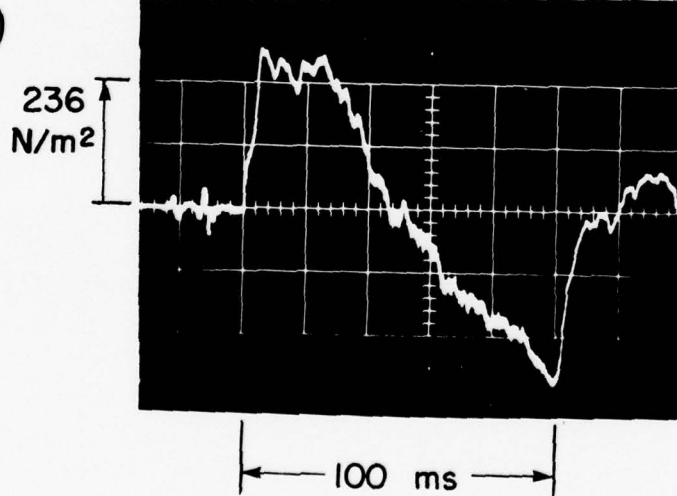
FIG. 24. SIMULATED SONIC BOOMS HAVING A DURATION OF 100 ms
(measured at a radial distance of 21.4 m).

a)

236 N/m²

RESERVOIR PRESSURE :

1.068 atm

b)

236 N/m²

1.136 atm

c)

236 N/m²
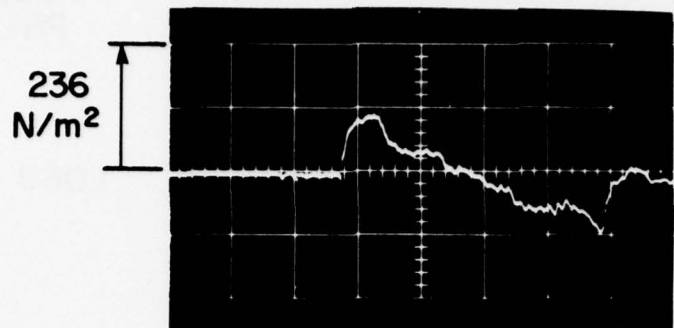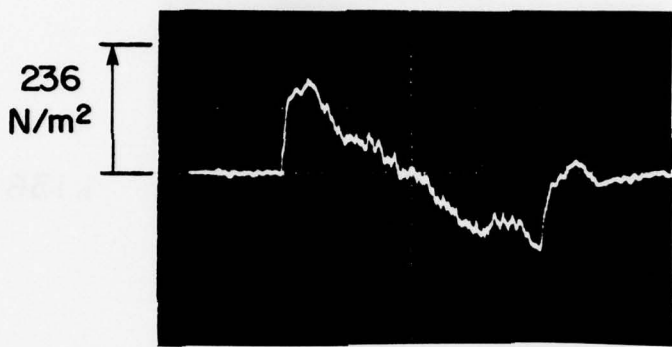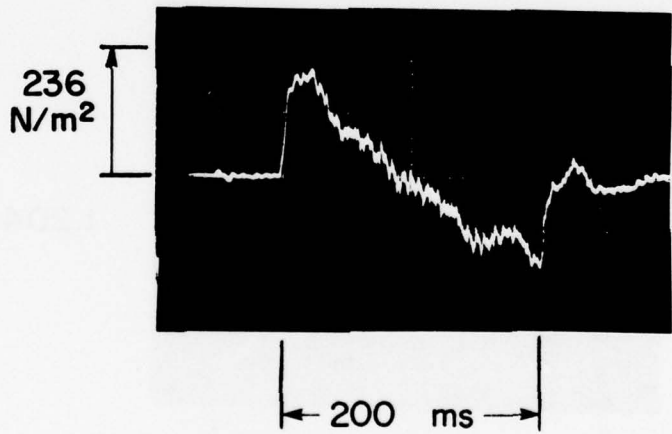
1.204 atm

|← 200 ms →|

FIG. 25. SIMULATED SONIC BOOMS HAVING A DURATION OF 200 ms
(measured at a radial distance of 21.4 m).

a)

94.5 N/m²

RESERVOIR PRESSURE :

1.068 atm

b)

94.5 N/m²

1.136 atm

c)

94.5 N/m²
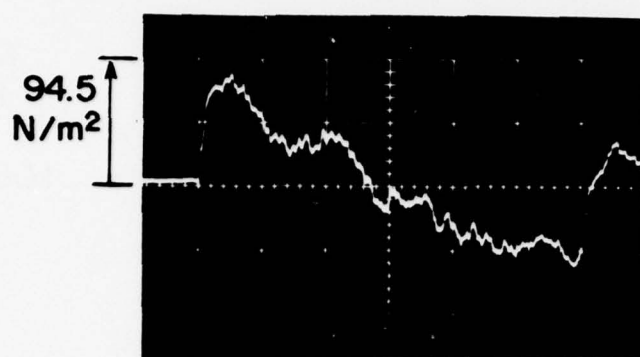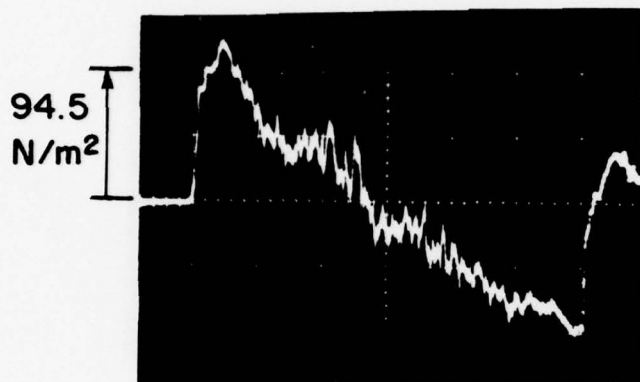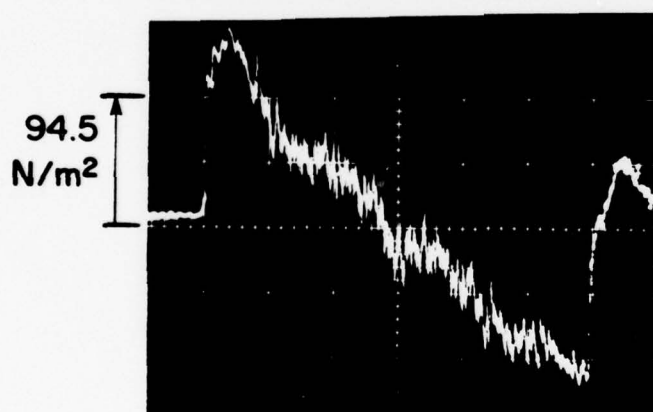
1.204 atm

|← 300 ms →|

FIG. 26.   SIMULATED SONIC BOOMS HAVING A DURATION OF 300 ms
(measured at a radial distance of 21.4 m).
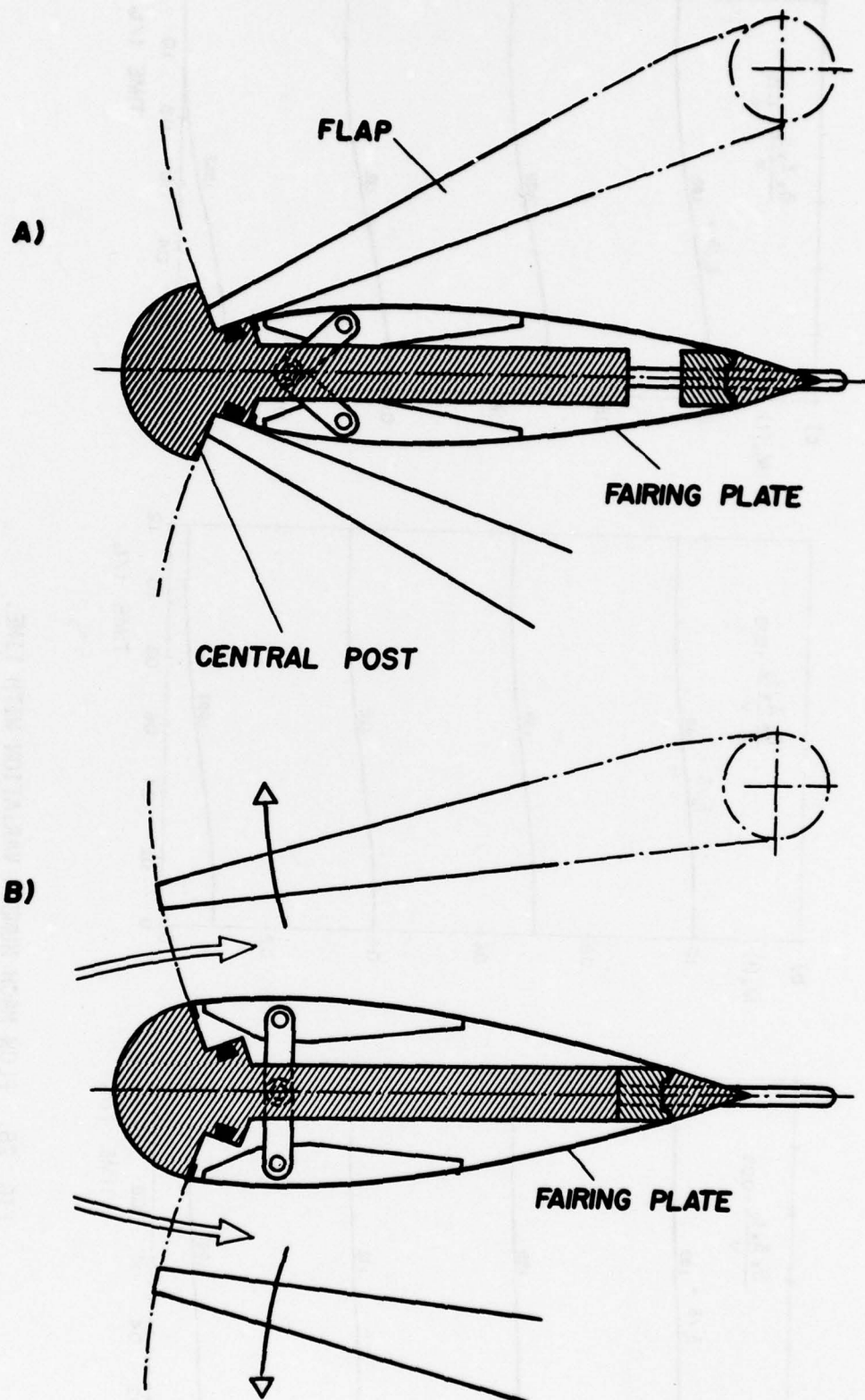
FIG. 27. MOTION OF THE CENTRAL-FAIRING PLATES AND VALVE FLAPS FOR A CENTRAL-FAIRING DESIGN WHICH GAVE A FAST RISE TIME.
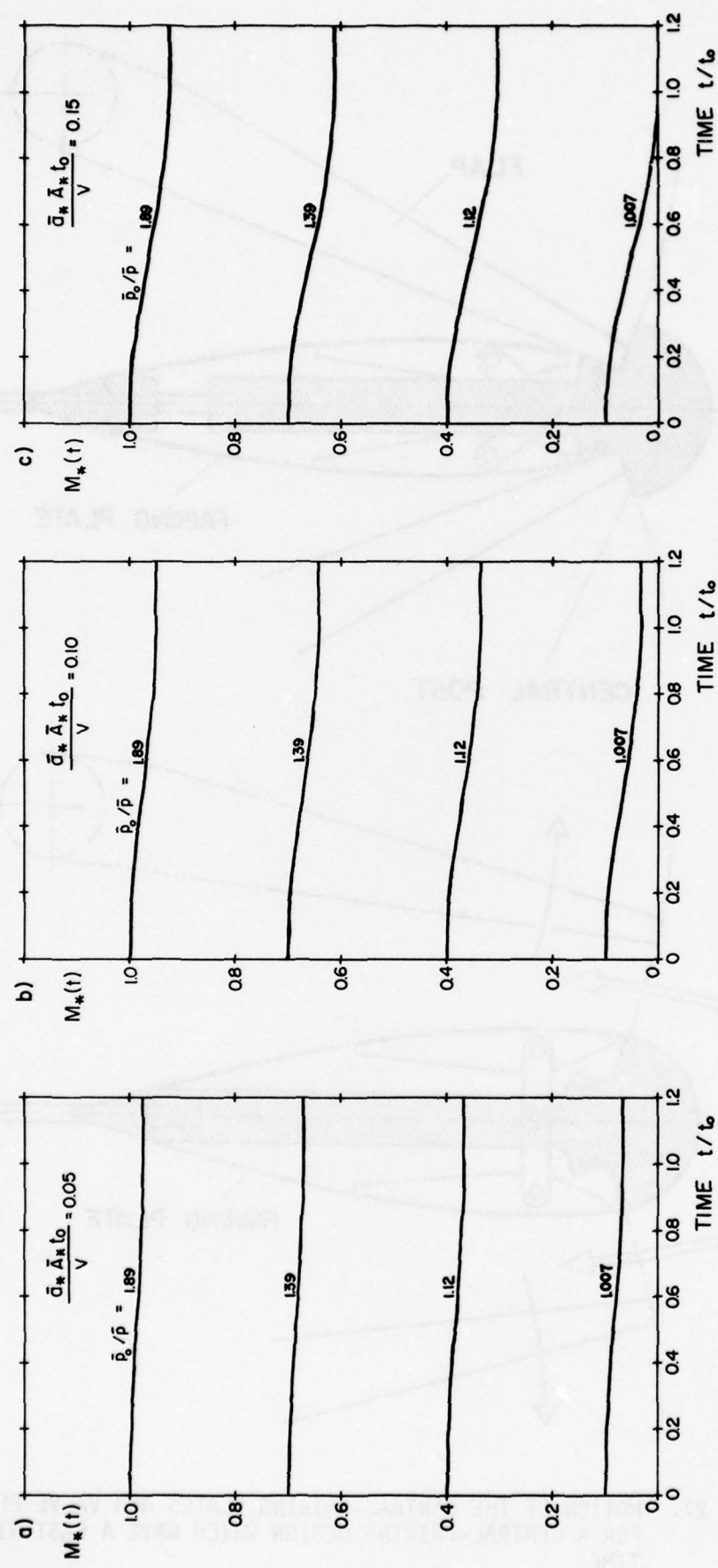
FIG. 28. FLOW MACH NUMBER VARIATION WITH TIME.
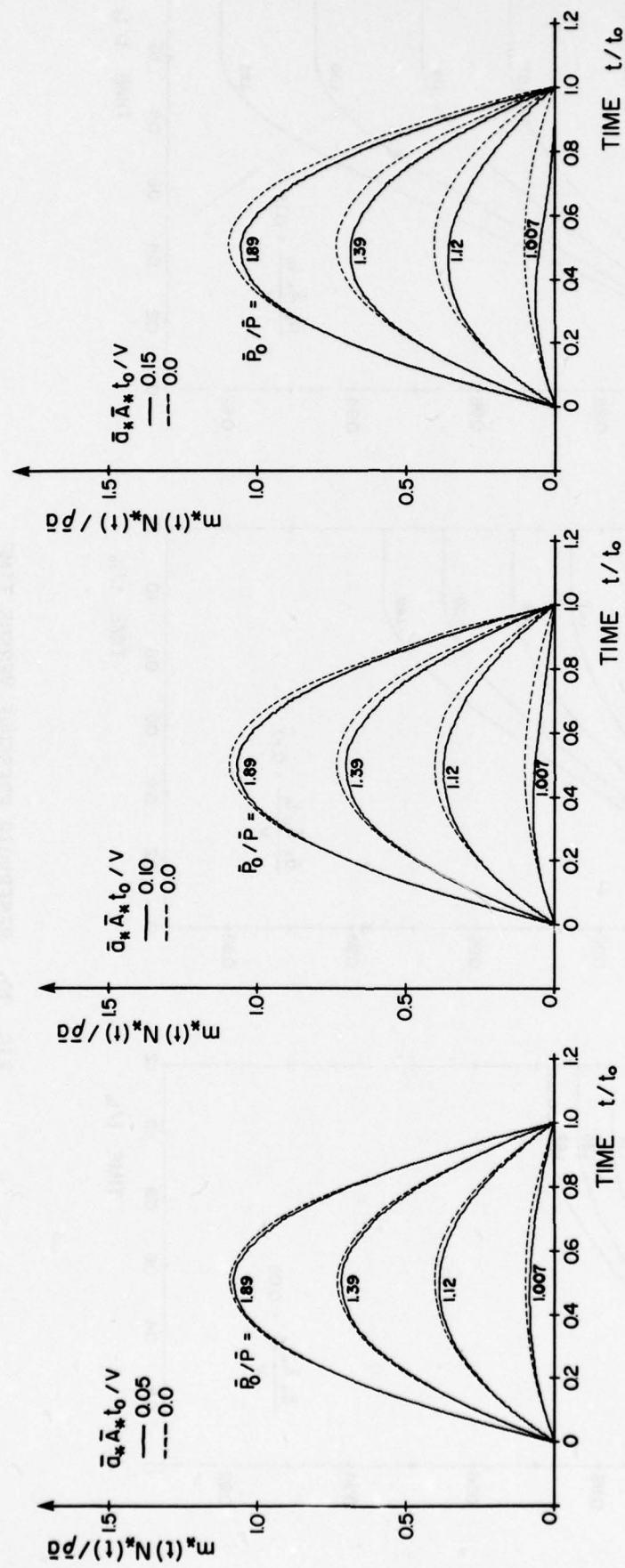
FIG. 29. MASS-FLOW-RATE VARIATION WITH TIME.
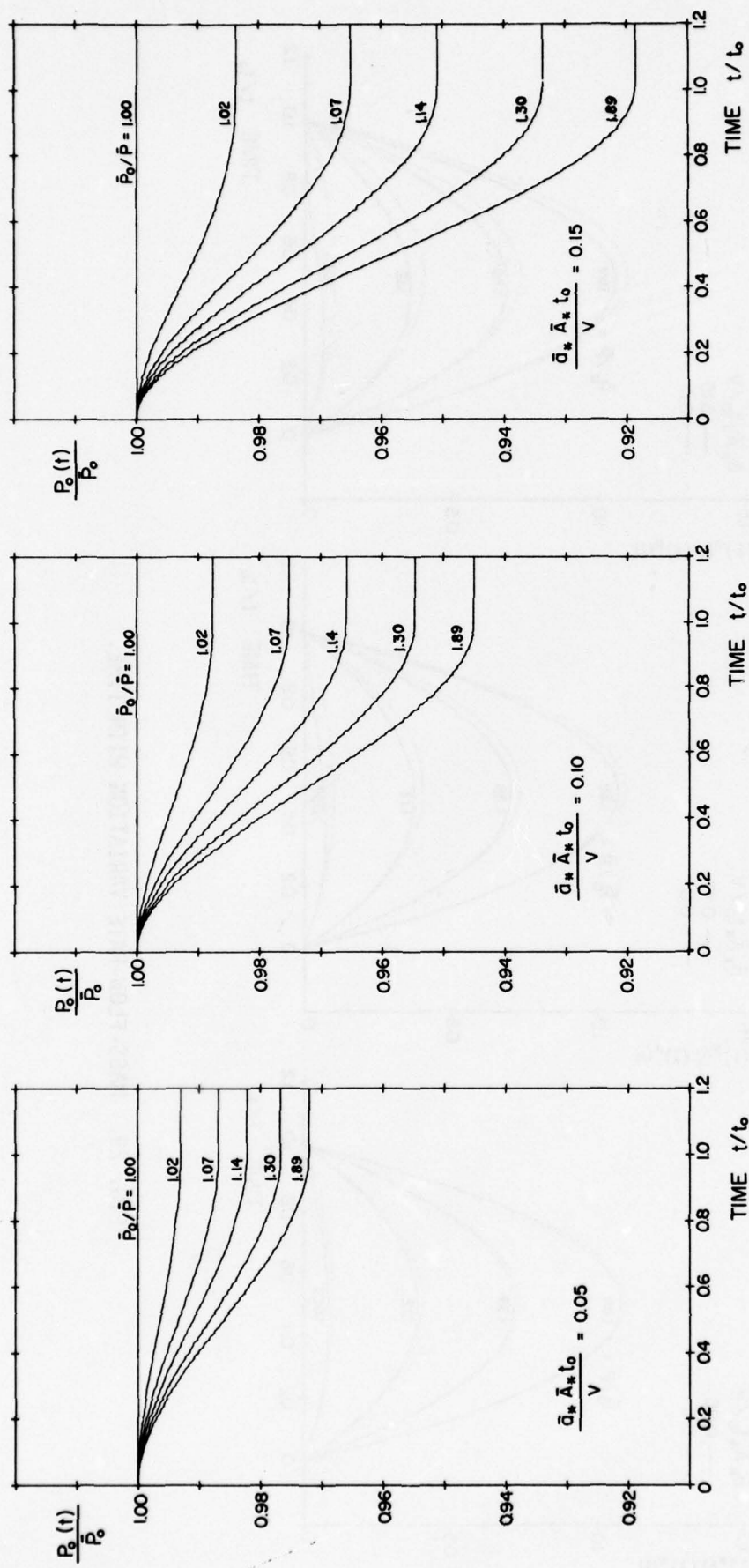
FIG. 30.   RESERVOIR PRESSURE VERSUS TIME.
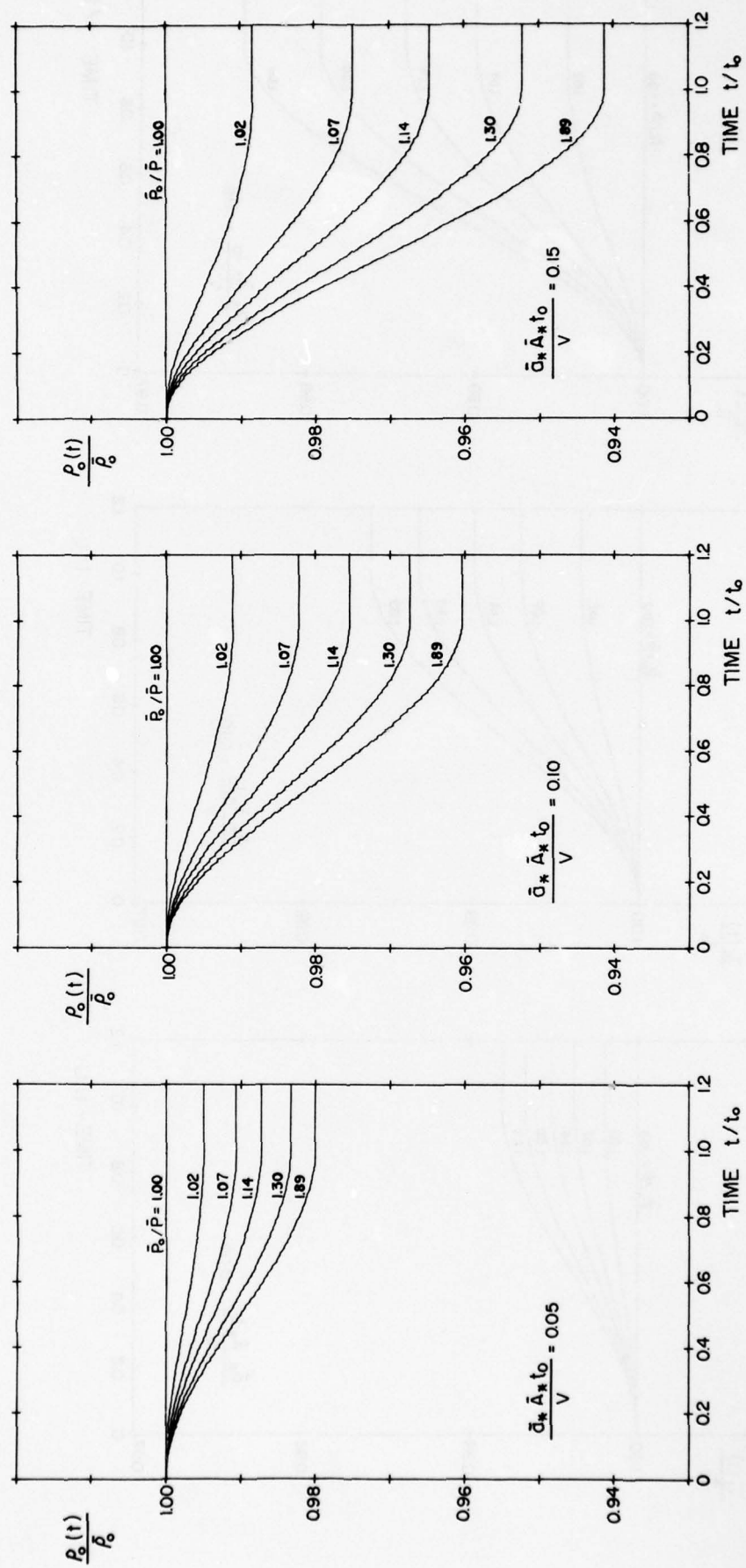
FIG. 31. RESERVOIR DENSITY VERSUS TIME.
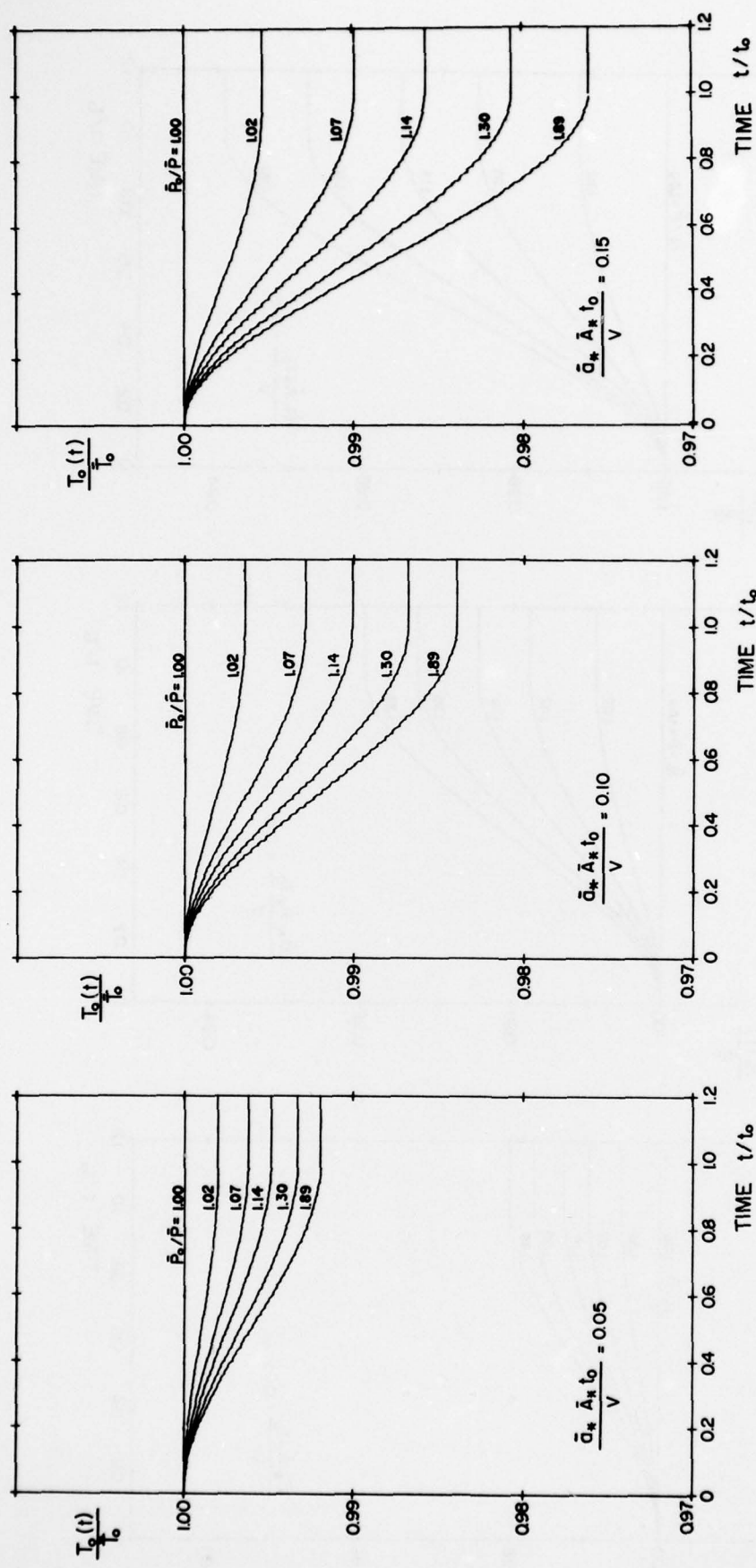
FIG. 32. RESERVOIR TEMPERATURE VERSUS TIME.
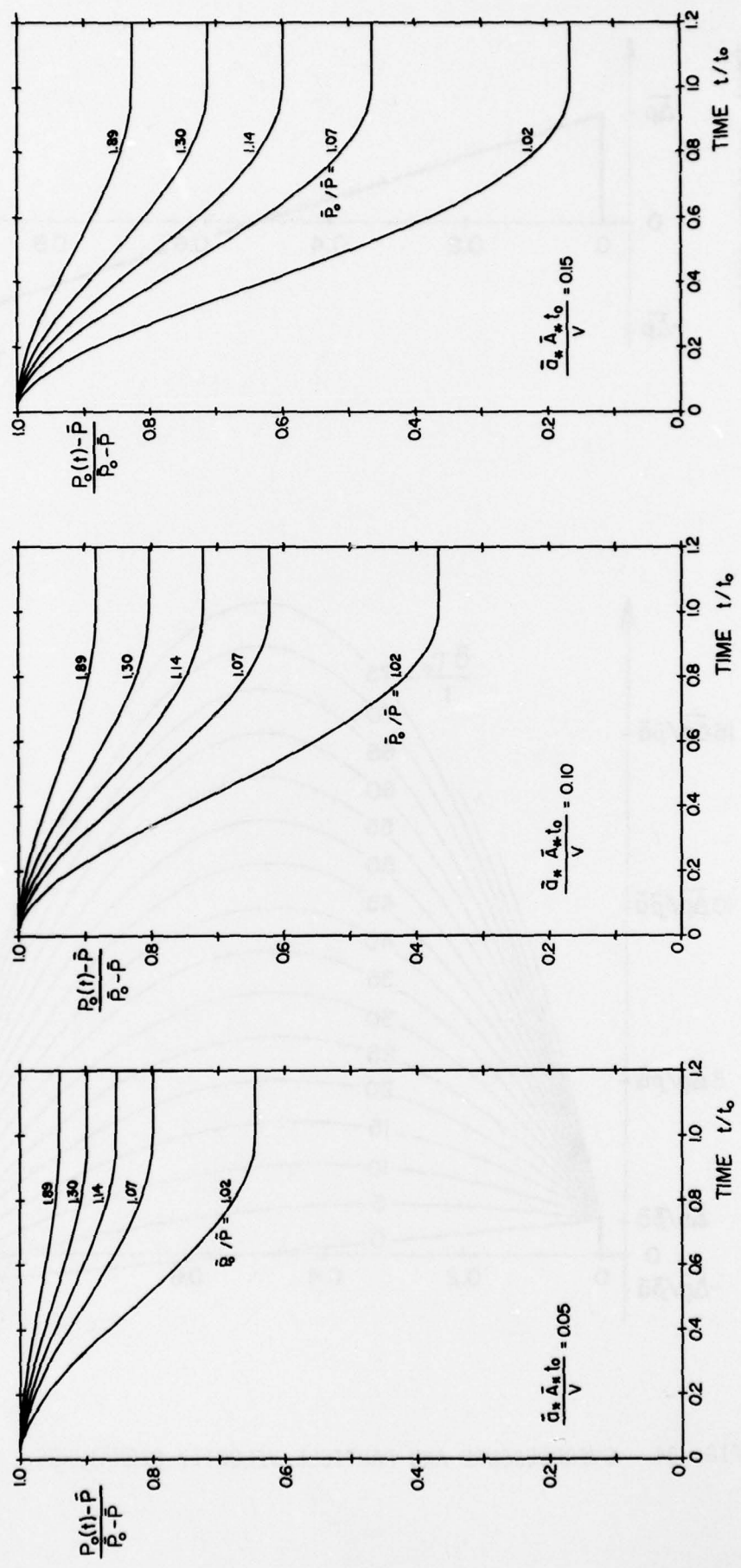
FIG. 33. NONDIMENSIONAL RESERVOIR OVERPRESSURE VERSUS TIME.
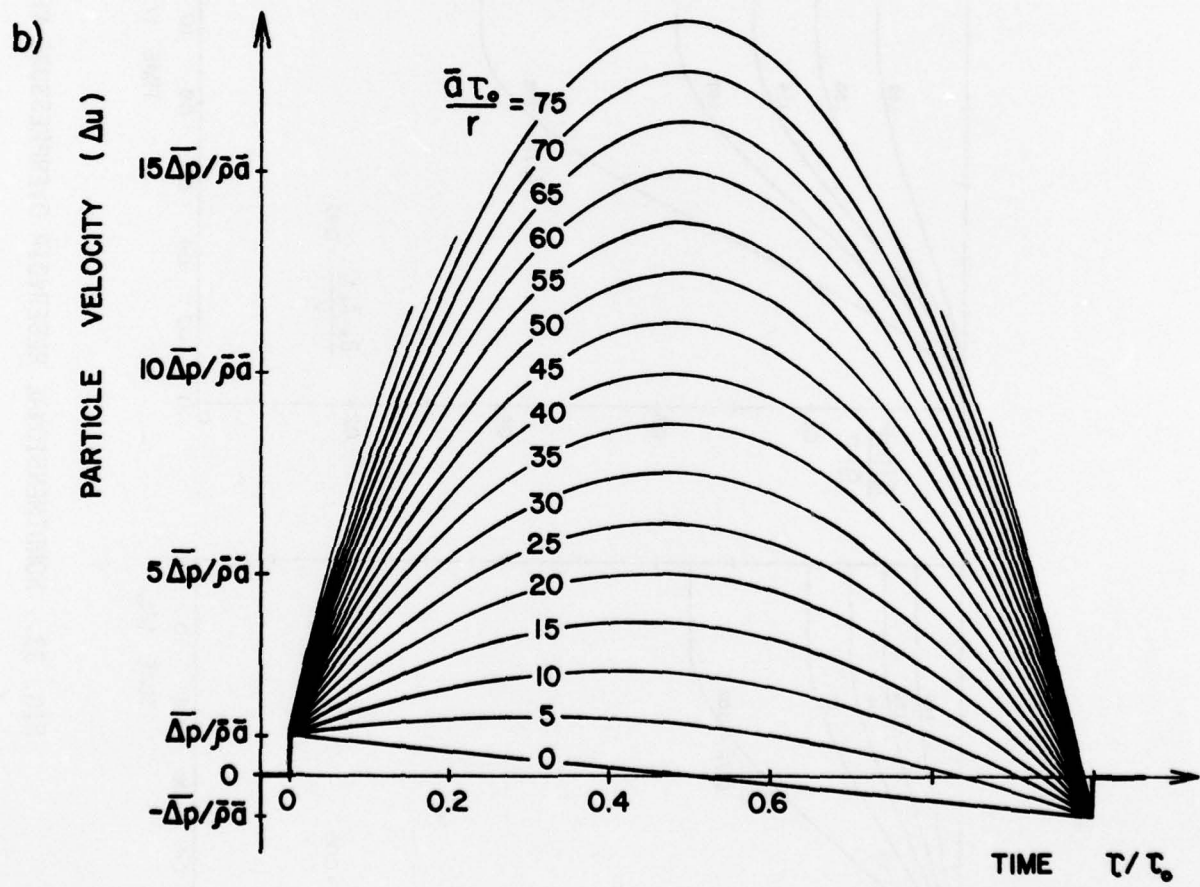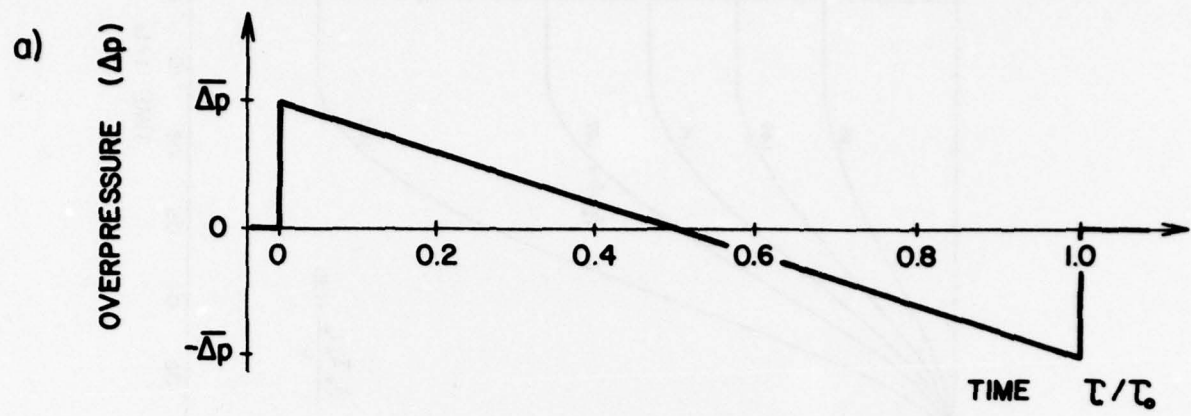
FIG. 34. OVERPRESSURE AND PARTICLE-VELOCITY SIGNATURES.
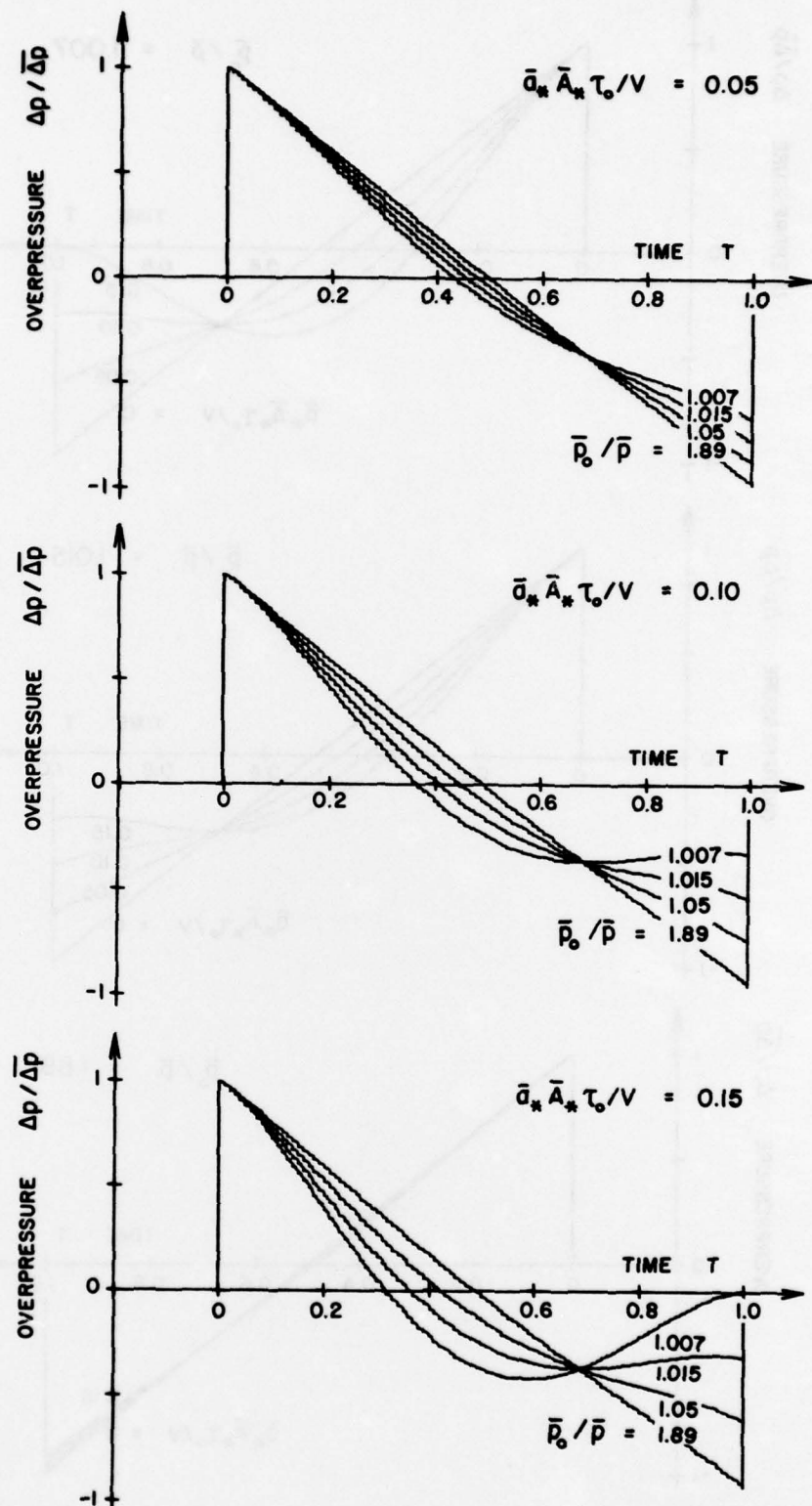
FIG. 35. EFFECTS OF THE PARAMETER $\bar{a}_* \bar{A}_* \tau_0/V$ AND RESERVOIR PRESSURE RATIO $\bar{p}_0/\bar{p}$ ON THE OVERPRESSURE SIGNATURE.
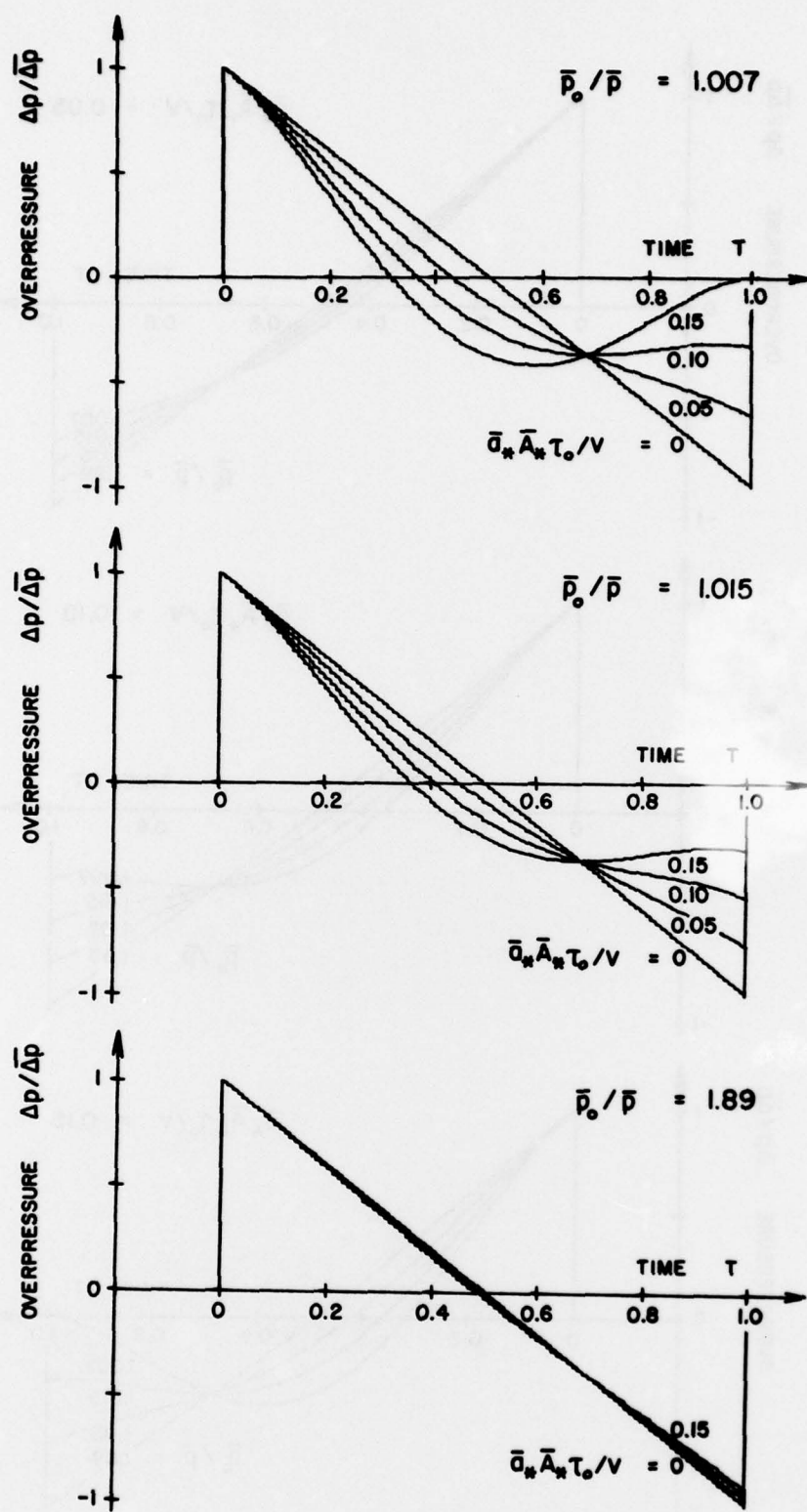
FIG. 36. EFFECTS OF THE RESERVOIR PRESSURE RATIO $\bar{p}_0/\bar{p}$ AND
PARAMETER $\bar{a}_*\bar{A}_*\tau_0/V$ ON THE OVERPRESSURE SIGNATURE.
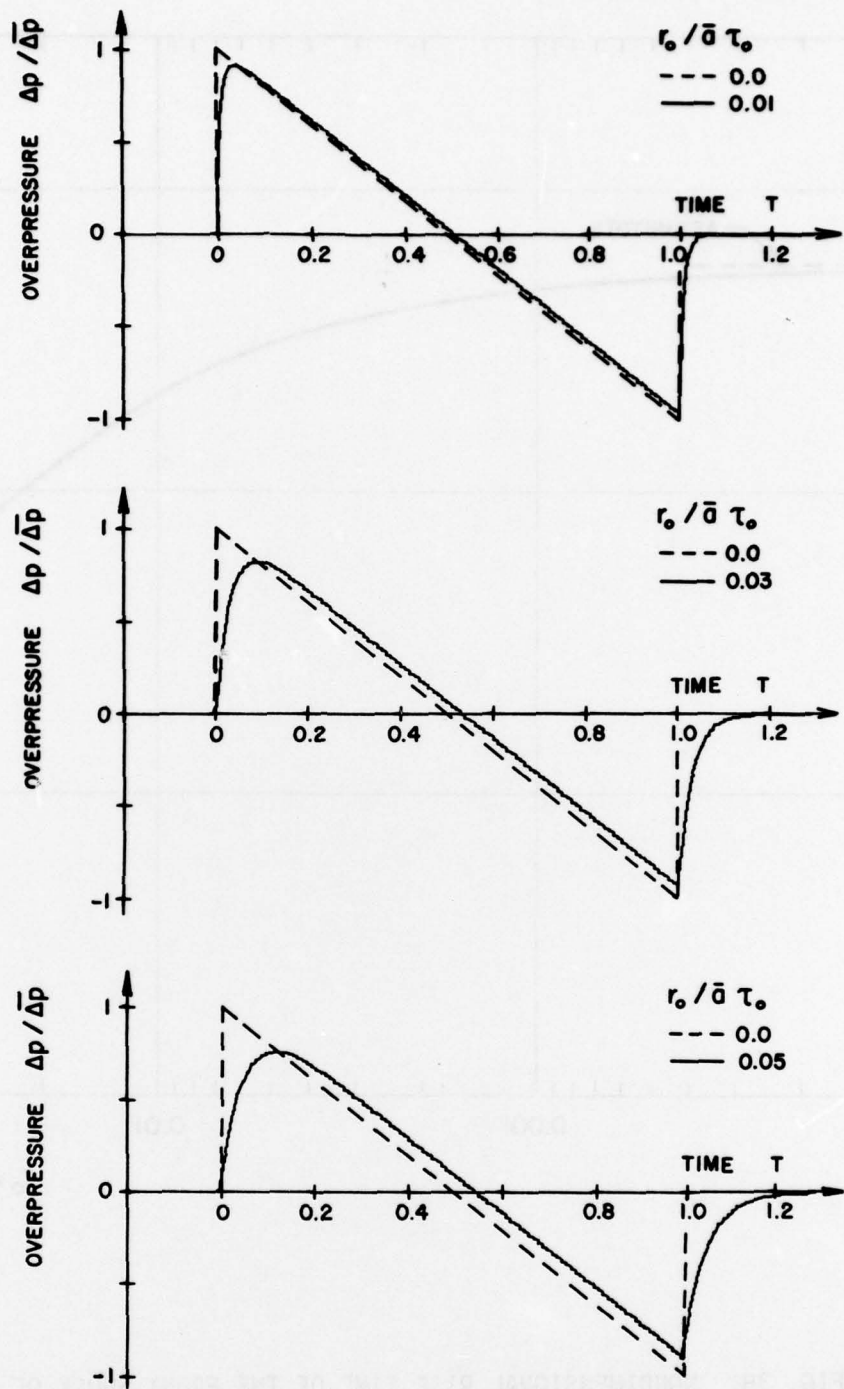
FIG. 37. COMPARISON OF INSTANTANEOUS AND FINITE RISE TIMES
OF N-SHAPED SIGNATURES.
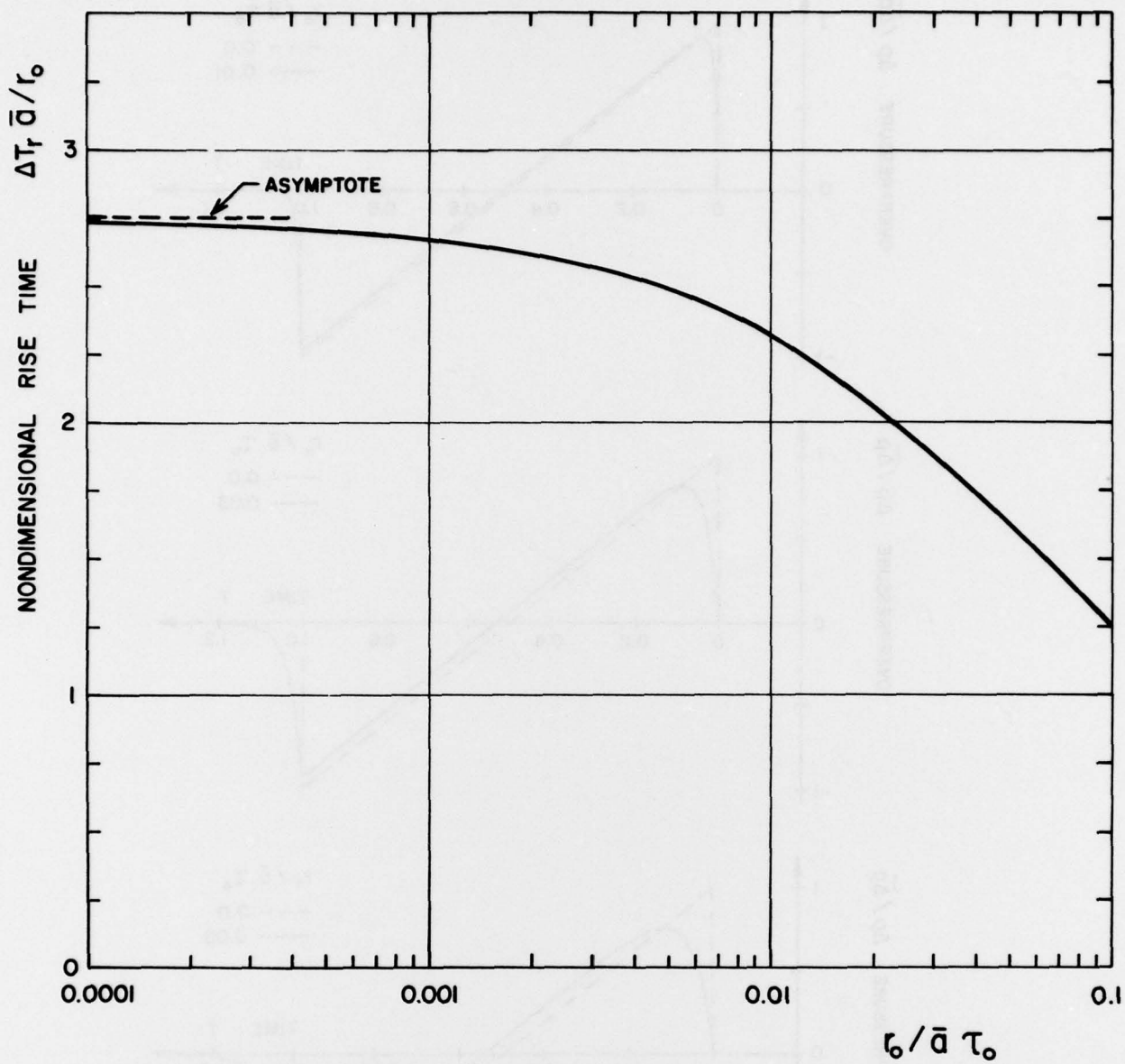
FIG. 38. NONDIMENSIONAL RISE TIME OF THE FRONT SHOCK OF A
SIMULATED SONIC BOOM VERSUS THE PARAMETER $r_0/\bar{a}\tau_0$.
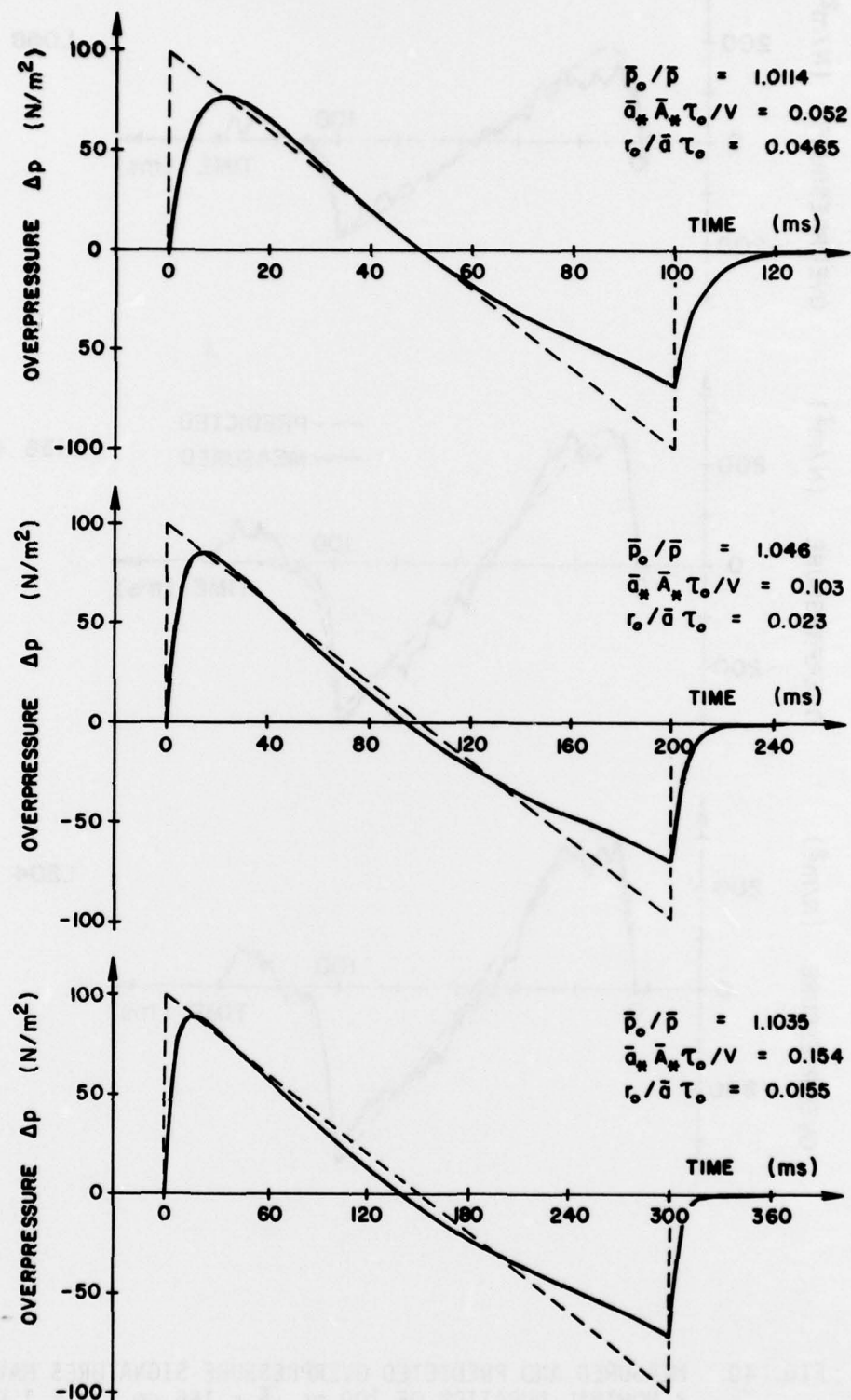
FIG. 39. COMPARISON OF IDEAL AND DISTORTED N-SHAPED OVERPRESSURE
SIGNATURES FOR THE UTIAS TRAVELLING-WAVE HORN
(r = 21.3 m, r_0 = 1.58 m, $\bar{A}_*$= 156 m², V = 10.2 m³,
$\bar{a}$ = 340 m/s).
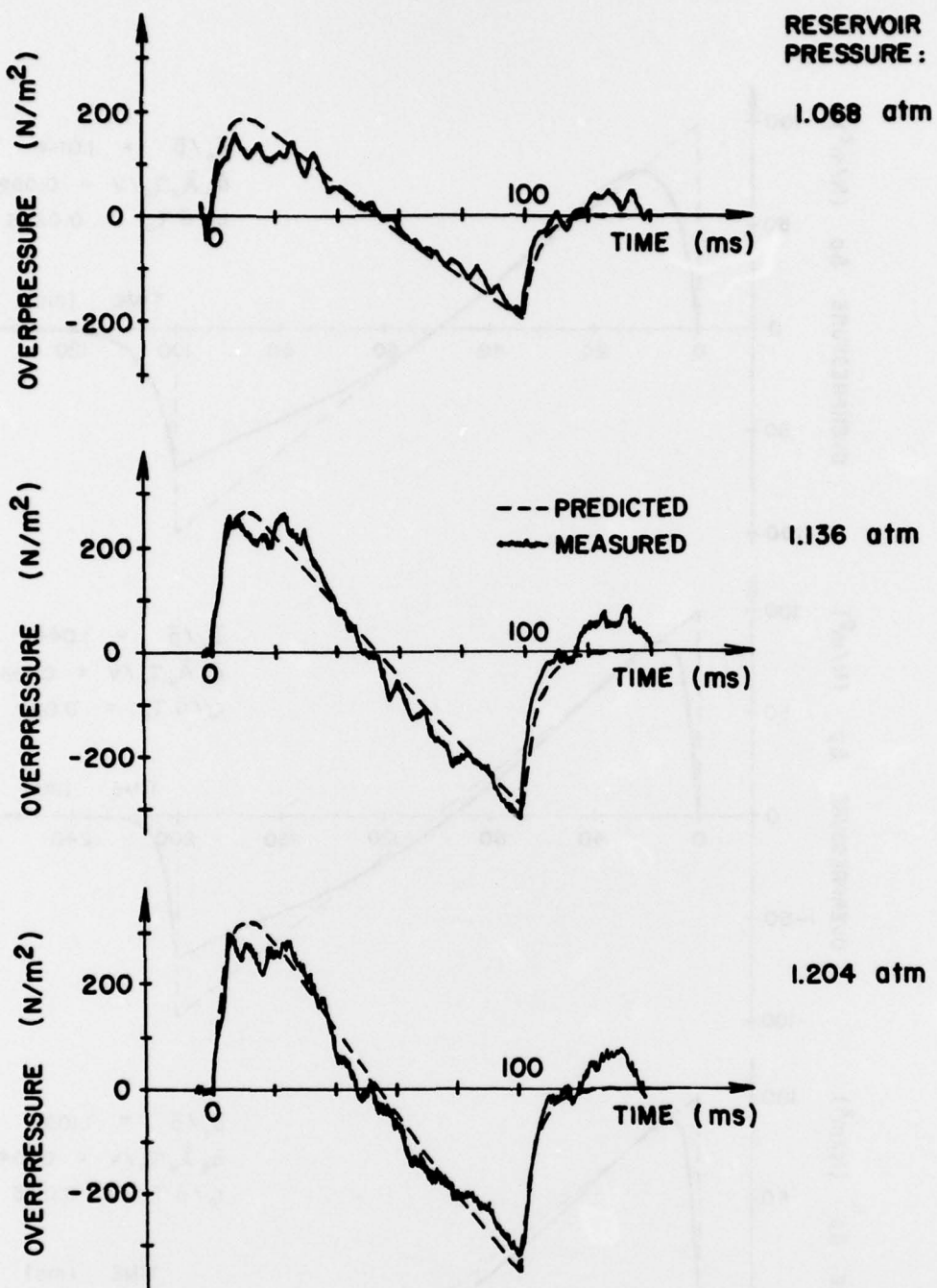
FIG. 40. MEASURED AND PREDICTED OVERPRESSURE SIGNATURES HAVING A NOMINAL DURATION OF 100 ms ($\bar{A}_* = 156$ cm, $r_* = 1.0$ m, $r_0 = 1.58$ m, $r = 21.3$ m, $V = 10.2$ m^3, $\bar{a} = 340$ m/s).
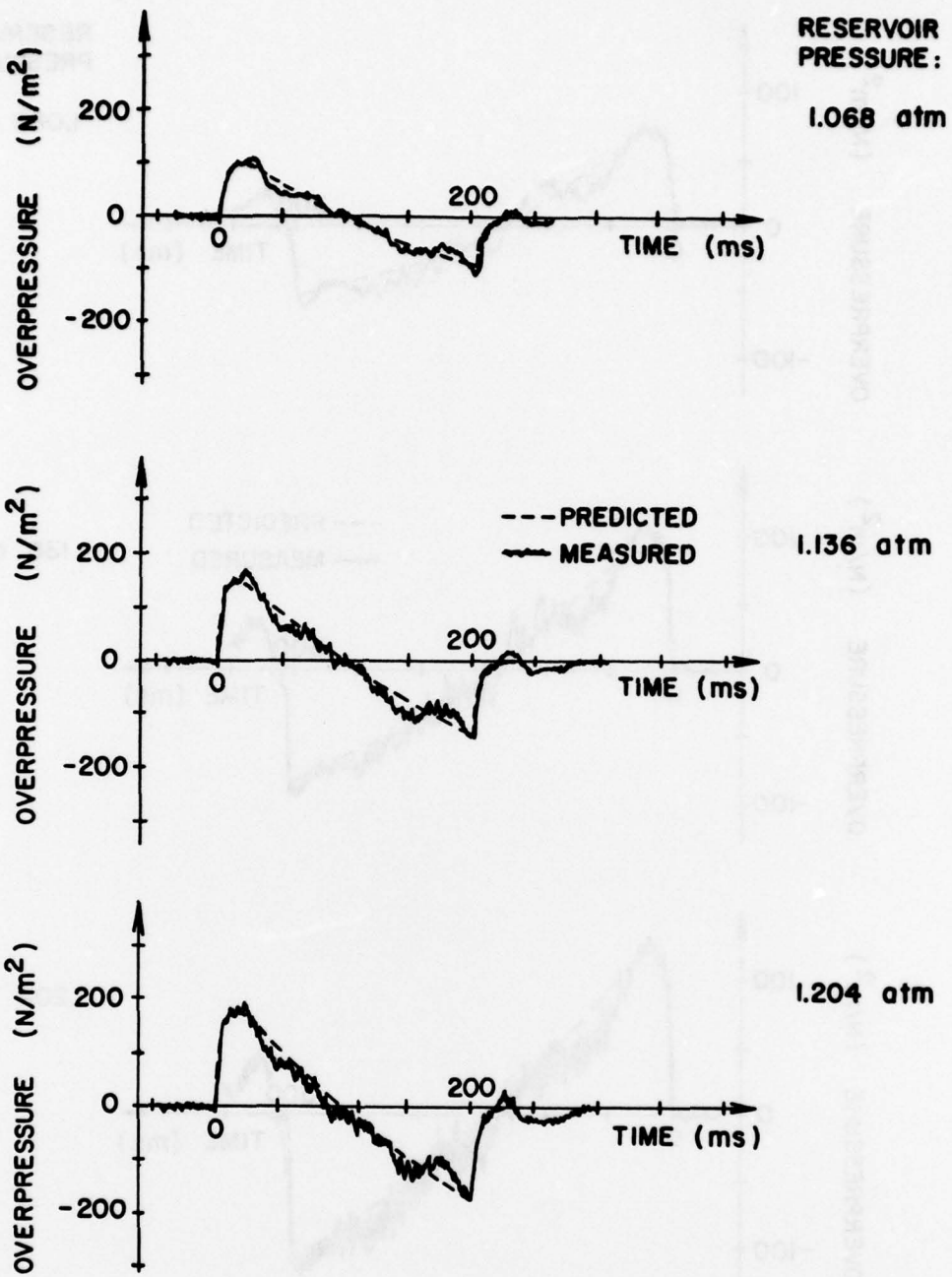
FIG. 41. MEASURED AND PREDICTED OVERPRESSURE SIGNATURES HAVING
A NOMINAL DURATION OF 200 ms ($\bar{A}_* = 156$ cm^2, $r_* = 1.0$ m,
$r_0 = 1.58$ m, $r = 21.3$ m, $V = 10.2$ m^3, $\bar{a} = 340$ m/s).
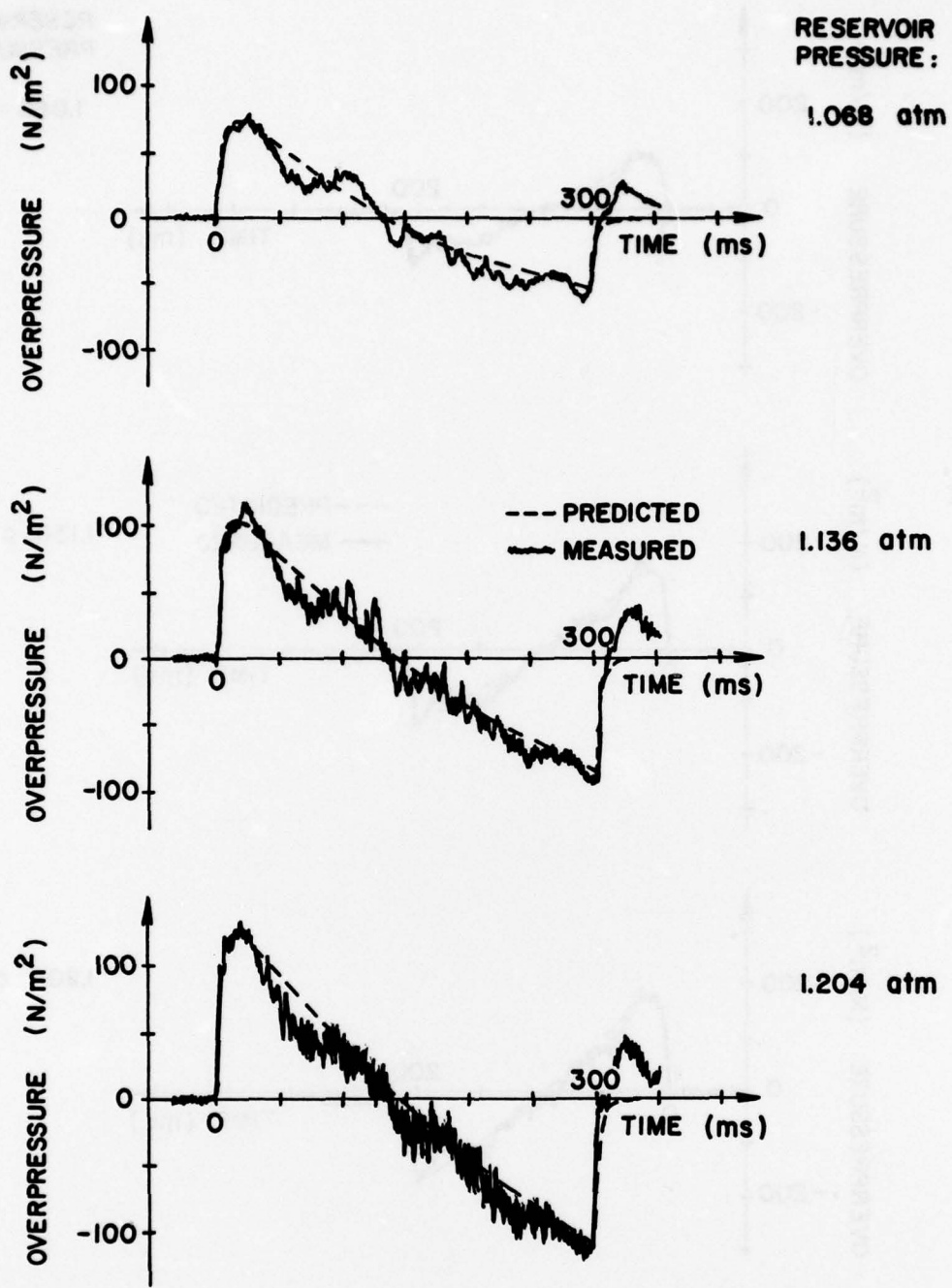
FIG. 42. MEASURED AND PREDICTED OVERPRESSURE SIGNATURES HAVING
A NOMINAL DURATION OF 300 ms) $\bar{A}_* = 156$ cm^2, $r_* = 1.0$ m,
$r_0 = 1.58$ m, $r = 21.3$ m, $V = 10.2$ m^3, $\bar{a} = 340$ m/s).
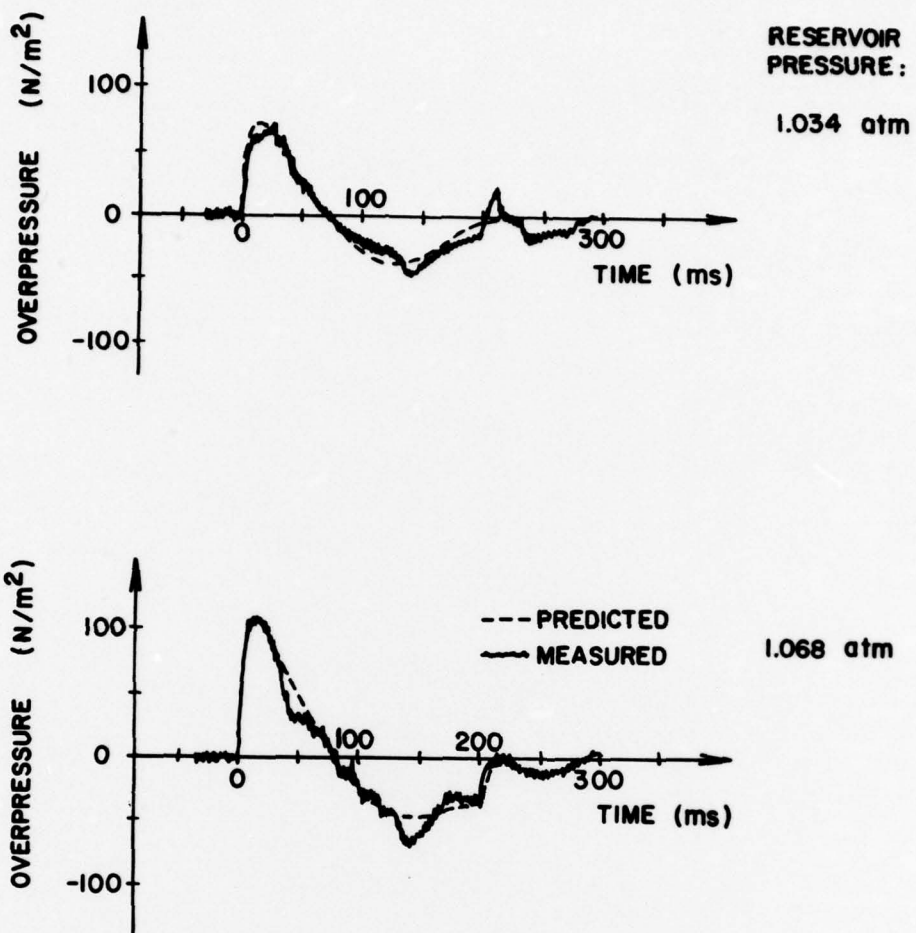
FIG. 43 MEASURED AND PREDICTED OVERPRESSURE SIGNATURES HAVING
A NOMINAL DURATION OF 200 ms ($\bar{A}_* = 156$ cm^2, $r_* = 1.0$ m,
$r_0 = 1.58$ m, $r = 21.3$ m, $V = 3.4$ m^3, $\bar{a} = 340$ m/s).

UTIAS REPORT NO. 208

Institute for Aerospace Studies, University of Toronto (UTIAS)
4925 Dufferin Street, Downsview, Ontario, Canada, M3H 5T6

A NEW TYPE FLAP VALVE FOR GENERATING SONIC BOOMS IN A PYRAMIDAL HORN

Gottlieb, J. J., Czerwinski, W., Wahba, N. N., Gnoyke, R. E.

Approx. 50 pages   Approx. 43 figures

I. Gottlieb, J. J., Czerwinski, W., Wahba, N. N., Gnoyke, R. E.   II. UTIAS Report No. 208

1. New type flap valve   2. Sonic-boom simulators   3. Low-jet-noise sonic-boom valve

A description is given of the design operation and performance of a radically new type of sonic-boom generating flap-valve. Included are the ancillary cam, clutch, flywheel and electric motor system, as well as a much larger air reservoir than used previously. An updated and greatly extended analysis describes the time varying reservoir conditions (e.g., pressure) and mass-flow rate of air through the flap valve, as well as the wave motion or characteristics of the travelling N-wave in the pyramidal concrete horn (25 m long with a 3 m x 3 m base) of the UTIAS travelling-wave sonic-boom simulation facility.

UTIAS REPORT NO. 208

Institute for Aerospace Studies, University of Toronto (UTIAS)
4925 Dufferin Street, Downsview, Ontario, Canada, M3H 5T6

A NEW TYPE FLAP VALVE FOR GENERATING SONIC BOOMS IN A PYRAMIDAL HORN

Gottlieb, J. J., Czerwinski, W., Wahba, N. N., Gnoyke, R. E.

Approx. 50 pages   Approx. 43 figures

I. Gottlieb, J. J., Czerwinski, W., Wahba, N. N., Gnoyke, R. E.   II. UTIAS Report No. 208

1. New type flap valve   2. Sonic-boom simulators   3. Low-jet-noise sonic-boom valve

A description is given of the design operation and performance of a radically new type of sonic-boom generating flap-valve. Included are the ancillary cam, clutch, flywheel and electric motor system, as well as a much larger air reservoir than used previously. An updated and greatly extended analysis describes the time varying reservoir conditions (e.g., pressure) and mass-flow rate of air through the flap valve, as well as the wave motion or characteristics of the travelling N-wave in the pyramidal concrete horn (25 m long with a 3 m x 3 m base) of the UTIAS travelling-wave sonic-boom simulation facility.

UTIAS REPORT NO. 208

Institute for Aerospace Studies, University of Toronto (UTIAS)
4925 Dufferin Street, Downsview, Ontario, Canada, M3H 5T6

A NEW TYPE FLAP VALVE FOR GENERATING SONIC BOOMS IN A PYRAMIDAL HORN

Gottlieb, J. J., Czerwinski, W., Wahba, N. N., Gnoyke, R. E.

Approx. 50 pages   Approx. 43 figures

I. Gottlieb, J. J., Czerwinski, W., Wahba, N. N., Gnoyke, R. E.   II. UTIAS Report No. 208

1. New type flap valve   2. Sonic-boom simulators   3. Low-jet-noise sonic-boom valve

A description is given of the design operation and performance of a radically new type of sonic-boom generating flap-valve. Included are the ancillary cam, clutch, flywheel and electric motor system, as well as a much larger air reservoir than used previously. An updated and greatly extended analysis describes the time varying reservoir conditions (e.g., pressure) and mass-flow rate of air through the flap valve, as well as the wave motion or characteristics of the travelling N-wave in the pyramidal concrete horn (25 m long with a 3 m x 3 m base) of the UTIAS travelling-wave sonic-boom simulation facility.

Available copies of this report are limited. Return this card to UTIAS, if you require a copy.

UTIAS REPORT NO. 208

Institute for Aerospace Studies, University of Toronto (UTIAS)
4925 Dufferin Street, Downsview, Ontario, Canada, M3H 5T6

A NEW TYPE FLAP VALVE FOR GENERATING SONIC BOOMS IN A PYRAMIDAL HORN

Gottlieb, J. J., Czerwinski, W., Wahba, N. N., Gnoyke, R. E.

Approx. 50 pages   Approx. 43 figures

I. Gottlieb, J. J., Czerwinski, W., Wahba, N. N., Gnoyke, R. E.   II. UTIAS Report No. 208

1. New type flap valve   2. Sonic-boom simulators   3. Low-jet-noise sonic-boom valve

A description is given of the design operation and performance of a radically new type of sonic-boom generating flap-valve. Included are the ancillary cam, clutch, flywheel and electric motor system, as well as a much larger air reservoir than used previously. An updated and greatly extended analysis describes the time varying reservoir conditions (e.g., pressure) and mass-flow rate of air through the flap valve, as well as the wave motion or characteristics of the travelling N-wave in the pyramidal concrete horn (25 m long with a 3 m x 3 m base) of the UTIAS travelling-wave sonic-boom simulation facility.

Available copies of this report are limited. Return this card to UTIAS, if you require a copy.

UTIAS REPORT NO. 208

Institute for Aerospace Studies, University of Toronto (UTIAS)
4925 Dufferin Street, Downsview, Ontario, Canada, M3H 5T6

A NEW TYPE FLAP VALVE FOR GENERATING SONIC BOOMS IN A PYRAMIDAL HORN

Gottlieb, J. J., Czerwinski, W., Wahba, N. N., Gnoyke, R. E.

Approx. 50 pages   Approx. 43 figures

I. Gottlieb, J. J., Czerwinski, W., Wahba, N. N., Gnoyke, R. E.   II. UTIAS Report No. 208

1. New type flap valve   2. Sonic-boom simulators   3. Low-jet-noise sonic-boom valve

A description is given of the design operation and performance of a radically new type of sonic-boom generating flap-valve. Included are the ancillary cam, clutch, flywheel and electric motor system, as well as a much larger air reservoir than used previously. An updated and greatly extended analysis describes the time varying reservoir conditions (e.g., pressure) and mass-flow rate of air through the flap valve, as well as the wave motion or characteristics of the travelling N-wave in the pyramidal concrete horn (25 m long with a 3 m x 3 m base) of the UTIAS travelling-wave sonic-boom simulation facility.

Available copies of this report are limited. Return this card to UTIAS, if you require a copy.

UTIAS REPORT NO. 208

Institute for Aerospace Studies, University of Toronto (UTIAS)
4925 Dufferin Street, Downsview, Ontario, Canada, M3H 5T6

A NEW TYPE FLAP VALVE FOR GENERATING SONIC BOOMS IN A PYRAMIDAL HORN

Gottlieb, J. J., Czerwinski, W., Wahba, N. N., Gnoyke, R. E.

Approx. 50 pages   Approx. 43 figures

I. Gottlieb, J. J., Czerwinski, W., Wahba, N. N., Gnoyke, R. E.   II. UTIAS Report No. 208

1. New type flap valve   2. Sonic-boom simulators   3. Low-jet-noise sonic-boom valve

A description is given of the design operation and performance of a radically new type of sonic-boom generating flap-valve. Included are the ancillary cam, clutch, flywheel and electric motor system, as well as a much larger air reservoir than used previously. An updated and greatly extended analysis describes the time varying reservoir conditions (e.g., pressure) and mass-flow rate of air through the flap valve, as well as the wave motion or characteristics of the travelling N-wave in the pyramidal concrete horn (25 m long with a 3 m x 3 m base) of the UTIAS travelling-wave sonic-boom simulation facility.

Available copies of this report are limited. Return this card to UTIAS, if you require a copy.